NASA/TP—2000–210481

A Comparison of Quasi-Static Indentation to Low-Velocity Impact

A.T. Nettles
Marshall Space Flight Center, Marshall Space Flight Center, Alabama

M.J. Douglas
Old Dominion University, Norfolk, Virginia

August 2000

The NASA STI Program Office...in Profile

Since its founding, NASA has been dedicated to the advancement of aeronautics and space science. The NASA Scientific and Technical Information (STI) Program Office plays a key part in helping NASA maintain this important role.

The NASA STI Program Office is operated by Langley Research Center, the lead center for NASA's scientific and technical information. The NASA STI Program Office provides access to the NASA STI Database, the largest collection of aeronautical and space science STI in the world. The Program Office is also NASA's institutional mechanism for disseminating the results of its research and development activities. These results are published by NASA in the NASA STI Report Series, which includes the following report types:

- TECHNICAL PUBLICATION. Reports of completed research or a major significant phase of research that present the results of NASA programs and include extensive data or theoretical analysis. Includes compilations of significant scientific and technical data and information deemed to be of continuing reference value. NASA's counterpart of peer-reviewed formal professional papers but has less stringent limitations on manuscript length and extent of graphic presentations.

- TECHNICAL MEMORANDUM. Scientific and technical findings that are preliminary or of specialized interest, e.g., quick release reports, working papers, and bibliographies that contain minimal annotation. Does not contain extensive analysis.

- CONTRACTOR REPORT. Scientific and technical findings by NASA-sponsored contractors and grantees.

- CONFERENCE PUBLICATION. Collected papers from scientific and technical conferences, symposia, seminars, or other meetings sponsored or cosponsored by NASA.

- SPECIAL PUBLICATION. Scientific, technical, or historical information from NASA programs, projects, and mission, often concerned with subjects having substantial public interest.

- TECHNICAL TRANSLATION. English-language translations of foreign scientific and technical material pertinent to NASA's mission.

Specialized services that complement the STI Program Office's diverse offerings include creating custom thesauri, building customized databases, organizing and publishing research results...even providing videos.

For more information about the NASA STI Program Office, see the following:

- Access the NASA STI Program Home Page at ***http://www.sti.nasa.gov***

- E-mail your question via the Internet to help@sti.nasa.gov

- Fax your question to the NASA Access Help Desk at (301) 621–0134

- Telephone the NASA Access Help Desk at (301) 621–0390

- Write to:
  NASA Access Help Desk
  NASA Center for AeroSpace Information
  7121 Standard Drive
  Hanover, MD 21076–1320

NASA/TP—2000–210481

A Comparison of Quasi-Static Indentation to Low-Velocity Impact

A.T. Nettles
Marshall Space Flight Center, Marshall Space Flight Center, Alabama

M.J. Douglas
Old Dominion University, Norfolk, Virginia

National Aeronautics and
Space Administration

Marshall Space Flight Center

August 2000

Available from:

NASA Center for AeroSpace Information
7121 Standard Drive
Hanover, MD 21076–1320
(301) 621–0390

National Technical Information Service
5285 Port Royal Road
Springfield, VA 22161
(703) 487–4650

TABLE OF CONTENTS

LIST OF FIGURES

LIST OF FIGURES (Continued)

LIST OF FIGURES (Continued)

LIST OF FIGURES (Continued)

LIST OF FIGURES (Continued)

LIST OF TABLES

LIST OF ACRONYMS

LaRC	Langley Research Center
LVDT	linear voltage displacement transducer
MSFC	Marshall Space Flight Center
NDE	nondestructive evaluation
TP	technical publication

TECHNICAL PUBLICATION

A COMPARISON OF QUASI-STATIC INDENTATION TO LOW-VELOCITY IMPACT

1. INTRODUCTION

Low-velocity impact events are expected to occur during the manufacturing and service life of composite parts and/or structures. Foreign body impact can occur during manufacturing, routine maintenance, or use of a laminated composite part. By dropping a 5-lb handtool less than 4 ft, an impact force anywhere between 100 to 1,500 lbf can occur, depending mainly on the transverse stiffness (flexural rigidity) of the impacted part at the site of the impact. Low-velocity impact events can occur during the service life of a composite in such forms as hail, runway debris, and collisions with other vehicles or animals. Impact events such as these can damage the integrity of the composite while leaving little or no visible damage.

There are two very distinct aspects to consider when designing composite structures/components—damage resistance and damage tolerance of composite materials. Damage resistance is the measure of a material's ability to resist damage, while damage tolerance measures the ability of a structure/component to carry service loads (or function as designed) with the presence of damage. Damage tolerance of carbon/epoxy composites is a very important aspect in the design criteria of composite structures. This is due to the relatively low strength of a carbon/epoxy laminate transverse to the fiber direction (through-the-thickness direction). The principal load-carrying mechanism in this direction is the epoxy matrix. The primary structural role of the matrix material is to provide stability to the fibers. During an impact event, the matrix will fail first, causing microcracks within a layer (lamina) and then delamination between the lamina layers. This can lead to the structure's inability to carry designed service loads, especially in compression.

This has led to much research on impact damage to laminated composite plates. Typically, laminated plates are impacted either by a "drop-weight" or "projectile" method. Drop-weight impacts usually consist of an instrumented striker (tup) that is secured to a carriage that falls along guideposts and collides with the plate. Projectile tests typically consist of firing a small spherical projectile at a composite plate with the use of a light gas gun. After an impact event has been performed, ultrasonic c-scans, x-radiography, and cross-sectional photomicroscopy are some of the common techniques used to document the damage area. Postimpact strength testing (mostly compression) is often performed to evaluate a material's or structure's damage tolerance.

It would be very beneficial to simulate an impact event using a "quasi-static" loading test. By using this test, damage initiation and propagation can be more easily detected, deflection can be directly measured with great accuracy, and maximum transverse force can be better controlled. Thus, the focus of the work in this technical publication (TP) was to examine if drop-weight impact tests and quasi-static loading tests give the same size, shape, and location of damage for a given maximum transverse load.

In the present study, all tests were conducted on laminated plates made from IM7/8552 prepreg. The plates tested were quasi-isotropic with a stacking sequence of $[+45,90,-45,0]_{ns}$, with n equal to 1,2,4, and 6. This is known as a $\pi/4$ quasi-isotropic stacking sequence.

2. PREVIOUS WORK

2.1 Background

The need for a static (or more commonly referred to as quasi-static) test method for modeling low-velocity foreign object impact events would prove to be very beneficial to researchers since much more data can be obtained from a quasi-static test than from an impact test. An American Standard Testing Materials standard has been proposed for transverse quasi-static loading of composite laminates, although the standard stops short of claiming to represent low-velocity impacts.[1] Since a "low-velocity" impact event lasts approximately 6–10 ms, there is debate as to whether or not a quasi-static indentation test truly represents a low-velocity impact event.

The first order of business is to determine whether or not an impact event is considered low velocity and can thus be subjected to further analysis as a quasi-static event. It has been clearly shown that projectile-type impacts in the ballistic range are governed by dynamic events and therefore could never be represented by a quasi-static test.[2–4] Some research efforts have been focused on defining the boundary between "low-velocity" and "dynamic" impact events. One study suggested that the impactor-to-target frequency ratio governs the type of event with a low (much less than unity) ratio, implying a quasi-static event.[5] A simpler method was obtained by Swanson[6] in which a rule has been established that if the impactor mass is more than 10 times the "lumped mass" of the target, then the impact event will be quasi-static in nature. The "lumped mass" is a function of the target shape and boundary conditions but is generally about one-half the mass of the entire target. However, for most practical purposes, it is fairly clear if an impact event is "low velocity." High-velocity/large-mass impacts are of little concern since the part will be so heavily damaged by such an event that an analysis is not needed and conversely a low-velocity/low-mass impact is of little concern since no damage will form.

Once an impact event is deemed to be "low velocity," the question remains as to whether or not a static indentation test can be performed that will duplicate certain aspects of the impact. Some of these aspects include permanent indentation, maximum displacement, and most importantly, amount and type of damage formed. All of these parameters must be compared against an independent variable that will be common to both tests. It has been suggested that this independent variable be the maximum transverse load.[4,7,8]

Permanent indentation after an impact or quasi-static loading test has been examined in a few studies.[9–11] The one common feature in all of these studies is the large amount of scatter in indentation depth data, to the point of rendering this measurement useless. Nevertheless, it was decided to examine this parameter in this study to see how much scatter would exist.

For load/deflection correlation it is imperative to have an instrumented impact apparatus. The interpretation of the signals has been greatly simplified with the use of commercially available systems that filter the load signals to reduce unwanted noise. Care must be taken to ensure that the filter being used does

not mask important load events. A complete analysis of instrumented impact testing is beyond the scope of this paper, but two excellent references are noted for the reader.[12,13]

The amount of damage formed by an impact event can be measured in a number of ways. Destructively, the impacted specimen can be sectioned and examined under high magnification, or a residual property can be measured (termed "damage tolerance"). Nondestructively, ultrasonic or x-radiography can give a planar indication of the type and extent of damage. Ultimately, the amount of damage formed by an impact event is the greatest concern to the engineer investigating such an occurrence, and since the impacted part may still be useable, nondestructive techniques are preferred. Thus the major portion of this paper will deal with the resulting damage as detected via nondestructive evaluation and whether or not the damage formed for a given transverse load is similar in low-velocity impact and quasi-static testing. Specific studies that have examined this are featured in section 2.2.

2.2 Impact Versus Quasi-Static Testing

Several studies[4,7,9,14,15] show a similarity between quasi-static indentation and drop-weight impact testing, while other studies[8,16,17] have shown a limit to the applicability of using quasi-static indentation to represent impact events. It must be noted that there are many variables involved in these tests such as boundary conditions, specimen size, specimen thickness, stacking sequence, impactor size, impactor shape, and type of fiber/resin system. The amount of impact damage formed in a laminated composite has been shown to be very sensitive to stacking sequence, regardless of thickness.[18] As plies are grouped together, larger areas of delaminations tend to form. It has been conventional wisdom in the aircraft industry to disperse the ply orientations in order to increase damage resistance. For example, a stacking sequence of $[+45,0,-45,90]_{2S}$ is preferable to one of $[+45_2,0_2,-45_2,90_2]_S$ in order to increase the damage resistance of the laminate.

Jackson and Poe[4] used 48-ply specimens with dispersed plies (a layup of $[45,0,-45,90]_{6S}$) in order to examine if a low-velocity impact event was similar to a quasi-static transverse loading event. The quasi-static indentation specimens were clamped over a 10.2-cm diameter circular opening and the impacted specimens were clamped over a 12.7-cm-square opening. Although these two boundary conditions are different, it was deemed not to be of a magnitude of difference to compare the delamination area of the results. The support size-to-specimen thickness ratio was ≈20 for these tests, which indicates a stiff impact target. For fiber/resin systems of both IM7/8551–7 and AS4/3506–6, no appreciable difference between the damage diameters as seen by c-scans were evident between the quasi-static and impact tests. In these tests, as a barely visible crater became more visible, the delamination results became more similar due to the elimination of scatter.

Kwon and Sankar[7] used 24- and 32-ply laminates with dispersed plies supported over a 2-in.-diameter circular opening. These specimens had an opening-to-thickness ratio of 17 and 12.5, respectively, indicating very stiff impact targets. For a limited amount of data, the static indentation and impact tests gave approximately the same delamination radius for a given transverse load.

Despite the title of a paper by Kaczmarek and Maison,[9] little information is obtained about damage area versus transverse load for impact and static indentation testing. What little information is given indicates that static and low-velocity impact testing gave "good similarity" when based on damage area as

detected by ultrasonic c-scans. The specimens were 16 plies thick with double groupings of all orientations. The layup sequence was $[45_2,0_2,-45_2,90_2]_S$ and the specimens were supported over a 12.5- by 7.5-cm opening. This gives a specimen opening-to-thickness ratio of ≈50, which is of moderate stiffness for an impact target.

Lee and Zahuta[14] used 16-ply quasi-isotropic panels with dispersed plies clamped over a 2.2- by 5-in. opening. This gives a specimen support-to-thickness ratio of ≈45, which indicates a moderately stiff to stiff impact target. The specimens were compared on a damage width rather than on a damage area basis. The results showed a good amount of scatter in the impact results with the static indentation tests yielding a slightly higher damage width for a given transverse load. On a lost energy basis, the results between static indentation and impact testing gave vastly different results with the impact tests losing much more energy for a given damage size. This was attributed to vibrations in the drop-weight crosshead absorbing much of the energy. This has also been a concern for researchers at NASA Marshall Space Flight Center (MSFC) where "lost energy" is deemed a dubious result at best.[19]

In a study at the University of Dayton Research Institute[15] a comparison between low-velocity impact and static indentation tests was based on load/deflection curves. The specimens were 48 plies thick with dispersed plies simply supported over a 12.3-cm-diameter ring. This gives a specimen support-to-thickness ratio of 20, which indicates a stiff target. The impact curve had the typical oscillations associated with an impact event but the static indentation curve superimposed over the impact curve fairly well, with incipient damage occurring at the same load and displacement for both. As far as damage is concerned, some of the specimens were cross sectioned and examined under magnification. There was no apparent difference in the type or extent of damage to the impacted specimens and the statically indented ones.

In a study at the Massachusetts Institute of Technology,[8] a slight difference in static indentation and impact testing was found. This study used panels fabricated with 12 plies grouped in sets of two. The panels were supported in a clamped-clamped/free-free configuration with a span of 25.2 cm and a width of 13 cm. These boundary conditions create a test specimen with a support size-to-thickness ratio of 170, a much more flexible specimen than those examined in previous studies thus far. For a given transverse load, the impacted panels showed more damage area as determined from x-ray analysis than the statically indented specimens. Numbers are not given, but the differences are within ≈50 percent; not huge, but different nonetheless. A plot of force versus deflection showed a vast (>100 percent) difference between static indentation and impact testing. This study also examined sandwich panels and it was found that the static indentation and impact tests were nearly identical. This was due to the extremely rigid support condition that a honeycomb panel gives its face sheets.

Elber[16] found some differences in maximum delamination length for a given transverse load between low-velocity impact and static indentation. In this study, 8-ply quasi-isotropic plates supported over a 2-in. circular opening were used. This gives a specimen support-to-thickness ratio of ≈50, which is between a stiff and flexible impact target. Load/deflection data were given and the two match well. However, for a given transverse load, those that were loaded statically had consistently longer delaminations than those that were impacted. This difference was between 15 and 40 percent for tests at four different load levels.

The largest difference between static indentation and impact testing in the literature surveyed was found by Highsmith.[17] This study employed 20-ply specimens with a layup of $[\pm 60, 0_4, \pm 60, 0_2]_S$ supported over a 2.5-in.-diameter circular opening, which gives a specimen support to thickness ratio of ≈25, representing a stiff target. Three different transverse load levels were selected and the resulting damage was evaluated using x-ray techniques. The lowest load level chosen in this study was just at the point of damage initiation; therefore, there is so much scatter in the data that a comparison cannot be made. At the two higher load levels, the specimens that were impacted showed about half as much delamination area for a given transverse load than the impacted specimens.

2.3 Conclusions From Past Studies

A summary of the results from past studies that compared quasi-static loading to impact loading based on a given transverse load is given in table 1.

From the studies examined thus far, it appears that a quasi-static indentation test can be used to simulate a low-velocity impact event in most cases; however, a more detailed study varying more parameters is needed. Most of the studies thus far have been on fairly stiff specimens. Larger ranges of stiffness need to be tested to draw a conclusion. The one study that did show a large difference in delamination area[17] has the most group plies with four zero-degree plies grouped together. It would be a rare case for an actual engineering laminate to have this kind of grouping. Thus it will be the intent of this study to examine laminates most commonly used in structures, those of the class $[45,90,-45,0]_{nS}$.

Table 1. Conclusions from previous studies.

Reference	Specimen Support/ Thickness Ratio[1]	Layup	Conclusions
4	20	$[45,0,-45,90]_{6S}$	No difference in c-scan diameter
7	17 12.5	$[0,45,90,-45]_{4S}$ $[0,22.5,45,67.5,-45,-22.5]_{2S}$	C-scan radius approx. same for limited data
9	50	$[45_2,0_2,-45_2,90_2]_S$	C-scan area shows no difference. Very little data
14	45	$[45,0,-45,90]_{2S}$	C-scan damage width showed static cases slightly higher than impact
15	20	$[0,45,-45,90]_{6S}$	Load/deflection curves similar
8	170	$[\pm 45_2,0_2]_S$	Impact showed more damage from x rays—load/deflection curves much different.
16	50	$[0,45,-45,90]_S$	From x rays, static specimens had a 15 –40 percent longer delamination length than impact specimens
17	25	$[\pm 60, 0_4, \pm 60, 0_2]_S$	Delamination areas of static specimens twice as large as impact specimens as determined from x rays

[1] The higher the number, the more flexible the plate.

3. EXPERIMENTAL PROCEDURE

3.1 Introduction

The intent of this study was to compare quasi-static indentation testing to drop-weight impact testing based on the maximum transverse load. In order to ensure a complete analysis of the two events, testing was divided into several different categories based on boundary conditions. These two categories were then subdivided into three additional groups based on plate stiffness. To ensure the repeatability of the experimental procedure, each impact test was performed on approximately four different specimens, while the quasi-static indentation test was performed on two different specimens. A decision was made to repeat the drop-weight impact testing numerous times because of the inherent data scatter. However, the repeatability became so constant during the latter stages of the testing that the number of impacted specimens for repeatability assurance was reduced.

Finally, the rate of the quasi-static indentation test was also investigated to find if there was any time dependency involved in quasi-static indentation testing. The two rates used were 0.05 in./min and 1 in./min.

3.2 Boundary Conditions

The two main categories of tests were dependent on the boundary conditions. Specimens were either clamped on all four edges or simply supported on all four edges. For simplicity, the specimens that were clamped on all four edges will be referred to as clamped and those simply supported on all four edges will be referred to as simply supported for the remainder of this TP. This was done to determine if the boundary conditions would have a major influence on the damage introduced for the same impact force. Since an impact event does not always occur directly in the center of two ribs in a grid-stiffened aircraft component nor on top of a rib, the boundary conditions will change. For example, if an impact event occurred somewhere between the center point of a grid and on top of a rib, the actual boundary conditions would be simulated more accurately in the lab as a combination of the clamped and simply supported.

To perform the simply supported test, the specimens were placed on the machined platen shown in figure 1. The platen was machined from a 5.08-cm-thick (2-in.-thick) aluminum plate with an outside square dimension of 40.64 cm (16 in.). A total of four platens were made with the square opening, N, shown in figure 1, machined to 5.08 cm (2 in.), 60.96 cm (4 in.), 15.24 cm (6 in.), and 30.48 cm (12 in.). This was done to explore the flexural/rigidity properties of the composite panels.

In order to perform the test with clamped boundary conditions, the platen in figure 1 was modified as shown in figure 2. A series of 0.64-cm (0.25-in.) holes were drilled and tapped into the aluminum plate 3.81 cm (1.50 in.) from the edge of the opening. The bolt holes were spaced 2.54 cm (1 in.) on center. The 1.27-cm-thick (0.50-in.-thick) plate shown in figure 2 was machined from a steel plate with holes placed in the same physical location as those in the platen.

The exterior dimension, *M*, in figure 2, was dependent on the opening size of the platen. For example, the platen with the 15.24-cm (6-in.) opening required a steel plate with exterior dimension (*M*) of 25.4 cm (10 in.). The laminated composite panel was placed between the 5.08-cm-thick (2-in.-thick) aluminum platen and the 1.27-cm (0.5-in.) steel plate. Allen-head bolts were then used to secure the specimen and a uniform torque of 5.65 J (50 in.-lbf) was applied to each bolt.

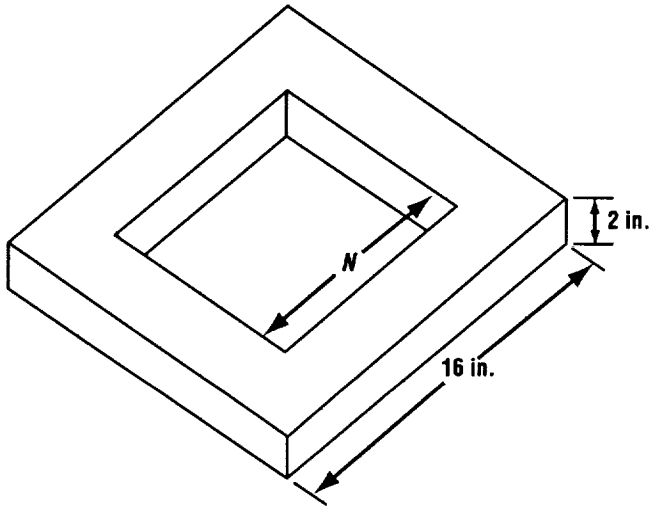

Figure 1. Test platen used for simply supported testing.

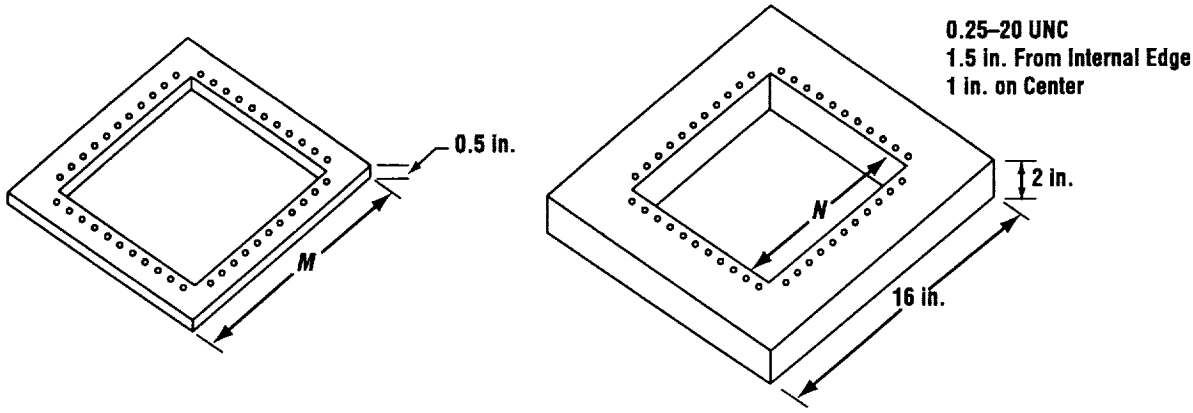

Figure 2. Modifications to test platen for clamped test.

3.3 Flexural Rigidity of Specimens

The three subgroups of tests involved the stiffness of the composite plate. It was decided that the stiffness was a function of the support opening versus the laminate plate thickness. The specimens were divided into three categories under this assumption: (1) Flex: ratio of 150, (2) medium: ratio of 50, and (3) stiff: ratio of 25.

During an impact event, this flex/stiff characteristic changes the mode of damage propagation as shown in figure 3. Figure 3 shows that for stiff laminates the contact forces caused the mode of failure, while for flexible laminates the failure propagates from the side opposite the impact site. This was characteristic of the brittle properties of the matrix materials used in advanced composites.

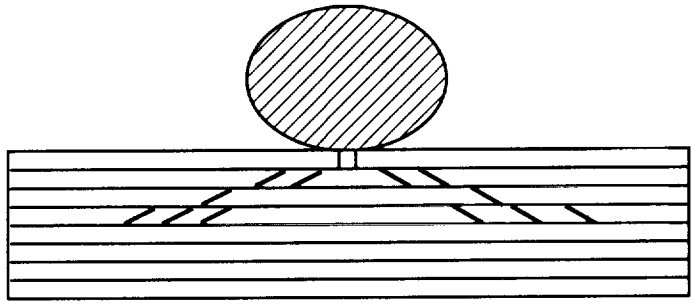

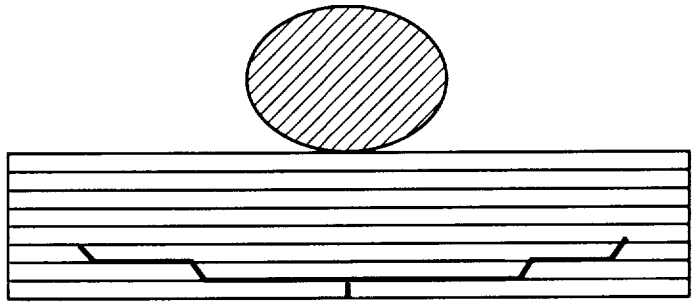

Figure 3. Impactor/laminate failure mode.

3.4 Materials

The plates used for this study were manufactured from Hexcel™ IM7/8552 prepreg. The epoxy resin, 8552, is a high-performance matrix that is used primarily in the aerospace industry for structural components. It offers exceptional toughness and damage tolerance. IM7 is an intermediate modulus carbon fiber with a tensile modulus of ≈27,580 MPa (40 msi). The manufacture's tensile strength and tensile modulus values for a unidirectional laminate of this fiber/resin system are listed in table 2.

Table 2. Material properties.

Property	Manufacturer's Value MPa (ksi)
Tensile strength	5,378 (780)
Tensile modulus	27,580 (40,000)

The quasi-isotropic laminated panels were layed up by hand, placed in a vacuum bag, and cured using the manufacturer's cure cycle shown in figure 4. The panels were fabricated into 61×91.4 cm (24×36 in.) plates. In order to obtain a large variety of flexural stiffnesses of carbon/epoxy laminates, the following four thicknesses were used: 8-, 16-, 32-, and 48-ply. The panels were fabricated utilizing the quasi-isotropic $\pi/4$ stacking sequence of $[+45,90,-45,0]_{ns}$, where n, was given the value of 1, 2, 4, and 6, respectfully.

Figure 5 is a schematic of an 8-ply laminate stacking sequence. From these panels, the test specimens were then machined into 10.16 cm (4 in.), 15.24 cm (6 in.), 20.32 cm (8 in.), and 35.56 cm (14 in.) squares. Appendix A lists all specimens, layups, and sizes. The specimens were machined using a tungsten carbide saw blade.

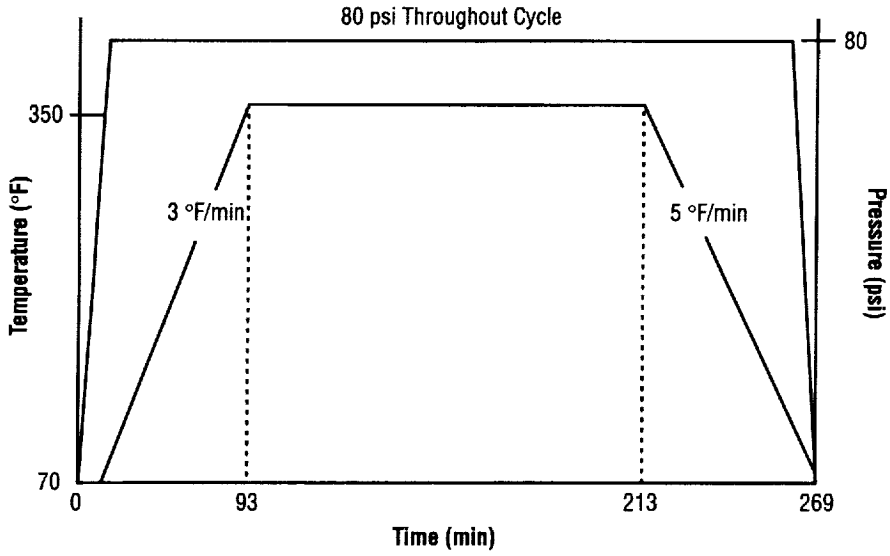

Figure 4. Typical cure cycle for IM7/8552 prepreg laminate.

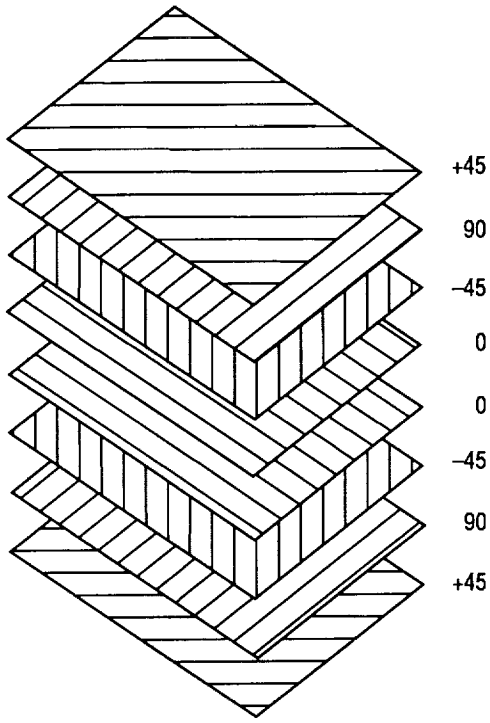

Figure 5. Schematic of an 8-ply laminate stacking sequence.

3.5 Mathematical Foundation

The impact tester measures the initial velocity by an electronic trip placed as close as possible to the surface of the impact specimen. By double-integrating the time versus load curve, deflection versus load plot was calculated. Although the computer software (GRC 930–I) performed this evaluation, the actual numbers were checked to ensure accuracy. The following equations were used:

$$F(t) = m\frac{d^2x}{dt^2}, \tag{1}$$

where

$F(t)$ is the force of the load cell (lbm*ft/sec^2)
m is the mass of the impactor (lbm)
d^2x/dt^2 is the acceleration (ft/sec^2).

From eq. (1), velocity was calculated numerically using eq. (2):

$$V(t) = \frac{-1}{m}\int F(t)dt + c_0 \ . \tag{2}$$

Using initial boundary conditions:

$$\text{at } t = 0$$
$$c_0 = V_o \ ,$$

where

$V(t)$ is the velocity of the load cell (ft/sec)
c_0 is a constant of integration
V_o is the initial velocity (ft/sec).

From eq. (2), deflection was calculated numerically using eq. (3):

$$X(t) = \left(\frac{-1}{m}\iint F(t)dtdt\right) + V_0 t \ , \tag{3}$$

where

$X(t)$ is the transverse deflection of the load cell as a function of time.

These numerical integrations were performed using the software package Kaledigraph™.

3.6 Impact Testing Procedure

The impact testing was performed at MSFC using a Dynatup 8200 drop-weight impact tester. The specimens were placed on the platen shown in figures 1 and 2, depending on boundary conditions, with the desired opening size (N). Table 3 lists the opening size used, dependent on the laminate plate thickness. This divided the test into the proper flexural/rigidity ratio being examined.

Table 3. Opening and laminate thickness ratio calculations.

Flex: Ratio of 150		
Number Plies	**Laminate Thickness mm (in.)**	**Opening Size (N) mm (in.)**
8	0.102 (0.04)	152.4 (6)
16	0.204 (0.08)	304.8 (12)
Medium: Ratio of 50		
8	0.102 (0.04)	50.8 (2)
16	0.204 (0.08)	101.6 (4)
48	6.096 (0.24)	304.8 (12)
Stiff: Ratio of 25		
16	0.204 (0.08)	50.8 (2)
32	4.064 (0.16)	101.6 (4)
48	6.096 (0.24)	152.4 (6)

Specimens were then impacted with a hemispherical-tipped steel tup. The drop-height and mass of the impactor was adjusted to give the desired damage mode. The damage desired was very little visual damage to the top of the specimen while achieving a measurable crack on the bottom surface. This level of damage was chosen since the onset of visual damage is such a critical state for an impact event. If penetration is allowed, boundary conditions and rate effects will not be as noticeable and if too low of an impact level is used, damage may not form at all. Tables 4 and 5 list the height, maximum load, and mass for each subgroup that was finally chosen before proceeding to the quasi-static indentation testing. Table 4 is for the clamped boundary conditions and table 5 is for the simply supported boundary conditions. Appendix A has a complete listing of the drop-height and maximum loads for each specimen tested.

Table 4. Maximum load and drop height for the clamped boundary conditions.

Clamped			
Flex: Ratio of 150			
Number Plies	**Specimen ID No.**	**Maximum Impact Force N (lbf)**	**Drop Height cm (in.)**
8	616–15f	1,930 (434)	30.48 (12)
16	616–04f	7,108 (1,598)	121.92 (48)
Medium: Ratio of 50			
8	728–11m	1,036 (233)	12.70 (5)
16	616–28m	3,728 (838)	35.56 (14)
48	61599–04m	26,823 (6,030)	119.38 (47)
Stiff: Ratio of 25			
16	616–32s	3,100 (697)	33.02 (13)
32	616–20s	7,268 (1,634)	71.12 (28)
48	727–05s	23,100 (5,193)	63.50 (25)

Table 5. Maximum load and drop height for the simply supported boundary conditions.

Simply Supported			
Flex: Ratio of 150			
Number Plies	**Specimen ID No.**	**Maximum Impact Force N (lbf)**	**Drop Height cm (in.)**
8	727–10f	1,873 (421)	44.45 (17.50)
16	728–06f	5,400 (1,214)	148.6 (58.50)
Medium: Ratio of 50			
8	728–03m	974 (219)	5.72 (2.25)
16	727–11m	3,728 (837)	49.53 (19.50)
48	61599–02m	23,562 (5,297)	119.38 (47.00)
Stiff: Ratio of 25			
16	727–20s	2,922 (657)	52.71 (20.75)
32	727–18s	9,853 (2,215)	124.46 (49.00)
48	727–02s	22,121 (4,973)	63.18 (24.88)

Time versus load data were measured and collected using the software package GRC 930–I. Figure 6 shows a typical time versus load plot for an impact test. From this data the load displacement graphs were calculated as discussed in section 3.5.

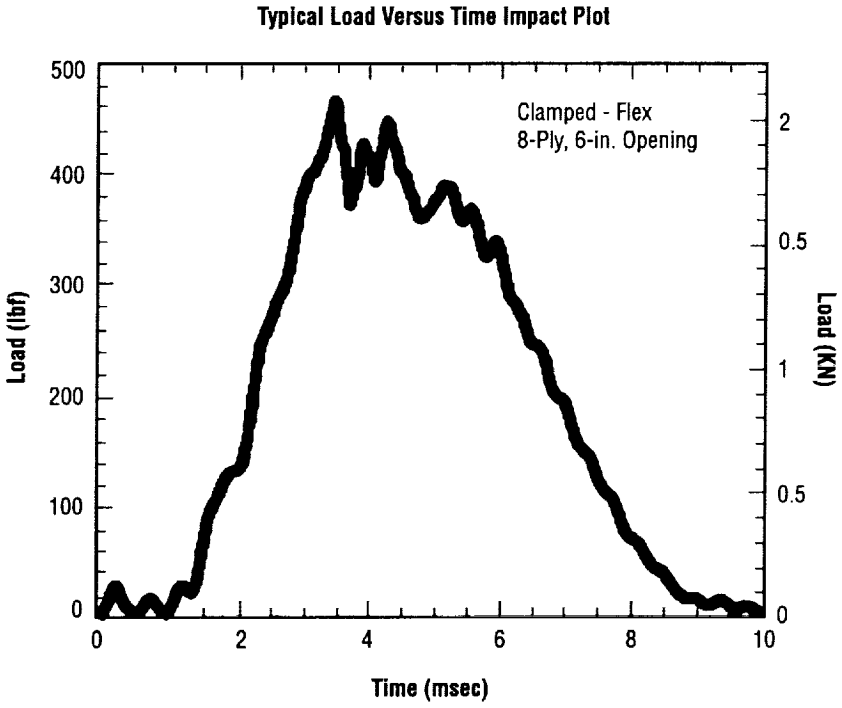

Figure 6. Typical time versus load plot.

In order to achieve the desired impact force on the 48-ply specimens, two different load cells were required. These specimens required an impact force >5,000 lbf; therefore, a 10,000-lbf load cell was used. To ensure the compatibility of the load cells, four drop-weight impact tests were performed. Both loads' cells were placed on the crosshead with an equal amount of weights placed at the same height, and then composite panels were impacted to compare maximum loads. The results of these tests are tabulated in table 6.

Table 6. 5,000- and 10,000-lb load cell comparison.

Specimen ID No.	Initial Energy J (ft-lb)	Initial Velocity M/sec (ft/sec)	Maximum Load N (lbf)	Load Cell
614E–1	15.89 (11.72)	4.3 (14.11)	5,449 (1,225)	10,000
614E–2	15.68 (11.57)	4.27 (14.02)	5,453 (1,226)	10,000
614E–3	15.82 (11.67)	4.29 (14.08)	5,351 (1,203)	5,000
614E–4	16.00 (11.80)	4.32 (14.16)	5,631 (1,266)	5,000

From these data it was concluded that both load cells were properly calibrated and giving good force values.

Figure 7 shows a typical load versus displacement plot. All load versus displacement plots for the impact test can be found in appendix B.

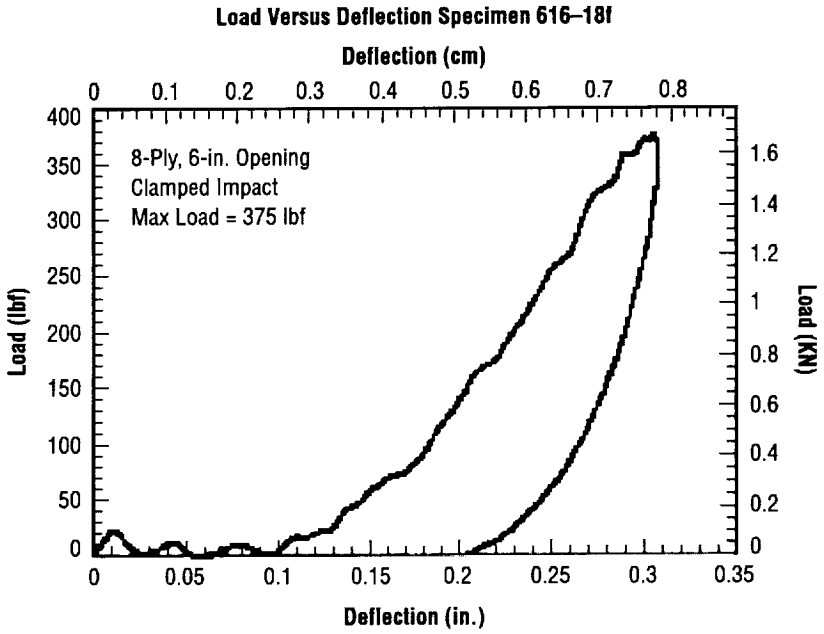

Figure 7. Typical load versus displacement plot for impact testing.

3.7 Static Indentation Testing Procedure

Once the impact testing was completed, the maximum impact force obtained for each of the different subgroups was used as the independent variable in the quasi-static indentation test. This was done primarily due to the ease of reproducing this value on a servohydraulic test frame. However, it did not turn out to be as easy as thought when the loading rate was increased to 1 in./min. Therefore, a small amount of scatter was introduced into the experimental data from the beginning. The majority of the quasi-static indentation tests were performed at NASA Langley Research Center (LaRC) on a 100-kip servohydraulic load frame. Figure 8 shows the test fixture used for all of the quasi-static indentation tests performed at LaRC. In order to perform a few tests at MSFC, a slight modification to the way the fixture was mounted in the load frame had to be accomplished. The platen shown in figure 8 was the same platen used for the impact test. For simplicity, the platen without the bolt holes is shown. The platen rested on top of the 5.08-cm-thick (2-in.-thick) aluminum uprights and could be removed without taking the fixture out of the test frame. The aluminum uprights were bolted to a 5.08-cm-thick (2-in.-thick) steel plate. The tang shown in figure 8 was also machined out of steel and was bolted to the underside of the steel plate. The impactor was placed in the upper crosshead of the servohydraulic load frame. In a limited number of tests, transverse deflection of the center point of the laminate, directly under the hemispherical tup, was measured using a linear voltage displacement transducer (LVDT). Figure 8 shows the location of the LVDT. The tests were run in stroke control at the two different load rates previously mentioned.

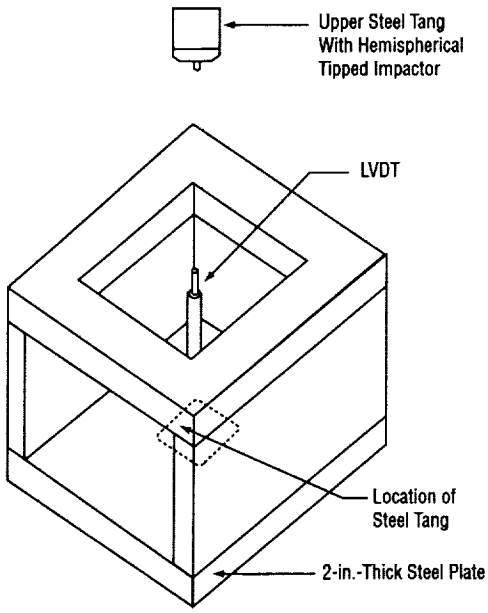

Figure 8. Test fixture for quasi-static indentation testing.

Load and transverse deflection data were collected using the WIN5000™ data acquisition system. Although the quasi-static indentation tests were repeated, it was not repeated to the magnitude of the impact testing. Each series of tests was performed twice. Since the dynamics of the quasi-static testing was not an issue, this was assumed an adequate number to ensure repeatability. Figure 9 is a typical load deflection plot for a quasi-static indentation test. Appendix C contains all of the load deflection plots from the quasi-static indentation testing.

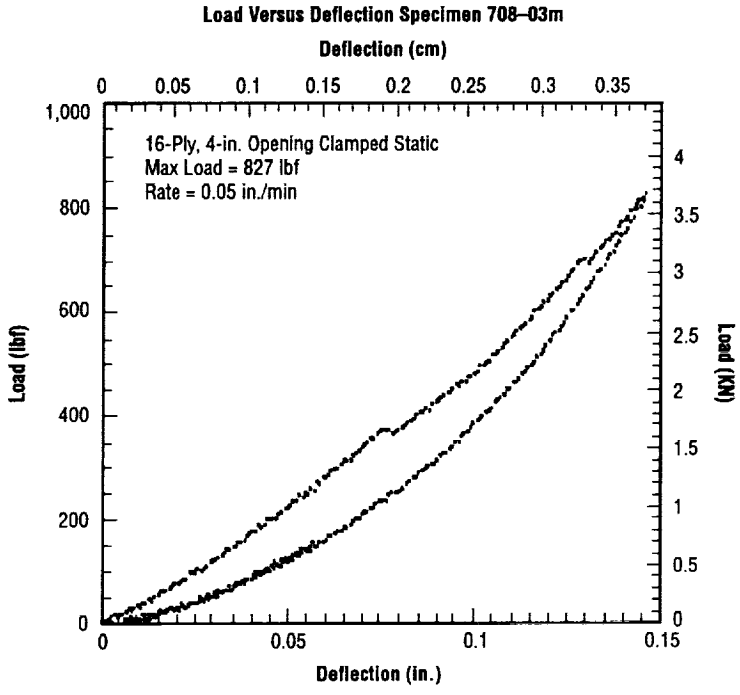

Figure 9. Typical load versus displacement plot for quasi-static indentation testing.

3.8 Nondestructive Analysis

Once the impact and quasi-static testing were completed, the specimen underwent three types of nondestructive analysis to document internal and external damage. These consisted of measuring dent depth on the impacted surface, crack lengths on the nonimpacted surface, and internal damage as determined from x-radiography.

After the specimens were impacted or subjected to quasi-static indentation testing, they were set aside for at least 24 hr so that the resulting dent would have time to relax to its equilibrium state. It was felt that this would be appropriate since a postflight inspection would be performed at least 24 hr after a flight. The dent depths were measured using a Starrett™ Model 644–44I dial depth gauge with an accuracy of 0.0254 mm (0.001 in.).

Any visible cracks on the nonimpacted surface of the specimens were measured.

After all the dent depths and crack lengths were measured, the specimens were then subjected to radiographic techniques to document the internal damage areas. The specimens were soaked on both sides with a zinc iodide penetrant solution for 24 hr and then x rayed using a Faxitron™ x-ray machine. A piece of photographic film was placed directly under the specimen to capture the image of the internal damage in the form of a negative. The exposure length and focal film distance was varied, depending on the specimens being x rayed. For example, specimens 61599–02 through 61599–05 (48-ply specimens) were exposed at 35 kV for 2 min with a focal length of 46 in. While the specimens with identification numbers 616–20 through 616–24 (32-ply specimens) were exposed at 35 kV for 1 min 15 sec at a focal length of 46 in. From the negatives, positives were made so that the planar damage area could be calculated. This was accomplished by superimposing a grid of 4 mm^2 (0.0062 $in.^2$) squares over the picture and then counting squares that were within the damage area. Figure 10 illustrates the process used. The specimen shown in figure 10 was a 16-ply clamped impact specimen, 616–04f, supported over the 30.48-cm (12-in.) opening. From this photo 192 squares were counted, which gives a planar delamination area of 768 mm^2 (1.19 $in.^2$). It should be noted that this is only a planar calculation and does not take into consideration the thickness of the specimen. The strain gauge that appears in the bottom righthand corner of figure 10 was put on the specimen after it had been impacted so the x ray could be oriented with the specimen if needed.

The planar area of delamination was the most important variable used in this study and was the main factor in determining if an impact event can be represented by a quasi-static indentation test.

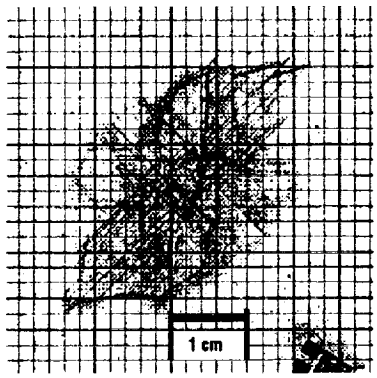

Figure 10. X-ray of impact specimen with 4 mm^2 grid superimposed.

4. RESULTS AND DISCUSSION

4.1 Introduction

Since the main purpose of the research being presented was to establish if quasi-static indentation testing was a true representation of a low-velocity impact event, this chapter will address this issue by comparing the experimental results obtained in the low-velocity impact testing to that of the quasi-static indentation testing. The impact testing will be discussed and then a comparison of the damage resistance of the material subjected to the two different events will be presented. Tables 7 and 8 list the specimens and the maximum loads used for comparison between impact and quasi-static testing. Once the specimens were tested, comparisons were made on the dent depth, crack length, and delamination area. From these comparisons, an understanding and analysis of the two types of testing procedures was achieved.

4.2 Drop-Weight Impact Testing

All of the load versus deflection plots for the drop-weight impact tests document the nonlinear characteristics inherent to large deflection of plates. This can be seen in appendix B. This nonlinear characteristic behavior makes it very difficult to accurately predict mathematically how the material will behave when subjected to a transverse load. For that reason, none of the classical laminate plate theories has been introduced for comparison in this paper.

The impact duration versus stiffness ratio plots shown in figures 11 and 12 show that the stiffness ratio has a direct effect on the duration of the impact. The impact duration increased as the stiffness ratio increased (i.e., the specimen became more "flexible") for both boundary conditions. All stiffness ratios had overlap in the duration of impact data and little difference can be noted between the two sets of boundary conditions. It is apparent from the data that the duration of impact is dependent upon much more than simply the support-to-thickness ratios of the plates, otherwise the data for ratios of 25, 50, and 150 would be clustered together in well-defined groups. The only noticeable trend between the two boundary conditions occurs on the most flexible specimens with a stiffness ratio of 150. For these data, the simply supported boundary condition gives a slightly longer duration of impact than the clamped boundary condition as long as all other parameters are held equal.

4.3 Quasi-Static Indentation Testing

Appendix C presents the load/deflection data generated for a limited number of the static indentation tests. The quasi-static test plots have very different behavior characteristics, depending on the stiffness ratio. For clarification, specimens ending in "f" indicate "flex" or a stiffness ratio of 150. Specimens ending in "m" indicate "medium" or a stiffness ratio of 50, and "s" indicates "stiff" or a stiffness ratio of 25.

For the "flex" specimens, the load/deflection curves demonstrate the extreme nonlinearity associated with large deflections of plates. The initial portion of the curve shows very little resistance to bending as a small load causes a large amount of deflection. However, as the membrane stresses begin to dominate,

Table 7. Identification numbers and maximum loads for clamped specimens.

	Type of Event	Specimen ID No.	Maximum Load N (lbf)
Flex: Support/Thickness Ratio of 150			
8-ply,	Impact	616–15f	1,930 (434)
6-in. opening	Static 0.05 in./min	708–10f	1,735 (390)
	Static 1 in./min	720–08f	1,899 (427)
16-ply,	Impact	616–04f	7,108 (1,598)
12-in. opening	Static 0.05 in./min	720–04f	6,993 (1,572)
	Static 1 in./min	720–05f	7,357 (1,654)
Medium: Support/Thickness Ratio of 50			
8-ply,	Impact	728–11m	1,036 (233)
2-in. opening	Static 0.05 in./min	722–04m	1,045 (235)
	Static 1 in./min	722–05m	939 (211)
16-ply,	Impact	616–28m	3,728 (838)
4-in. opening	Static 0.05 in./min	708–02m	3,705 (833)
	Static 1 in./min	720–06m	3,857 (867)
48-ply,	Impact	616–04m	26,823 (6,030)
12-in. opening	Static 0.05 in./min	817–01m	26,293 (5,911)
	Static 1 in./min	818–02m	28,290 (6,360)
Stiff: Support/Thickness Ratio of 25			
16-ply,	Impact	616–32s	3,100 (697)
2-in. opening	Static 0.05 in./min	722–02s	2,918 (656)
	Static 1 in./min	722–08s	2,931 (659)
32-ply,	Impact	616–20s	7,313 (1,644)
4-in. opening	Static 0.05 in./min	706–01s	7,455 (1,676)
	Static 1 in./min	708–07s	7,455 (1,676)
48-ply,	Impact	727–05s	23,100 (5,193)
6-in. opening	Static 0.05 in./min	720–01s	23,429 (5,267)
	Static 1 in./min	817–03s	23,389 (5,258)

the amount of load needed to cause a given amount of deflection increases greatly. Little damage is noted in these specimens until the maximum load is reached. This suggests a damage mode associated with large bending stresses.

The "medium" specimens all show a "kink" in the initial loading portion of the load/deflection curves associated with initial damage. Higher shear stresses are developed in the stiffer specimens, which results in delamination-type failures within the laminate. The curves are seen to be slightly nonlinear until the initial damage is formed, at which point the curves demonstrate more nonlinearity.

The "stiff" specimens also have the initial load drop along the loading curve, which appears to be of a larger magnitude than in the "medium" specimens. This follows since the stiff specimens will develop larger shear stresses which will release more energy when delamination does occur. Also of note is the change of stiffness at the very beginning of the load/deflection curve. This is associated with the contact stresses between the impactor and the plate. As the impactor first touches the plate, it begins to "dent into" the specimen, causing an indentation in the specimen. As the impactor goes deeper into the specimen, the contact stresses are spread out and the impactor stops indenting into the specimen.

Table 8. Identification numbers and maximum loads for simply supported specimens.

	Type of Event	Specimen ID No.	Maximum Load N (lbf)
Flex: Support/Thickness Ratio of 150			
8-ply,	Impact	727–10f	1,873 (421)
6-in. opening	Static 0.05 in./min	817–11f	1,859 (418)
	Static 1 in./min	817–04f	1,859 (418)
16-ply,	Impact	728–06f	5,400 (1,214)
12-in. opening	Static 0.05 in./min	818–06f	5,458 (1,227)
	Static 1 in./min	818–04f	5,667 (1,270)
Medium: Support/Thickness Ratio of 50			
8-ply,	Impact	728–03m	974 (219)
2-in. opening	Static 0.05 in./min	819–02m	907 (204)
	Static 1 in./min	819–08m	1,059 (238)
16-ply,	Impact	727–12m	3,701 (832)
4-in. opening	Static 0.05 in./min	819–016m	3,677 (827)
	Static 1 in./min	819–10m	3,777 (849)
48-ply,	Impact	61599–02m	23,562 (5,297)
12-in. opening	Static 0.05 in./min	818–07m	23,878 (5,368)
	Static 1 in./min	818–02m	28,304 (6,363)
Stiff: Support/Thickness Ratio of 25			
16-ply,	Impact	727–20s	2,922 (657)
2-in. opening	Static 0.05 in./min	819–04s	2,918 (656)
	Static 1 in./min	819–06s	2,931 (656)
32-ply,	Impact	727–18s	9,853 (2,215)
4-in. opening	Static 0.05 in./min	819–14s	9,866 (2,218)
	Static 1 in./min	819–12s	10,898 (2,450)
48-ply,	Impact	727–02s	22,121 (4,973)
6-in. opening	Static 0.05 in./min	817–08s	22,726 (5,109)
	Static 1 in./min	817–06s	21,476 (4,828)

4.4 Nondestructive Analysis

As mentioned earlier, three different types of nondestructive analysis techniques were used. All nondestructive evaluation (NDE) analysis results are tabulated in appendix D. Since visible damage that occurs from an impact event is most easily measured, all analysis will be presented with the dent depth as the independent variable.

When an impact event occurs to a laminated component, visual damage is not always apparent, although there can be severe underlying damage. It has been proposed that if a correlation between the measurable dent depth, usually the only visible damage, and underlying delamination or measurable crack length on the nonimpacted surface, then a damage resistance concern could be easily addressed. For this reason the dent depths were measured and documented for all specimens and used as the independent variable for all subsequent comparisons.

4.5 Crack Length

The specimens listed in tables 7 and 8 were used to generate the dent depth versus crack length plots shown in figures 13 and 14. Figure 13 is for the clamped boundary condition and figure 14 is for the simply supported boundary condition. For these two figures, a least-squares linear approximation was performed to find if any linear correlation between the two variables was present.

In figure 14 the data represented by the open squares were not included for the least-squares linear approximation. This was done because it fell outside of what was considered valid scatterbands. Equation (4) is the calculated linear approximation:

$$C = -0.347 + 224d \quad , \tag{4}$$

where

C is the crack length (in.)
d is the dent depth (in.).

From eq. (4) when the crack length (C) was set equal to zero and the equation solved for the dent depth (d), a value of 0.0015 in. was calculated. This would suggest that a carbon/epoxy structure/component could sustain a low-velocity impact event that produces a dent depth of 0.0015 in. and not have any measurable crack length on the nonimpacted surface.

Equation (5) is the linear approximation, calculated using the least-squares approach, as performed for figure 14:

$$C = -0.309 + 202d \quad , \tag{5}$$

where

C is the crack length (in.)
d is the dent depth (in.).

If the same analysis is performed on eq. (5) as performed on eq. (4), the value for the maximum dent depth without cracking was calculated to be 0.00153 in.

Although the two equations are in general agreement, they do not take into account the stiffness ratio of the composite plates. As previously mentioned, the stiffness ratio has a direct effect on the failure mode of the composite plates. Therefore, a correlation needs to be found that is not as generalized as this approach.

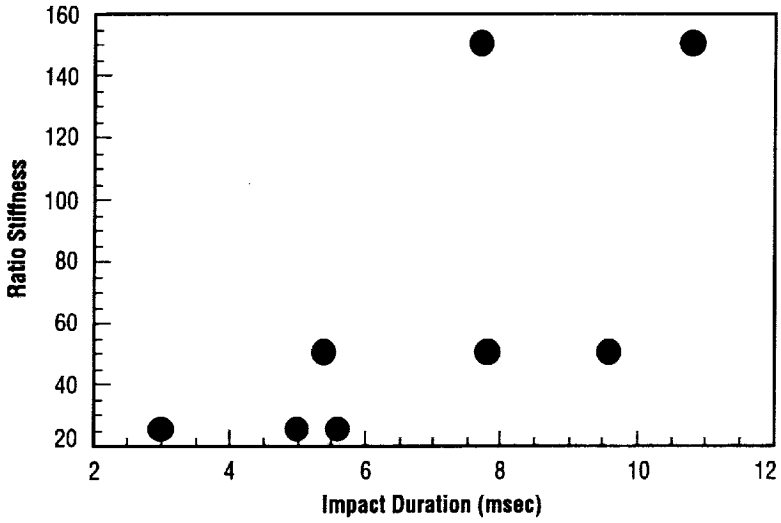

Figure 11. Impact duration versus stiffness ratio for clamped boundary conditions.

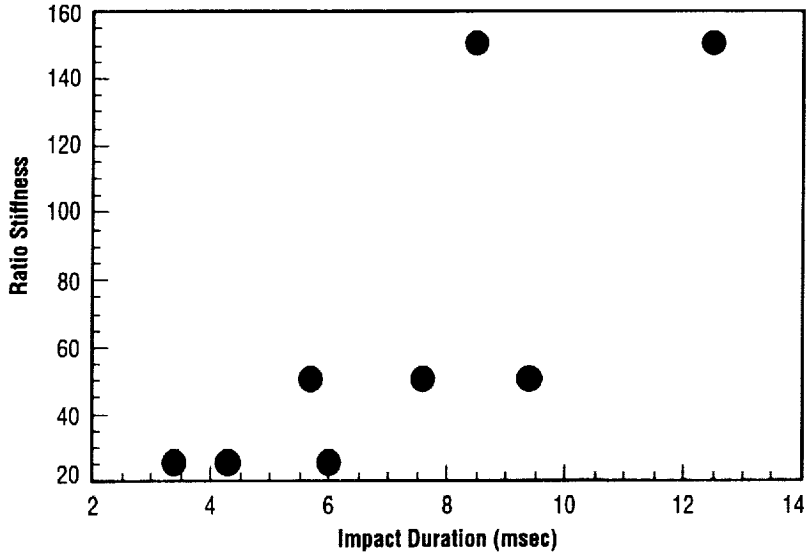

Figure 12. Impact duration versus stiffness ratio for simply supported boundary conditions.

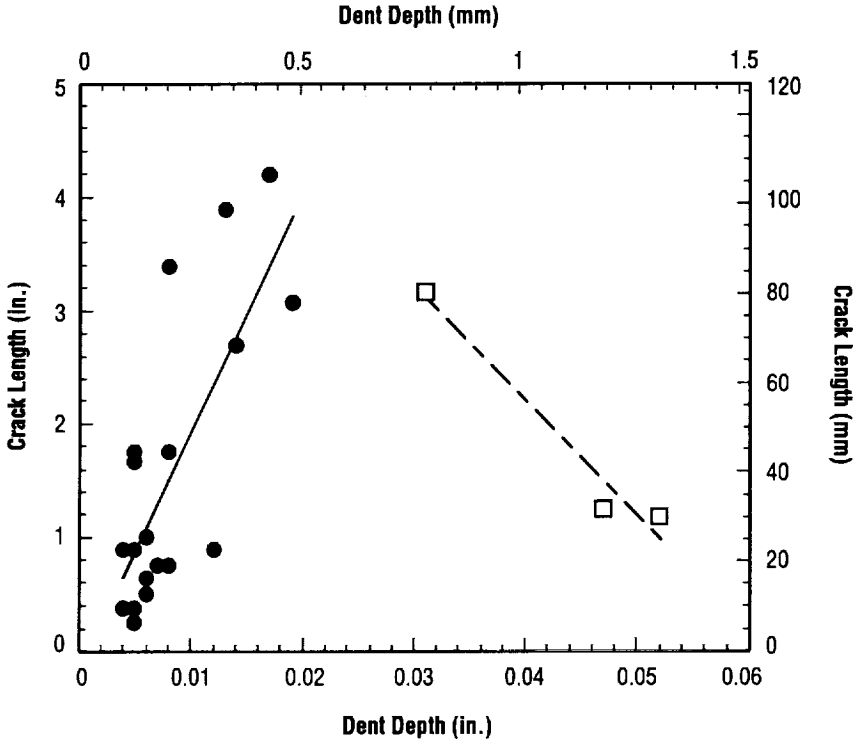

Figure 13. Crack length versus dent depth clamped boundary conditions.

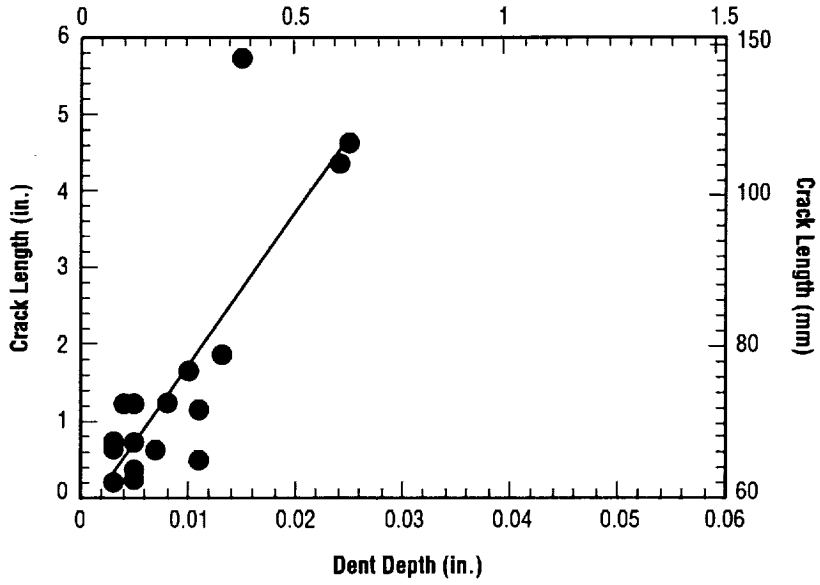

Figure 14. Crack length versus dent depth simply supported boundary conditions.

4.6 Delamination Area

For the delamination area comparisons, the same analysis will be performed as in the case of the crack lengths. Figures 15 and 16 are plots of delamination area versus dent depth for the clamped and simply supported boundary conditions, respectfully. The least-squares linear approximations are presented in eqs. (6) and (7); however, the physical interpretations of these equations take on a different approach.

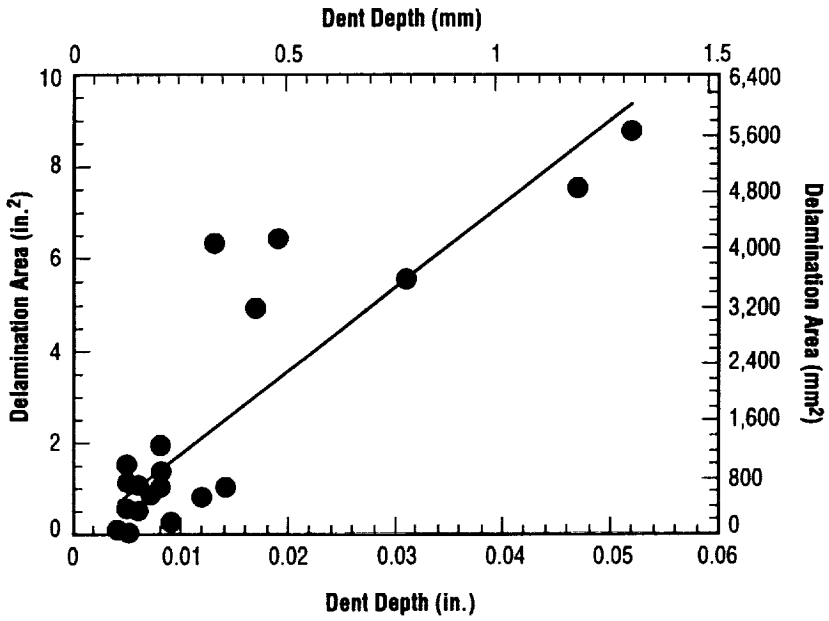

Figure 15. Delamination area versus dent depth clamped boundary conditions.

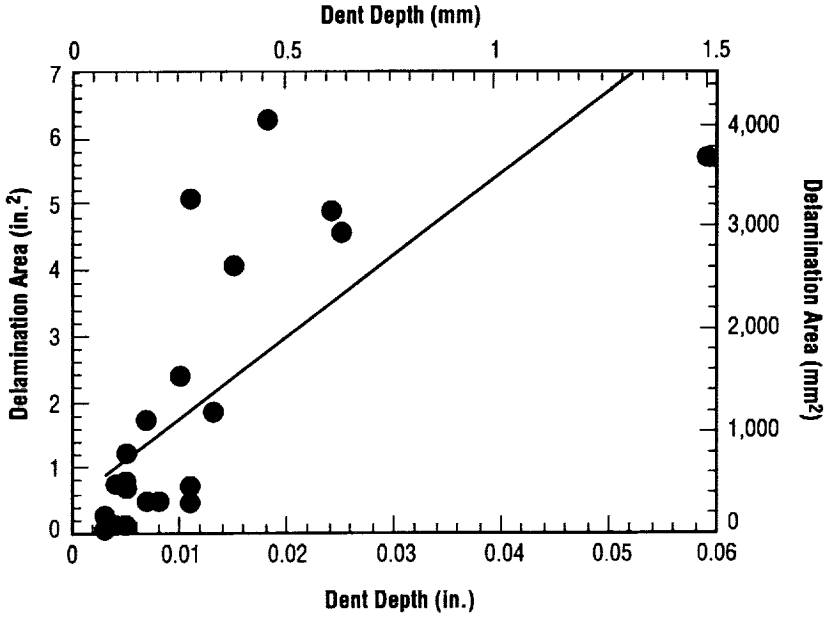

Figure 16. Delamination area versus dent depth simply supported boundary conditions.

Equation (6) is the linear approximation to the data presented in figure 15:

$$A = 0.005 + 178d \ , \tag{6}$$

where

A is the delamination area (in.^{2})
d is the dent depth (in.).

Unlike the dent depth discussion, in order to understand the physical meaning, if there is any, of eq. (6), the dent depth (d) was allowed to become zero. Doing this leads to a value of delamination area (A) equal to 0.005 in^2.

Equation (7) for figure 16 is presented as:

$$A = 0.52 + 124d \ , \tag{7}$$

where

A is the delamination area (in.^{2})
d is the dent depth (in.).

Using the same analysis as performed on eq. (6), a delamination area of 0.52 in.^{2} is found. This value is extremely large compared to the value for eq. (6). One could argue that because of the simply supported boundary conditions, this is possible. The simply supported boundary conditions allow for a larger amount of flexure to the composite plate, which in turn would produce more internal stress, alluding to large internal delaminations for the same applied load.

These data imply that after an impact event has occurred to a carbon/epoxy component/structure, underlying damage can occur with no visual evidence. Again, this analysis is overly simplified and a more indepth analysis needs to be found to better predict internal damage to laminated structures.

4.7 Comparison of Quasi-Static Indentation Testing and Drop-Weight Impact Testing

This section presents the main topic of this TP—"Does a statically applied transverse load yield the same damage as a low-velocity impact load of the same magnitude?" Using damage area as detected by x-ray analysis was deemed the most suitable method to do this since internal damage can be detected with this method. Figures 17–24 present delamination area as a function of applied transverse load for both low-velocity impacts and quasi-static loads of two rates. Each figure contains data for both clamped and simply supported specimens to test Jackson's assertion[4] that the delamination area should be independent of this parameter.

Figures 17 and 18 present data for the case of "flexible" laminates (support/thickness ratio of 150). The open symbols represent the simply supported boundary condition.

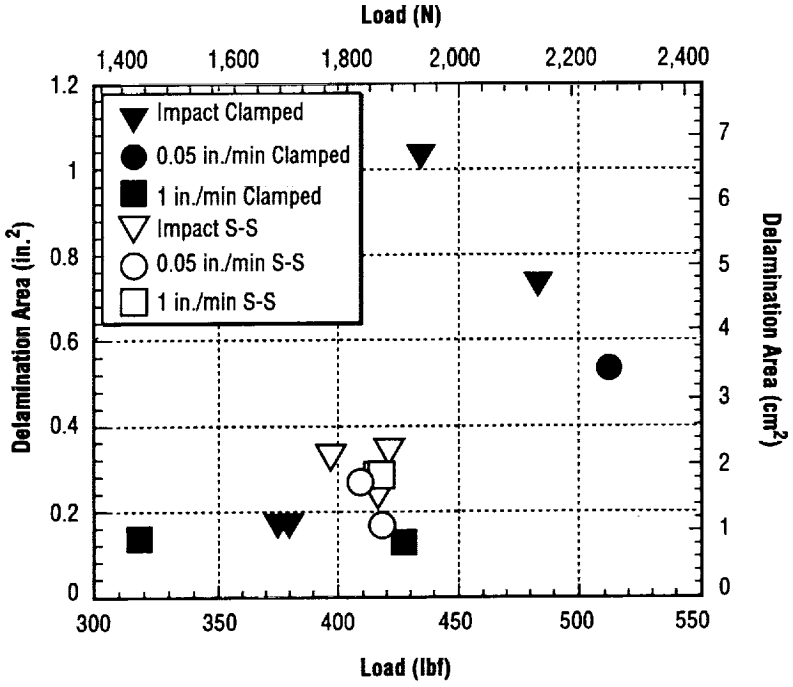

Figure 17. Delamination area versus maximum load for 8-ply specimens over 6-in. opening.

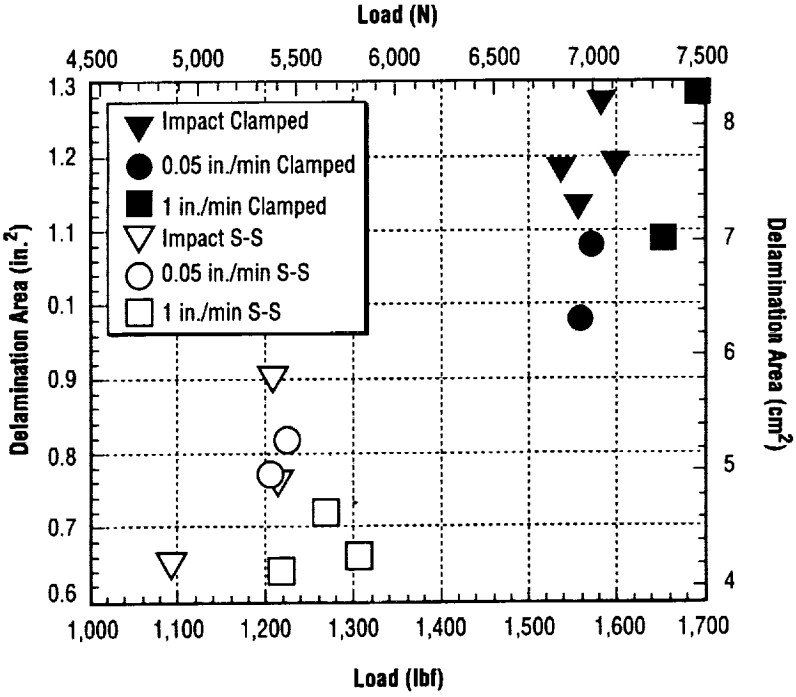

Figure 18. Delamination area versus maximum load for 16-ply specimens over 12-in. opening.

Figures 19–21 present data for the case of "medium" laminates (support/thickness ratio of 50). The open symbols represent the simply supported boundary condition.

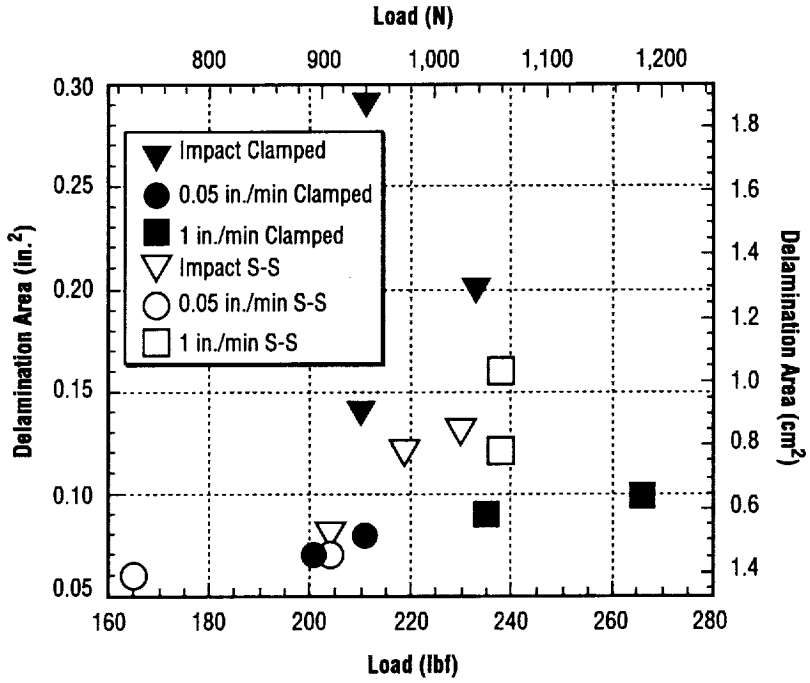

Figure 19. Delamination area versus maximum load for 8-ply specimens over 2-in. opening.

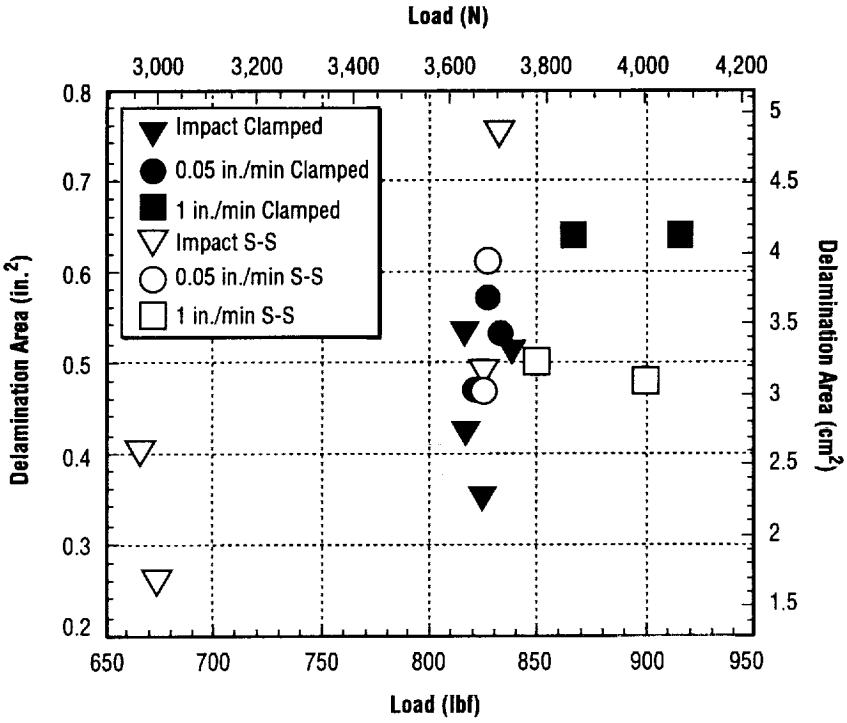

Figure 20. Delamination area versus maximum load for 16-ply specimens over 4-in. opening.

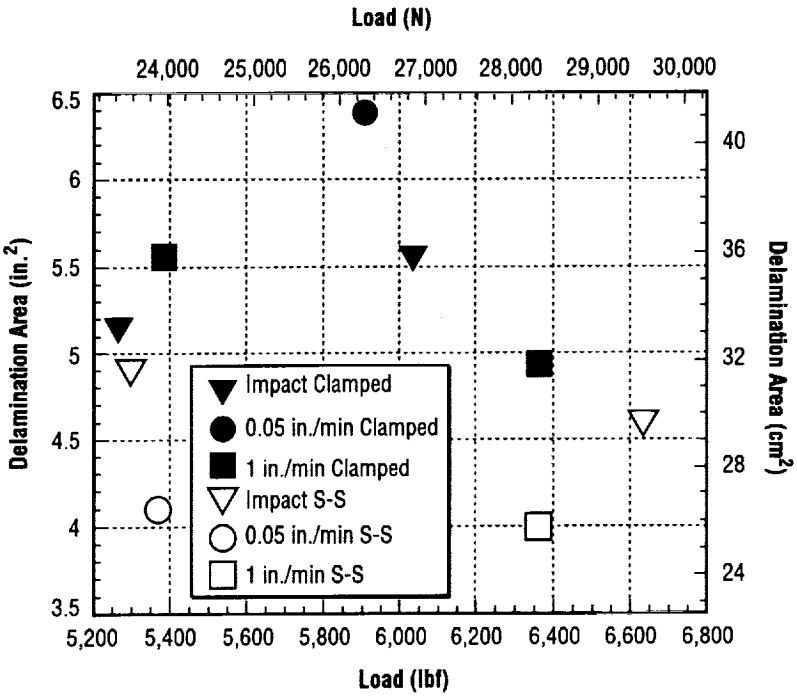

Figure 21. Delamination area versus maximum load for 48-ply specimens over 12-in. opening.

Figures 22–24 present data for the case of "stiff" laminates (support/thickness ratio of 25). The open symbols represent the simply supported boundary condition.

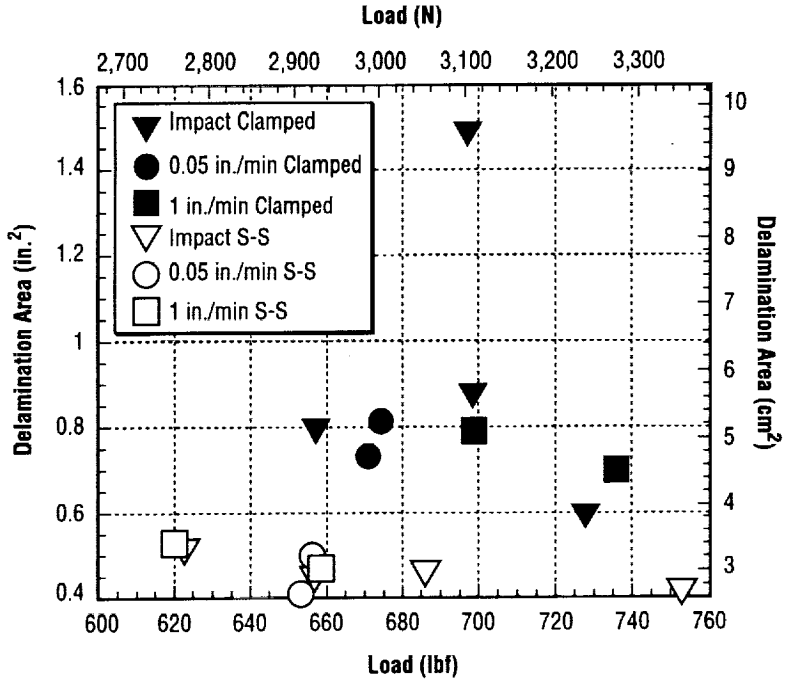

Figure 22. Delamination area versus maximum load for 16-ply specimens over 2-in. opening.

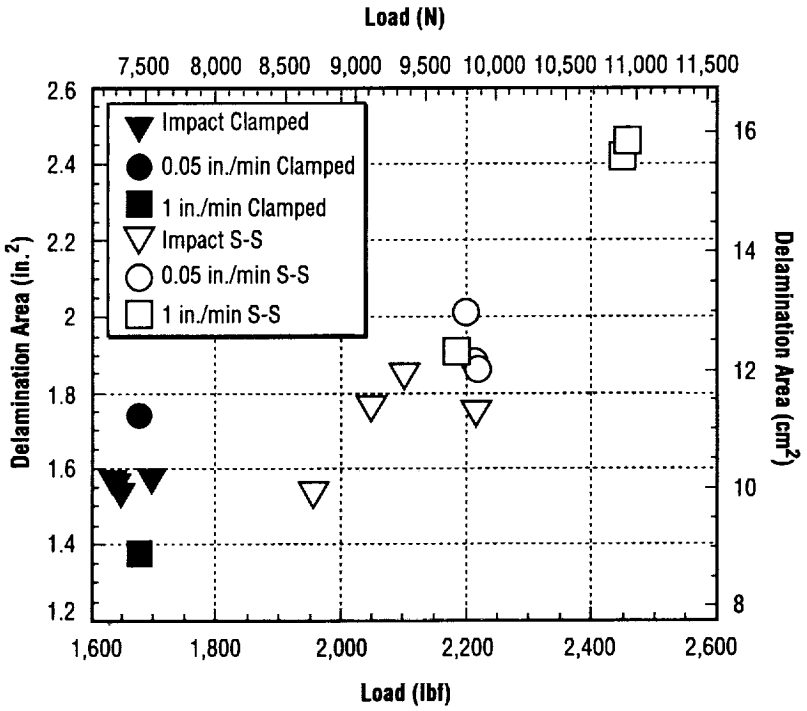

Figure 23. Delamination area versus maximum load for 32-ply specimens over 4-in. opening.

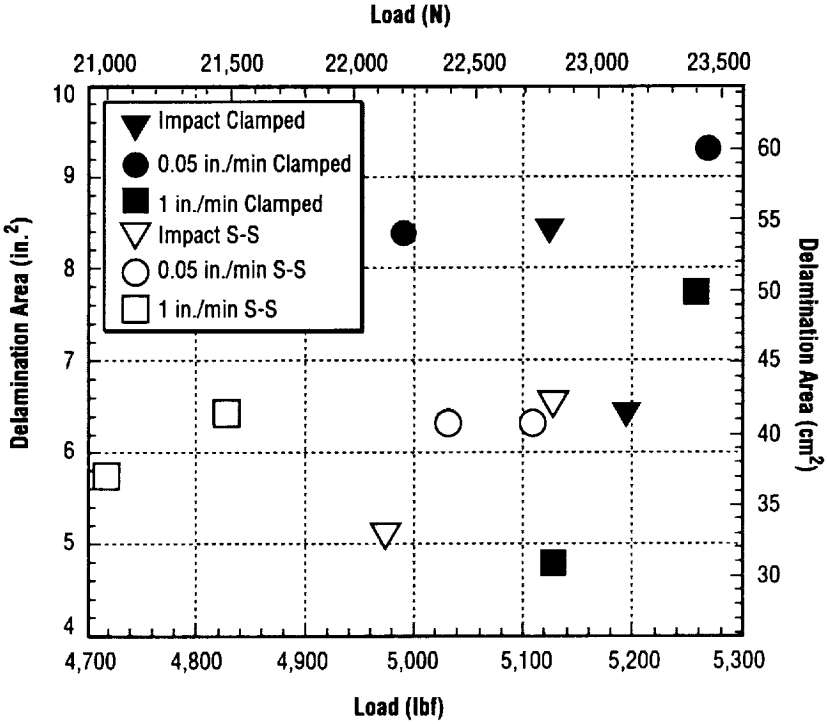

Figure 24. Delamination area versus maximum load for 48-ply specimens over 6-in. opening.

For the "flexible" laminates, there is no difference between the impacted specimens and those tested quasi-statically at either rate. The effects of the boundary conditions show no difference for the 8-ply specimens supported over the 6-in. opening, whereas a distinct difference is seen for the 16-ply specimens supported over the 12-in. opening. This difference is due to the clamped specimens being loaded to a higher level, resulting in a larger delamination area.

The "medium" specimens have no distinct trends between boundary conditions or rate of loading. The impact test results fall in well with the static indentation tests in figures 19–21. Boundary conditions also appear to have no effect on the maximum load versus delamination area.

Figures 22–24 represent the opposite extreme from the "flexible" specimens in that the contact damage is the dominant failure mode. Again, there is no discernable difference between impact and static indentation results. In figure 22, the simply supported specimens show slightly less damage for the same magnitude of maximum load than the clamped specimens; however, this difference is slight.

Overall, the low-velocity impact tests can be represented by static indentation testing at rates of 0.05 and 1 in. per minute, regardless of specimen rigidity and boundary conditions. There is enough inherent scatter in both types of tests that all data fall within this scatter. It must be kept in mind that these results are only valid for laminates of the $\pi/4$ type and laminates with different layups or clumped plies may yield different results.

Another check of the validity of using static indentation tests to represent impact tests, a comparison of the load/deflection data, can be made.

Figures 25–31 show static indentation load/deflection data superimposed over impact load/deflection data. The static data are represented by filled symbols, while the impact data are represented by open symbols. Static load/deflection data were not available for all of the static tests since a faulty LVDT was used; thus, only the valid data are presented.

On the loading portion of the curves, the data agree well. However, for the unloading portion of the curves, the impact data consistently indicate that more energy was lost during the event since there is a much larger hysteresis in the impact curves. However, from the delamination area data, it was anticipated that the energy lost should be about the same. It has always been suspected that most of the energy lost in this type of impact testing is lost due to vibrations within the impact apparatus, not in damage to the specimen. When the falling crosshead and tup impact the composite plate, the head will tend to rebound at an angle that is not parallel to the guideposts. Thus, a sideways force is exerted on the guideposts which causes them to vibrate and interfere with the "natural" rebound of the impactor.

Figures 25, 27, and 30 represent this erroneous "loss of energy" data quite well. Figure 25 is a flexible specimen and the loading portions of the curves agree well for both the static and impact cases. However, for unloading, the impact data show a much larger deflection than the static data for a given load on the rebound. Furthermore, the maximum displacement does not coincide with the maximum load, rather it is seen to occur during the unloading portion of the curve and is quite a bit larger than the displacement at the maximum load for two of the four impact specimens. Figures 27 and 30 also demonstrate this behavoir and are data for medium and stiff plates, respectfully, so this phenomena is not a function of how rigid the target is.

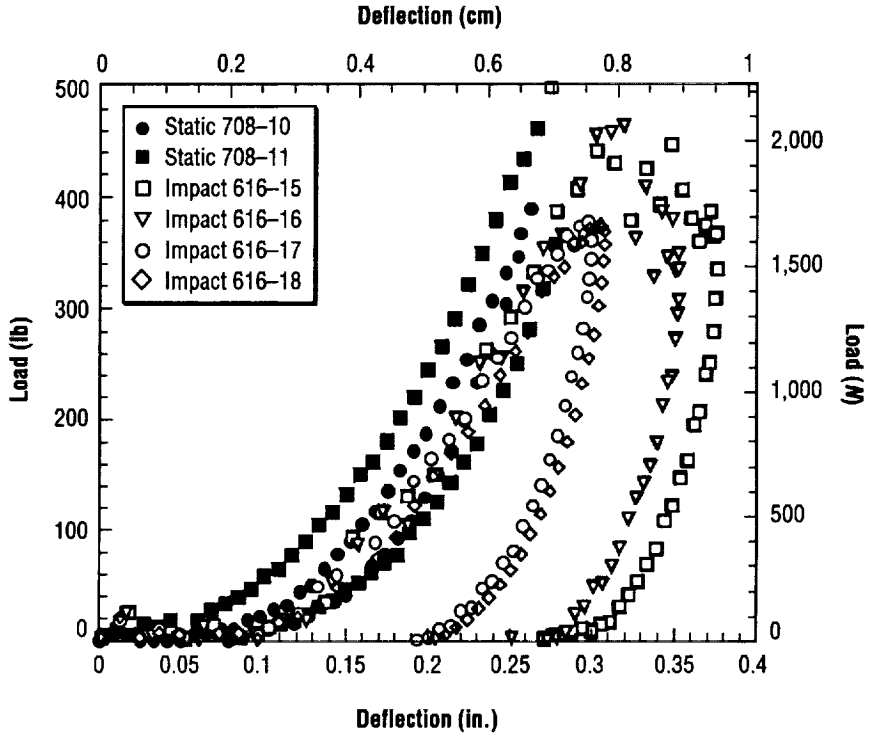

Figure 25. Static indentation data superimposed over impact data for 8-ply clamped specimens over a 6-in. opening.

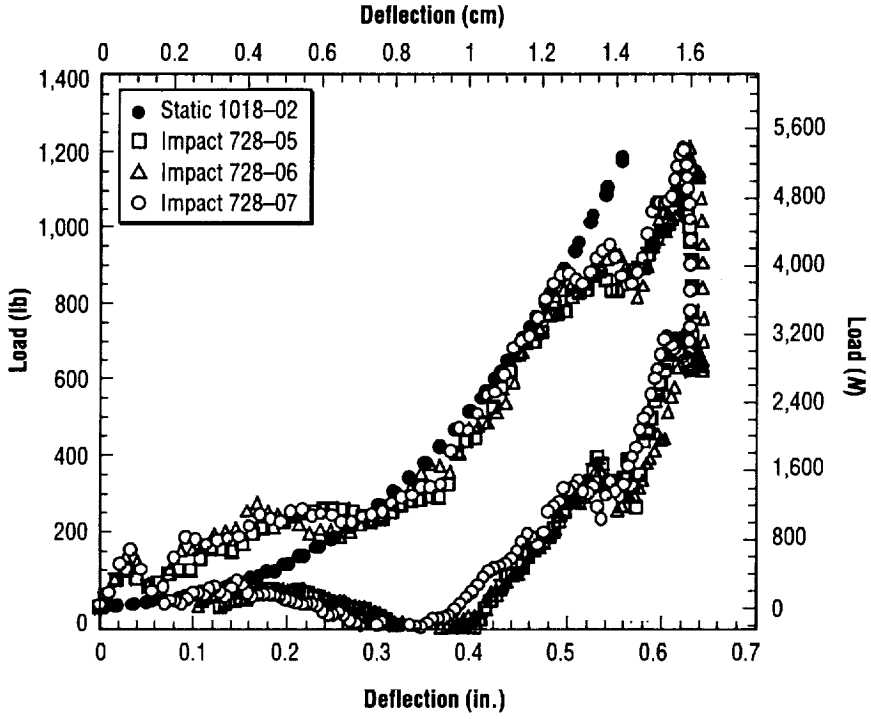

Figure 26. Static indentation data superimposed over impact data for 16-ply simply supported specimens over a 12-in. opening.

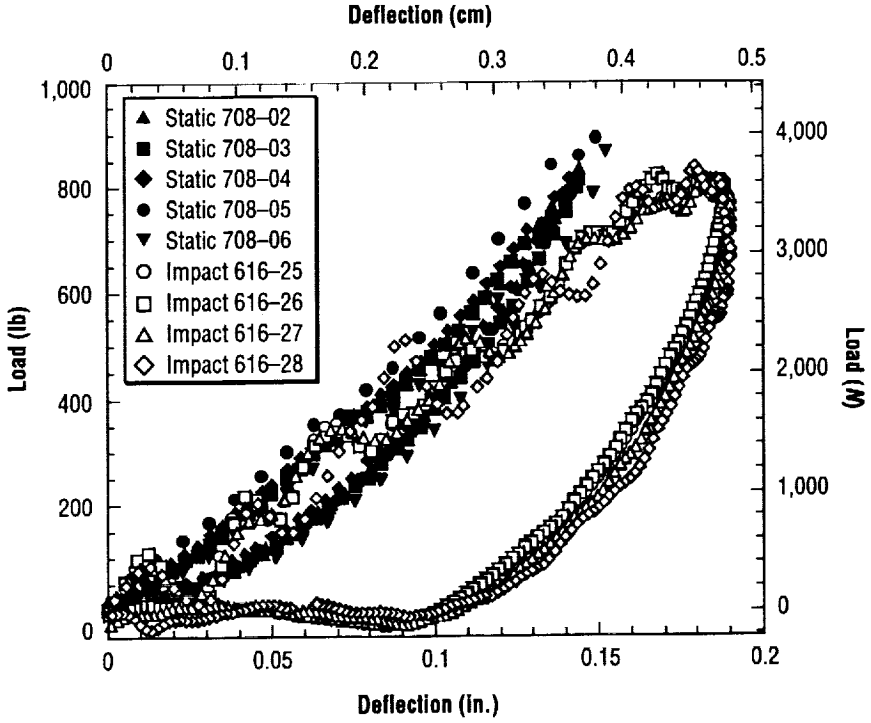

Figure 27. Static indentation data superimposed over impact data for 16-ply clamped specimens over a 4-in. opening.

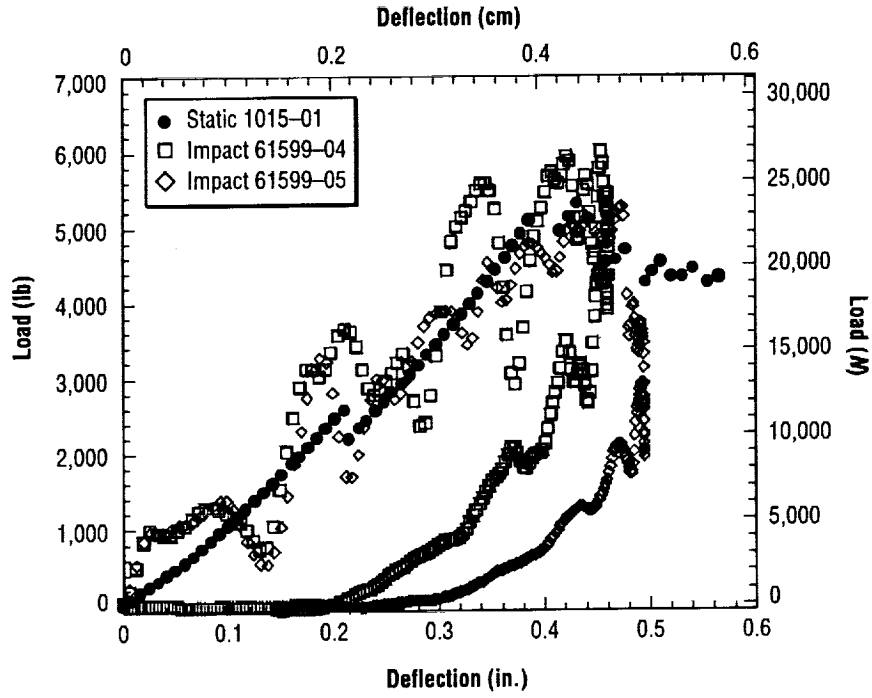

Figure 28. Static indentation data superimposed over impact data for 48-ply clamped specimens over a 12-in. opening.

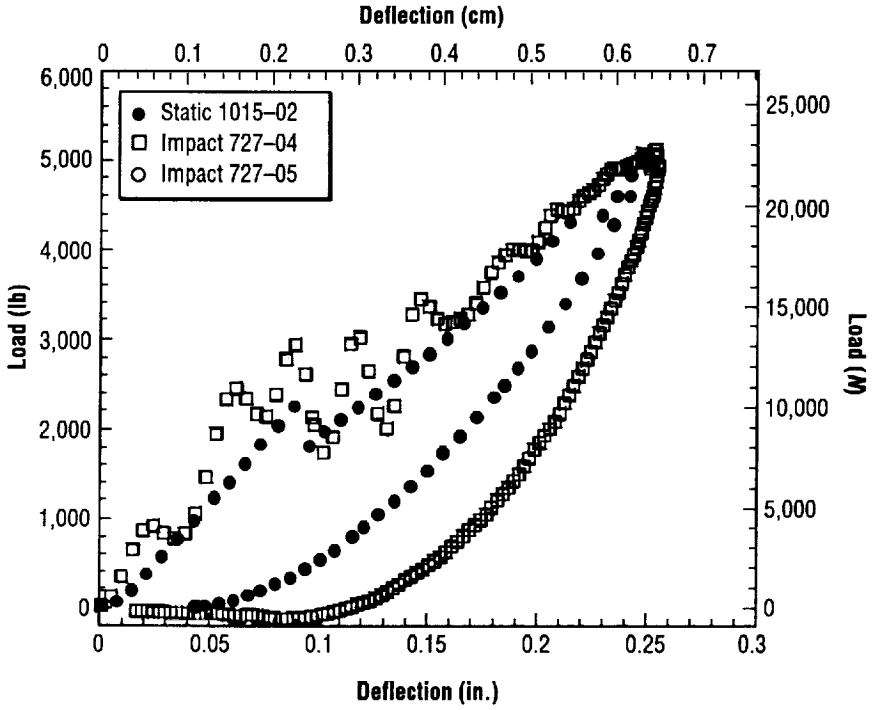

Figure 29. Static indentation data superimposed over impact data for 48-ply clamped specimens over a 6-in. opening.

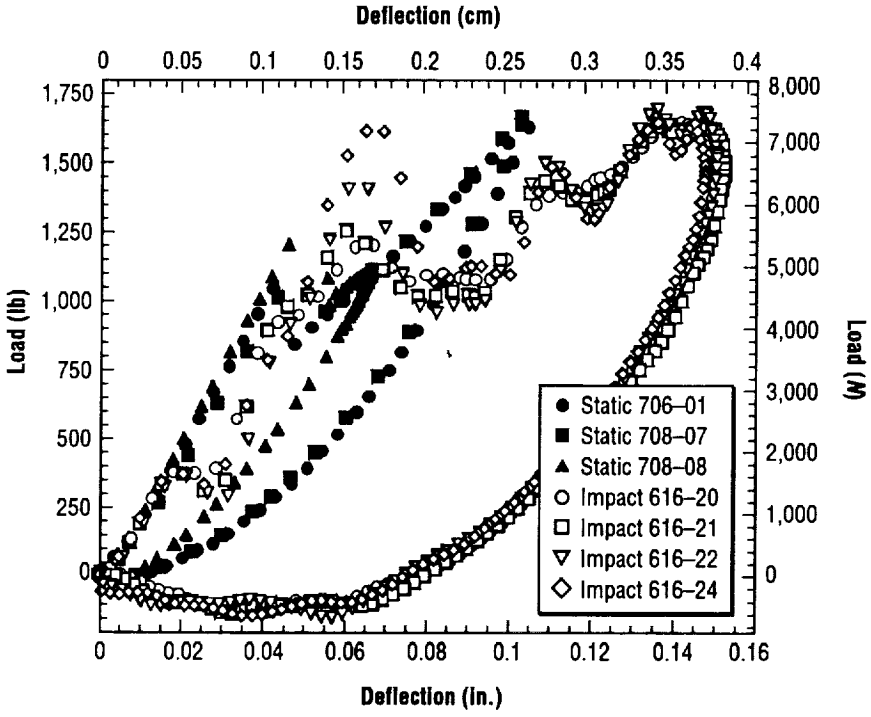

Figure 30. Static indentation data superimposed over impact data for 32-ply clamped specimens over a 4-in. opening.

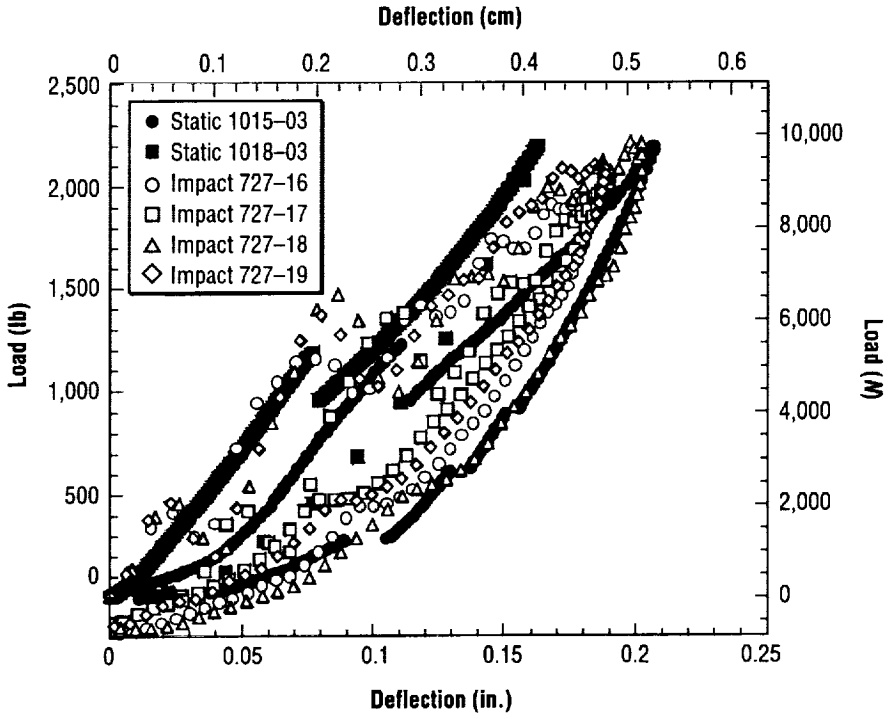

Figure 31. Static indentation data superimposed over impact data for 32-ply simply supported specimens over a 4-in.opening.

An argument may be made that this is due to the inertial effects of the plate, that after the "collision" of the impactor and plate, the plate continues to move downward due to its own inertia. This argument would indicate that heavier plates would show more difference in load/deflection data for static indentation and impact since heavier plates will have more inertia. However, figure 29 is a 48-ply plate over a 6-in. opening whereas figure 25 is an 8-ply plate over the same size opening, yet the lighter plate shows more of a difference.

Figure 26 does not have unloading data for the static case, but the loading portions of the curves agree quite well.

Figure 28 is unique in that during the static indentation test, the maximum load, as determined from the impact tests, could not be reached since the impactor began penetrating through the plate before this load was obtained.

5. CONCLUSIONS

Major conclusions of this study are as follows:

1. Static indentation tests can be used to represent low-velocity impact events when the damage is compared by maximum transverse force. This is true of plates that experience flexural-type damage, contact-type damage, and a combination of the two. Layups other than those of the $\pi/4$ type may not yield these same results.

2. Duration of an impact event is dependent upon the transverse stiffness of the plate. The stiffer the plate, the shorter the duration of impact. Boundary conditions have little effect on this behavior.

3. Much nonlinear behavior is observed in the load/deflection curves for flexible laminates. As the laminate becomes stiffer, more linearity is seen and a distinct drop in load due to delamination becomes more pronounced.

4. Load/deflection plots of static indentation and low-velocity impact are similar.

5. Dent depth results produce a great deal of scatter, which makes any conclusions concerning this parameter difficult.

APPENDEX A—IMPACT SPECIMEN IDENTIFICATION NUMBERS

Tables 9–14 show clamped and simply supported data for impact specimens.

Table 9. Clamped flex.

8 Ply on 6-in. Platen					
Specimen ID No.	Drop Height cm (in.)	Maximum Load N (lbf)	Impact Energy J (ft-lbf)	Impact Velocity m/sec (ft/sec)	Maximum Deflection cm (in.)
616–15f	30 (12)	1,930 (434)	7.5 (5.6)	2.42 (7.95)	No data
616–16f	25 (10)	2,148 (483)	6.4 (4.7)	2.22 (7.29)	0.90 (0.35)
616–17f	15 (6)	1,673 (376)	3.7 (2.8)	1.71 (5.60)	0.76 (0.30)
616–18f	15 (6)	1,668 (375)	3.8 (2.8)	1.71 (5.60)	0.78 (0.31)

16 Ply on 12-in. Platen					
Specimen ID No.	Drop Height cm (in.)	Maximum Load N (lbf)	Impact Energy J (ft-lbf)	Impact Velocity m/sec (ft/sec)	Maximum Deflection cm (in.)
616–01f	122 (48)	6,841 (1,538)	30.1 (22.2)	4.86 (15.94)	1.49 (0.59)
616–02f	122 (48)	6,921 (1,556)	29.7 (30.1)	4.82 (15.81)	1.49 (0.59)
616–03f	122 (48)	7,037 (1,582)	30.3 (22.3)	4.86 (15.96)	1.47 (0.58)
616–04f	122 (48)	7,108 (1,598)	30.3 (22.3)	4.87 (15.97)	1.44 (0.57)

Table 10. Clamped medium.

8 Ply on 2-in. Platen					
Specimen ID No.	Drop Height cm (in.)	Maximum Load N (lbf)	Impact Energy J (ft-lbf)	Impact Velocity m/sec (ft/sec)	Maximum Deflection cm (in.)
616–37m	12.7 (5)	1,045 (235)	3.3 (2.4)	2.10 (6.89)	0.31 (0.12)
616–38m	12.7 (5)	939 (211)	2.3 (1.7)	1.76 (5.78)	No data
728–09m	12.7 (5)	936 (210)	3.0 (2.2)	1.61 (5.28)	No data
728–11m	12.7 (5)	1,036 (233)	2.9 (2.1)	1.57 (5.14)	0.46 (0.18)

16 Ply on 4-in. Platen					
Specimen ID No.	Drop Height cm (in.)	Maximum Load N (lbf)	Impact Energy J (ft-lbf)	Impact Velocity m/sec (ft/sec)	Maximum Deflection cm (in.)
616–25m	35.6 (14)	3,634 (817)	8.6 (6.4)	2.61 (8.55)	0.48 (0.19)
616–26m	35.6 (14)	3,629 (816)	8.7 (6.4)	2.61 (8.57)	0.48 (0.19)
616–27m	35.6 (14)	3,665 (824)	8.7 (6.4)	2.61 (8.55)	0.48 (0.19)
616–28m	35.6 (14)	3,728 (838)	8.9 (6.5)	2.60 (8.53)	0.48 (0.19)

48 Ply on 12-in. Platen					
Specimen ID No.	Drop Height cm (in.)	Maximum Load N (lbf)	Impact Energy J (ft-lbf)	Impact Velocity m/sec (ft/sec)	Maximum Deflection cm (in.)
61599–04m	119 (47)	26,823 (6,030)	155 (115)	4.71 (15.46)	1.26 (0.50)
61599–05m	119 (47)	23,420 (5,265)	157 (115)	4.73 (15.52)	1.17 (0.46)

Table 11. Clamped stiff.

16 Ply on 2-in. Platen					
Specimen ID No.	Drop Height cm (in.)	Maximum Load N (lbf)	Impact Energy J (ft-lbf)	Impact Velocity m/sec (ft/sec)	Maximum Deflection cm (in.)
616–29s	34.3 (13.5)	3,239 (728)	8.4 (6.2)	2.57 (8.43)	0.43 (0.17)
616–30s	26.7 (10.5)	2,922 (657)	6.4 (4.7)	2.23 (7.33)	0.34 (0.13)
616–31s	33.0 (13.0)	3,105 (698)	8.1 (6.0)	2.52 (8.27)	0.42 (0.17)
616–32s	33.0 (13.0)	3,100 (697)	8.0 (5.9)	2.51 (8.24)	0.41 (0.16)

32 Ply on 4-in. Platen					
Specimen ID No.	Drop Height cm (in.)	Maximum Load N (lbf)	Impact Energy J (ft-lbf)	Impact Velocity m/sec (ft/sec)	Maximum Deflection cm (in.)
616–20s	71.1 (28)	7,313 (1,644)	17.2 (12.7)	3.67 (12.05)	0.38 (0.15)
616–21s	71.1 (28)	7,268 (1,634)	17.4 (12.8)	3.69 (12.12)	0.39 (0.15)
616–22s	71.1 (28)	7,544 (1,696)	17.1 (12.6)	3.66 (12.00)	0.38 (0.15)
616–24s	71.1 (28)	7,322 (1,646)	17.5 (12.9)	3.70 (12.14)	No Data

48 Ply on 6-in. Platen					
Specimen ID No.	Drop Height cm (in.)	Maximum Load N (lbf)	Impact Energy J (ft-lbf)	Impact Velocity m/sec (ft/sec)	Maximum Deflection cm (in.)
727–04s	63.5 (25)	22,788 (5,123)	80.7 (59.5)	3.40 (11.15)	0.65 (0.26)
727–05s	63.5 (25)	23,100 (5,193)	80.7 (59.5)	3.40 (11.15)	0.64 (0.25)

Table 12. Simply supported flex.

8 Ply on 6-in. Platen					
Specimen ID No.	Drop Height cm (in.)	Maximum Load N (lbf)	Impact Energy J (ft-lbf)	Impact Velocity m/sec (ft/sec)	Maximum Deflection cm (in.)
727-06f	44.4 (17.5)	1,850 (416)	10.2 (7.5)	2.9 (9.6)	No data
727-07f	44.4 (17.5)	1,766 (397)	9.6 (7.1)	2.9 (9.3)	1.18 (0.47)
727-08f	44.4 (17.5)	1,850 (416)	10.2 (7.5)	2.9 (9.6)	1.23 (0.48)
727-09f	44.4 (17.5)	1,873 (421)	10.1 (7.5)	2.9 (9.6)	1.34 (0.53)
727-10f	44.4 (17.5)	1,873 (421)	9.7 (7.1)	2.9 (9.4)	1.24 (0.49)

16 Ply on 12-in. Platen					
Specimen ID No.	Drop Height cm (in.)	Maximum Load N (lbf)	Impact Energy J (ft-lbf)	Impact Velocity m/sec (ft/sec)	Maximum Deflection cm (in.)
728-05f	132 (52.0)	4,862 (1,093)	29.7 (21.9)	4.8 (15.8)	1.61 (0.63)
728-06f	149 (58.5)	5,400 (1,214)	32.2 (23.8)	5.0 (16.5)	1.64 (0.64)
728-07f	149 (58.5)	5,373 (1,208)	31.6 (23.3)	5.0 (16.3)	No data

Table 13. Simply supported medium.

8 Ply on 2-in. Platen					
Specimen ID No.	Drop Height cm (in.)	Maximum Load N (lbf)	Impact Energy J (ft-lbf)	Impact Velocity m/sec (ft/sec)	Maximum Deflection cm (in.)
728–02m	7.6 (3.0)	1,023 (230)	1.8 (1.3)	1.23 (4.04)	0.29 (0.11)
728–03m	5.7 (2.3)	974 (219)	1.3 (0.9)	1.03 (3.38)	0.23 (0.09)
728–04m	4.5 (1.8)	907 (204)	1.1 (0.8)	0.96 (3.16)	No data

16 Ply on 4-in. Platen					
Specimen ID No.	Drop Height cm (in.)	Maximum Load N (lbf)	Impact Energy J (ft-lbf)	Impact Velocity m/sec (ft/sec)	Maximum Deflection cm (in.)
727–11m	49.5 (19.5)	3,723 (837)	11.9 (8.8)	3.18 (10.43)	0.63 (0.25)
727–12m	46.4 (18.3)	3,701 (832)	10.6 (7.8)	2.30 (9.83)	0.58 (0.23)
727–13m	39.4 (15.5)	3,670 (825)	8.3 (6.1)	2.65 (8.71)	0.52 (0.20)
727–14m	24.1 (9.5)	2,998 (674)	5.6 (4.1)	2.18 (7.15)	0.44 (0.17)
727–15m	24.1 (9.5)	2,963 (666)	5.3 (3.9)	2.13 (6.99)	0.34 (0.17)

48 Ply on 12-in. Platen					
Specimen ID No.	Drop Height cm (in.)	Maximum Load N (lbf)	Impact Energy J (ft-lbf)	Impact Velocity m/sec (ft/sec)	Maximum Deflection cm (in.)
61599–02m	119 (47)	23,562 (5,297)	158 (116)	4.75 (15.57)	1.42 (0.56)
61599–03m	119 (47)	29,492 (6,630)	159 (116)	4.75 (15.58)	1.42 (0.56)

Table 14. Simply supported stiff.

16 Ply on 2-in. Platen					
Specimen ID No.	Drop Height cm (in.)	Maximum Load N (lbf)	Impact Energy J (ft-lbf)	Impact Velocity m/sec (ft/sec)	Maximum Deflection cm (in.)
727–20s	52.7 (20.8)	2,922 (657)	4.5 (3.3)	1.95 (6.40)	0.28 (0.11)
727–21s	20.3 (8.0)	2,771 (623)	4.5 (3.3)	1.96 (6.42)	0.28 (0.11)
727–22s	16.5 (6.5)	3,350 (753)	3.9 (2.8)	1.81 (5.95)	0.27 (0.11)
728–01s	16.5 (6.5)	3,051 (686)	3.9 (2.9)	1.82 (5.97)	0.27 (0.10)

32 Ply on 4-in. Platen					
Specimen ID No.	Drop Height cm (in.)	Maximum Load N (lbf)	Impact Energy J (ft-lbf)	Impact Velocity m/sec (ft/sec)	Maximum Deflection cm (in.)
727–16s	104 (41.0)	8,696 (1,955)	22.2 (12.7)	4.35 (14.27)	0.46 (0.18)
727–17s	112 (44.3)	9,101 (2,047)	24.0 (12.8)	4.52 (14.82)	0.48 (0.19)
727–18s	125 (49.0)	9,853 (2,215)	27.1 (12.6)	4.80 (15.74)	0.51 (0.20)
727–19s	125 (49.0)	9,346 (2,101)	24.1 (12.9)	4.53 (14.86)	0.48 (0.19)

48 Ply on 6-in. Platen					
Specimen ID No.	Drop Height cm (in.)	Maximum Load N (lbf)	Impact Energy J (ft-lbf)	Impact Velocity m/sec (ft/sec)	Maximum Deflection cm (in.)
727–02s	63.2 (24.9)	22,121 (4,973)	79.2 (58.4)	3.36 (11.04)	0.70 (0.27)
727–03s	63.2 (24.9)	22,810 (5,128)	82.6 (60.9)	3.39 (11.12)	No data

APPENDIX B—LOAD VERSUS DEFLECTION PLOTS FOR IMPACT SPECIMENS

Impact specimen load versus deflection plots are displayed in figures 32–82.

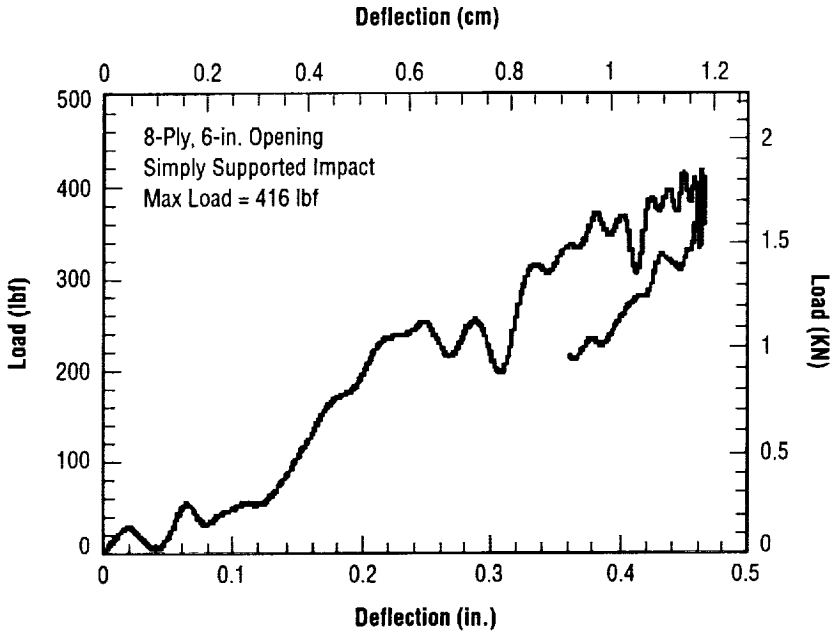

Figure 32. Load versus deflection specimen 727–06f.

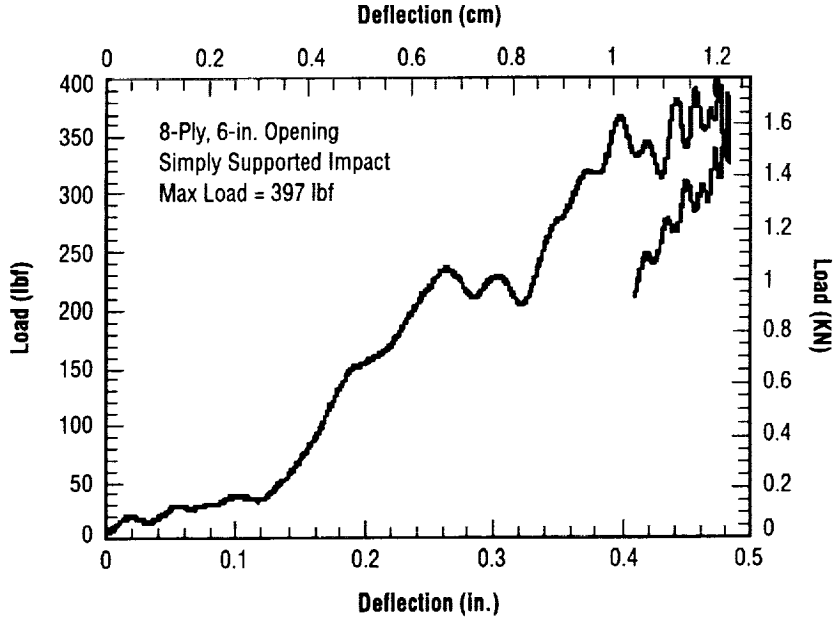

Figure 33. Load versus deflection specimen 727–07f.

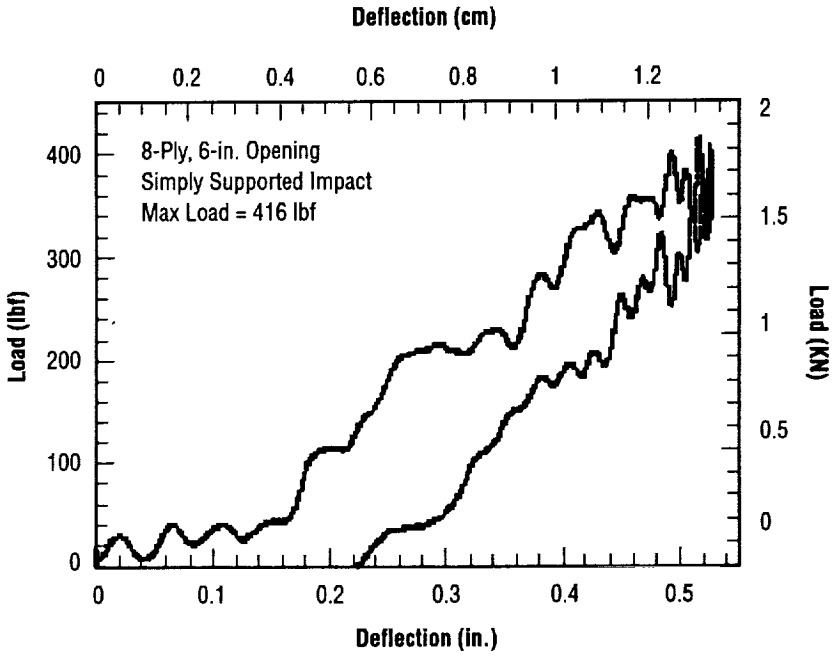

Figure 34. Load versus deflection specimen 727–08f.

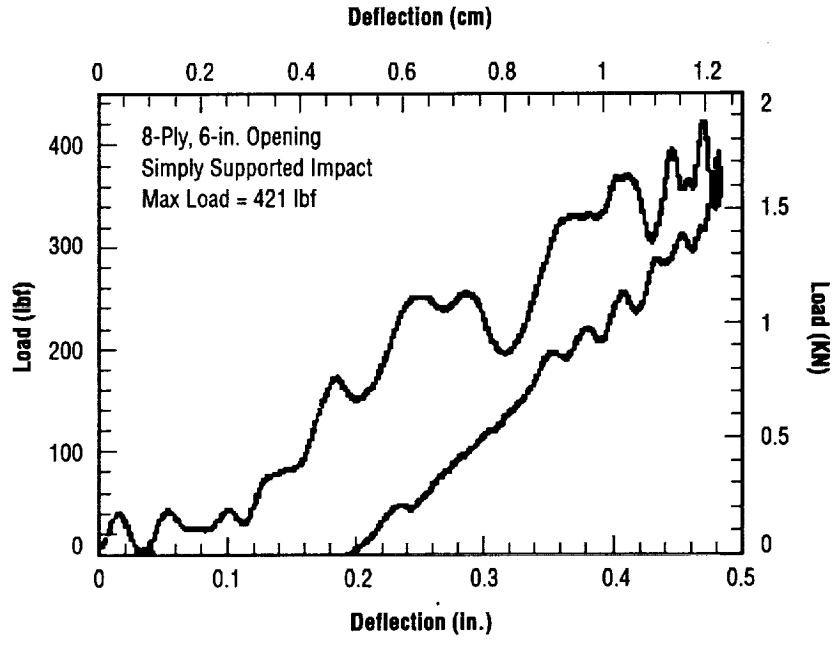

Figure 35. Load versus deflection specimen 727–09f.

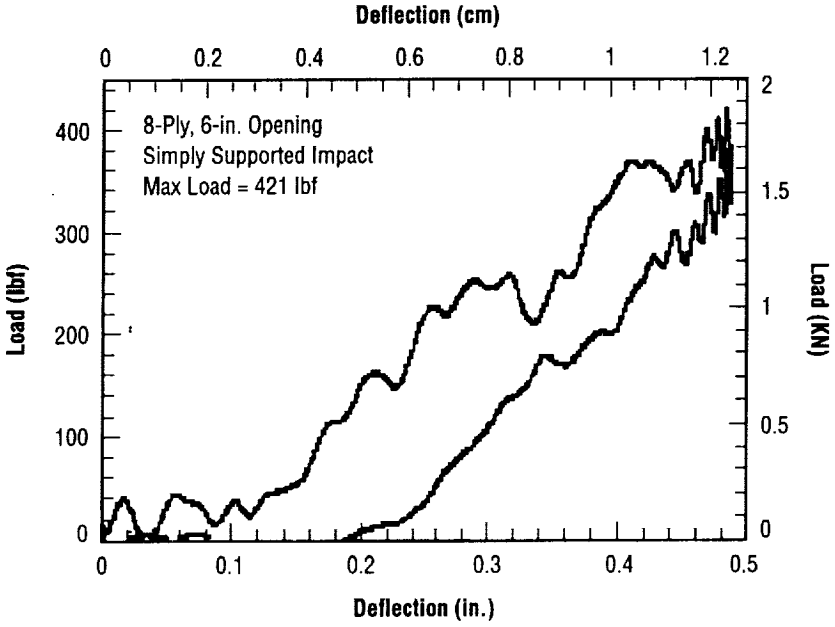

Figure 36. Load versus deflection specimen 727–10f.

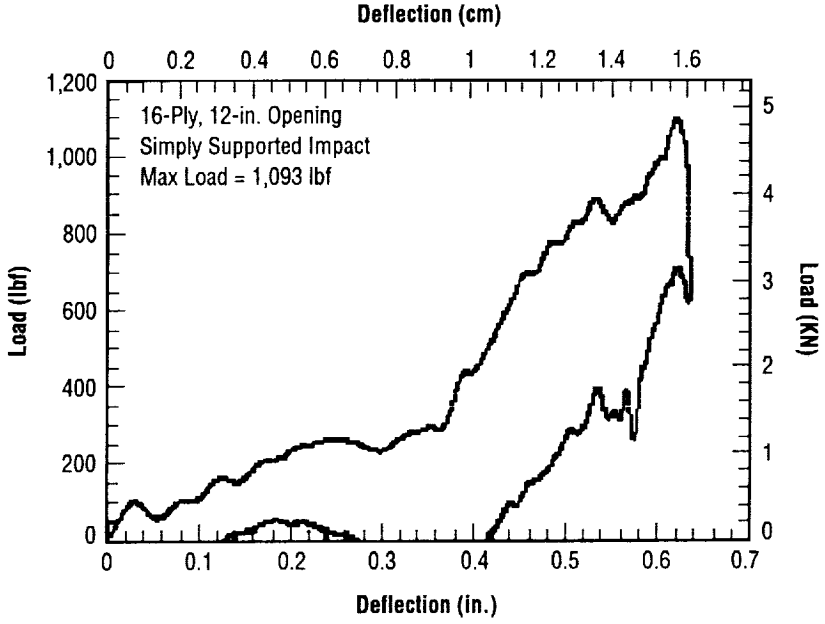

Figure 37. Load versus deflection specimen 728–05f.

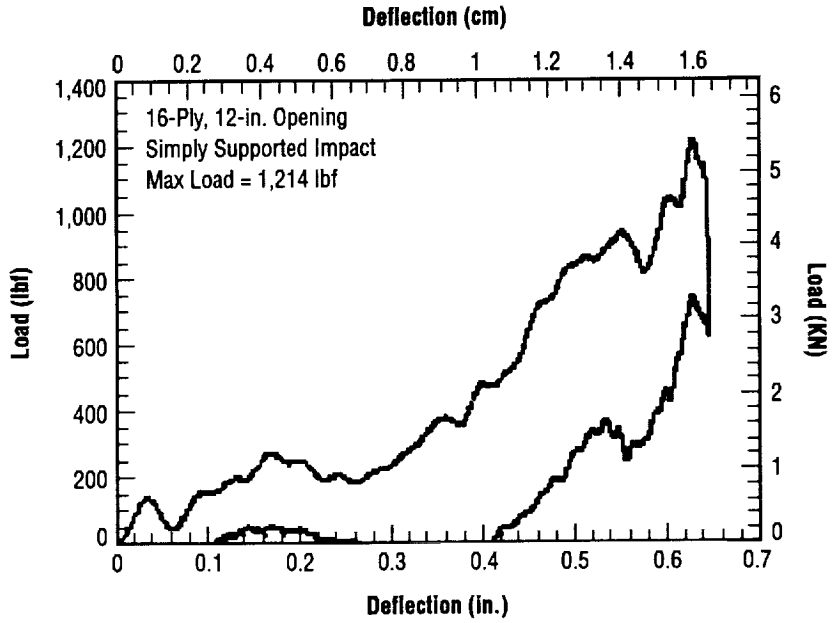

Figure 38. Load versus deflection specimen 728–06f.

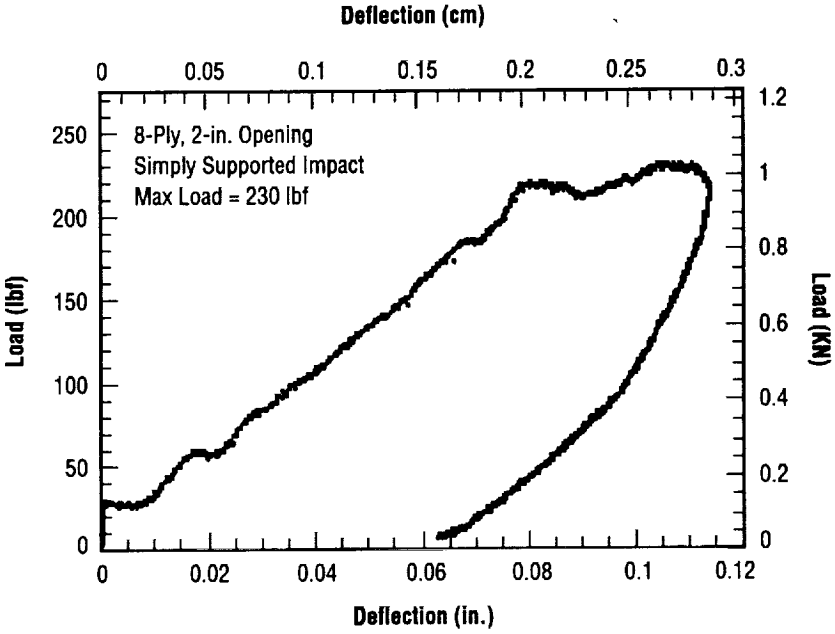

Figure 39. Load versus deflection specimen 728–02m.

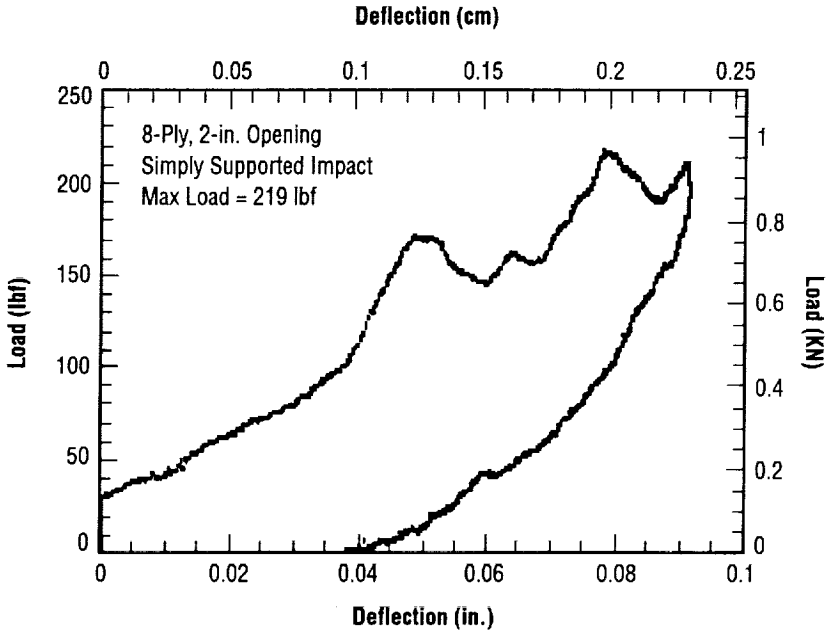

Figure 40. Load versus deflection specimen 728–03m.

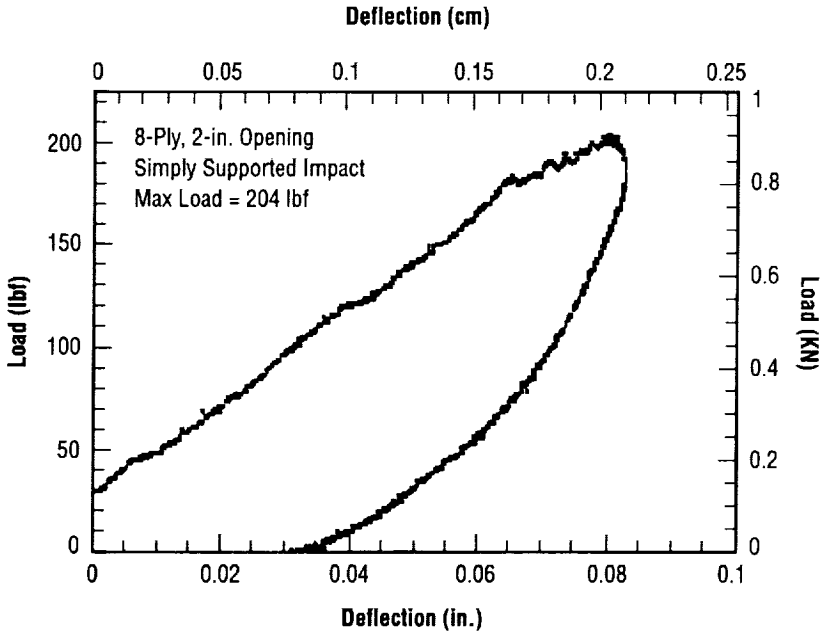

Figure 41. Load versus deflection specimen 728–04m.

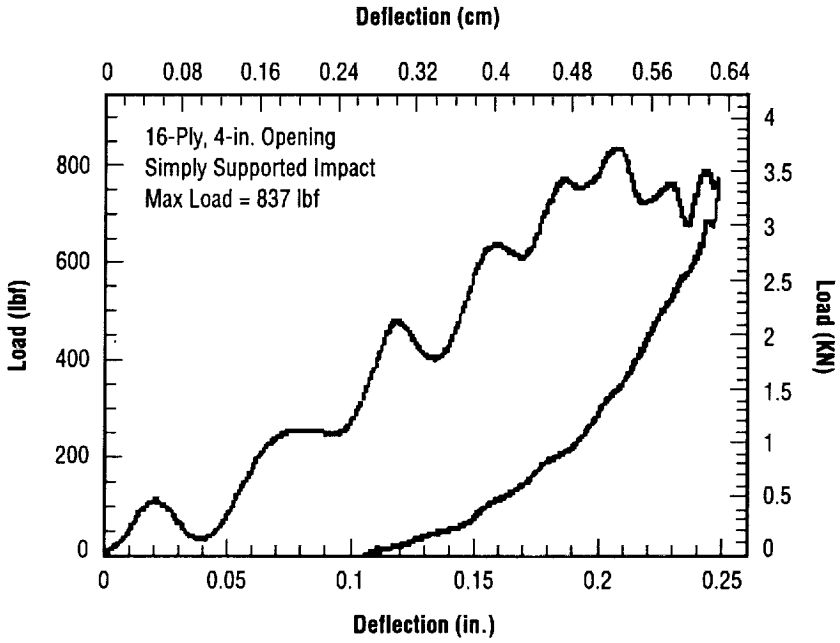

Figure 42. Load versus deflection specimen 727–11m.

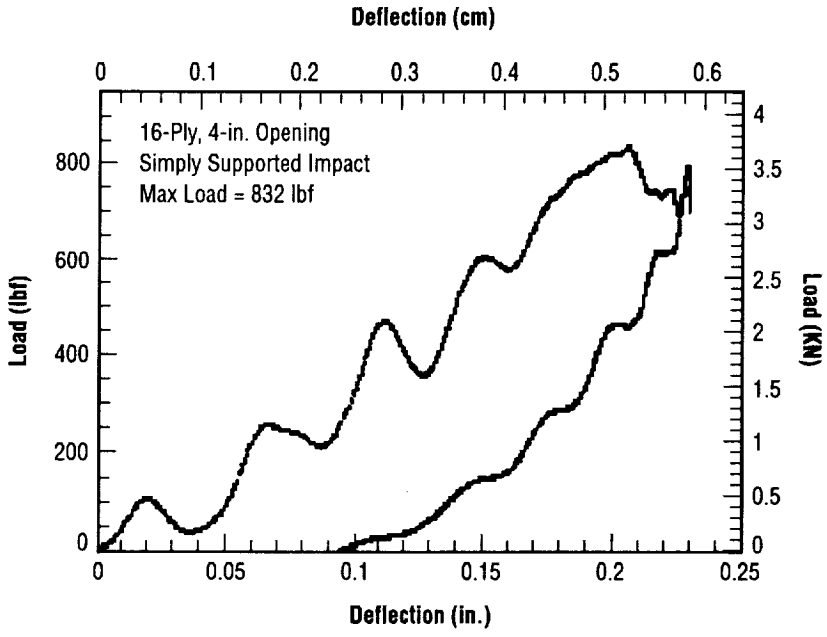

Figure 43. Load versus deflection specimen 727–12m.

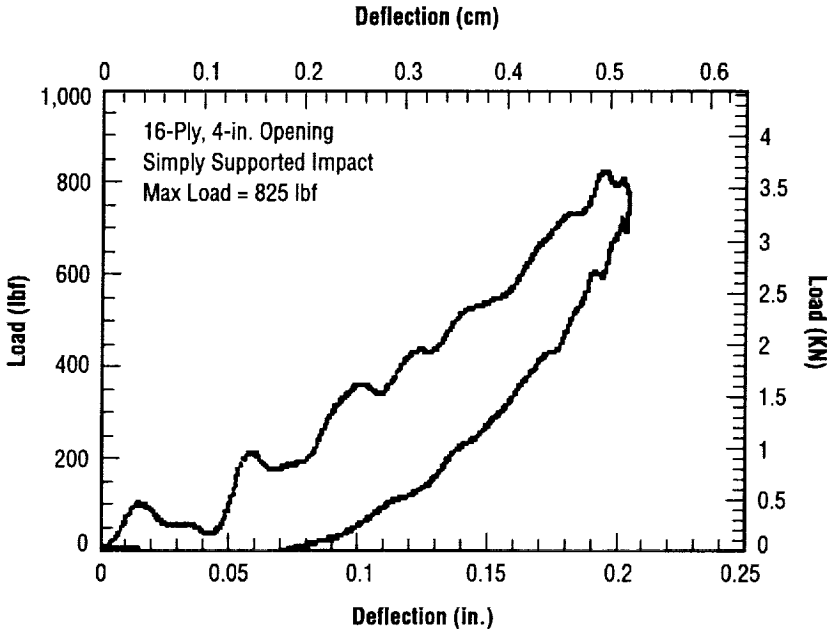

Figure 44. Load versus deflection specimen 727–13m.

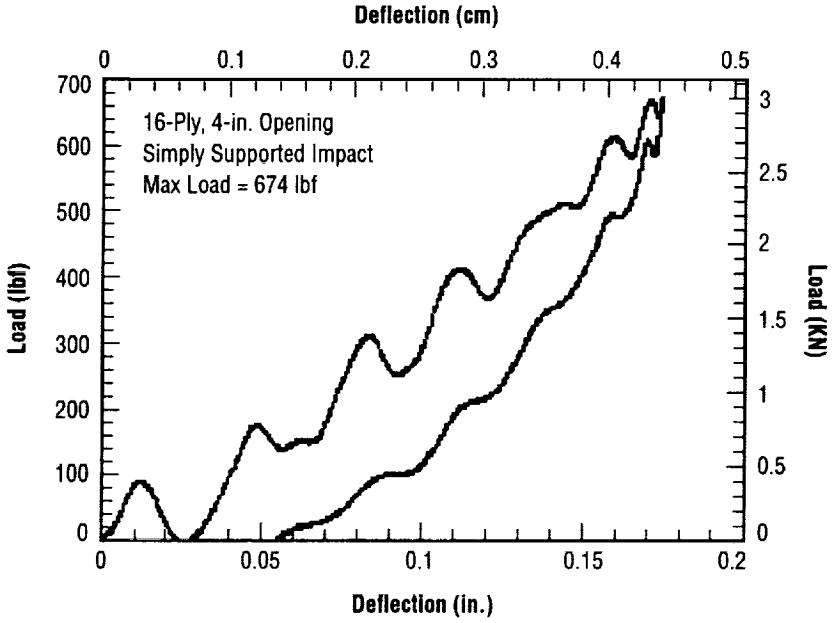

Figure 45. Load versus deflection specimen 727–14m.

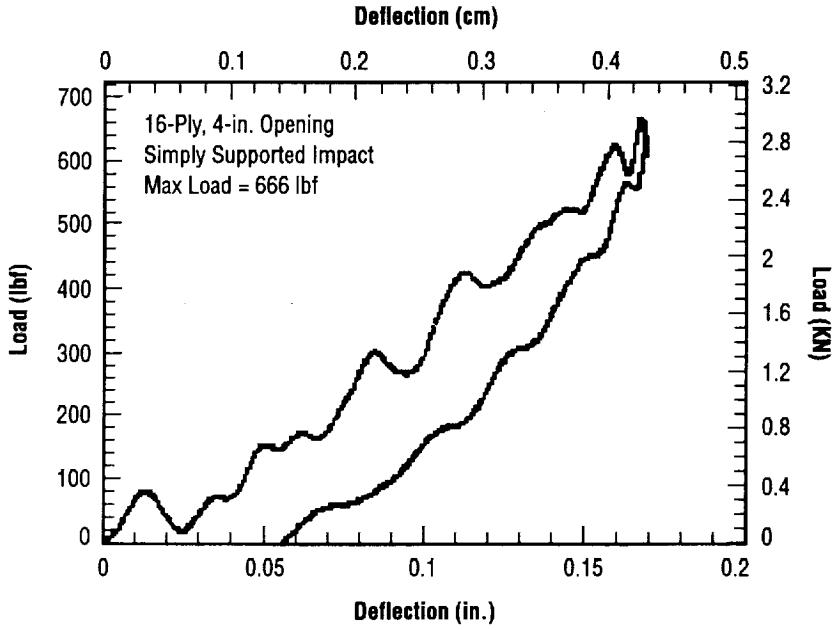

Figure 46. Load versus deflection specimen 727–15m.

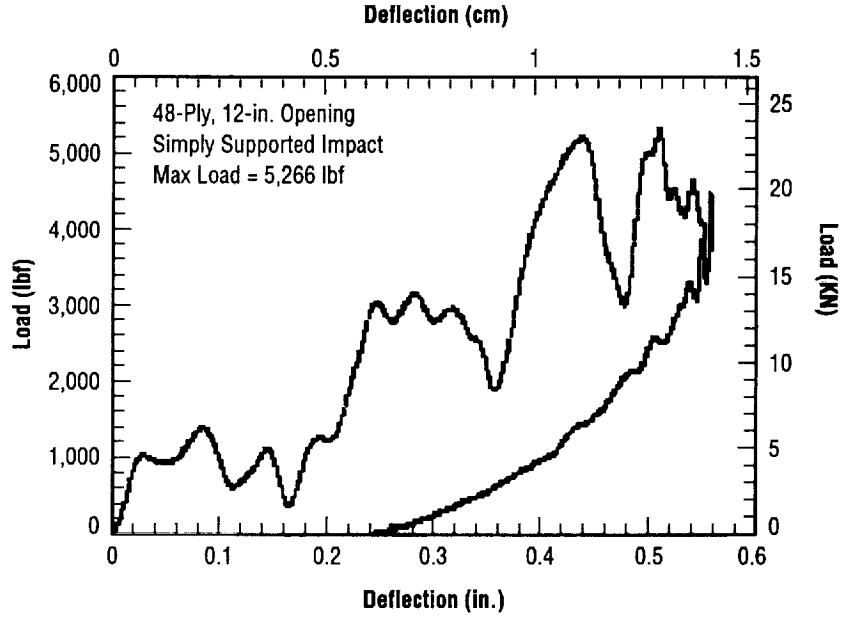

Figure 47. Load versus deflection specimen 61599–02m.

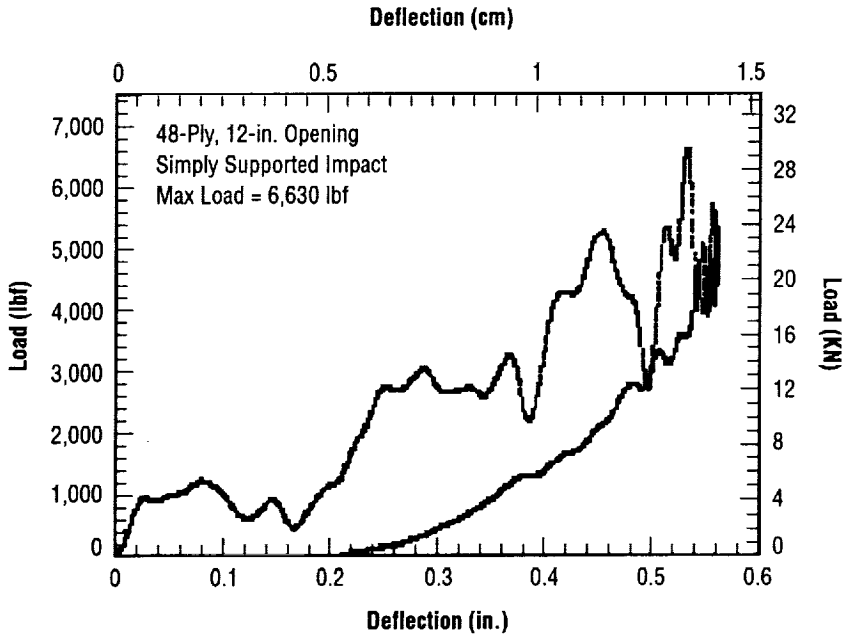

Figure 48. Load versus deflection specimen 61599–03m.

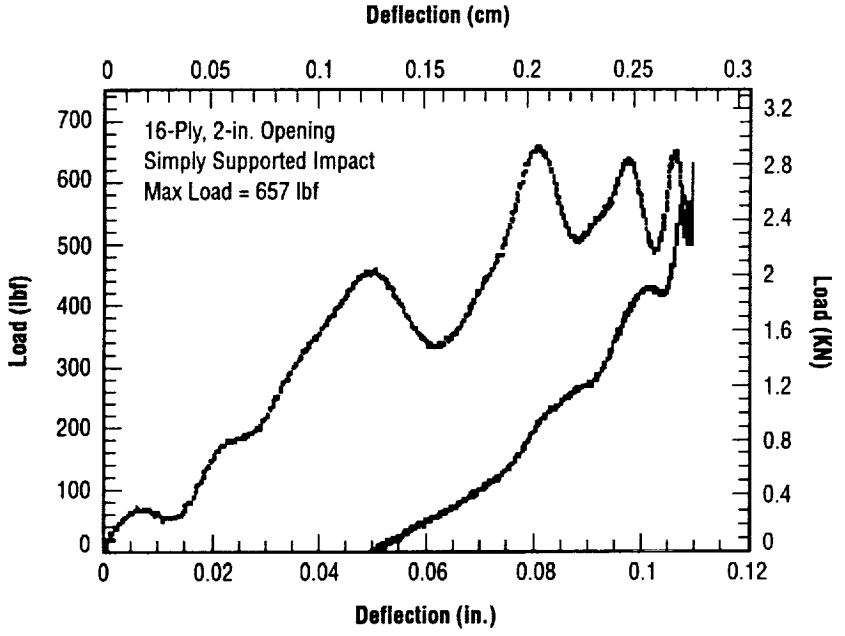

Figure 49. Load versus deflection specimen 727–20s.

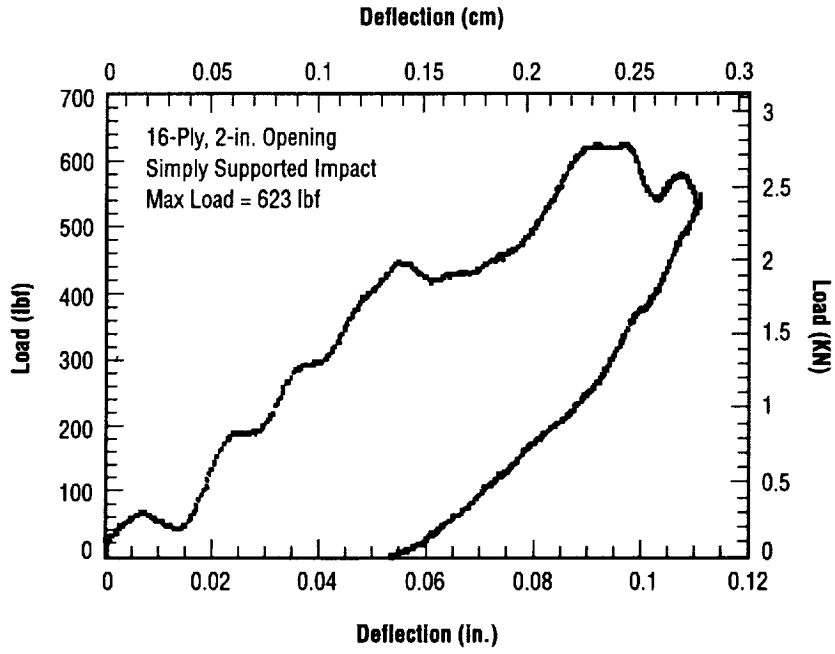

Figure 50. Load versus deflection specimen 727–21s.

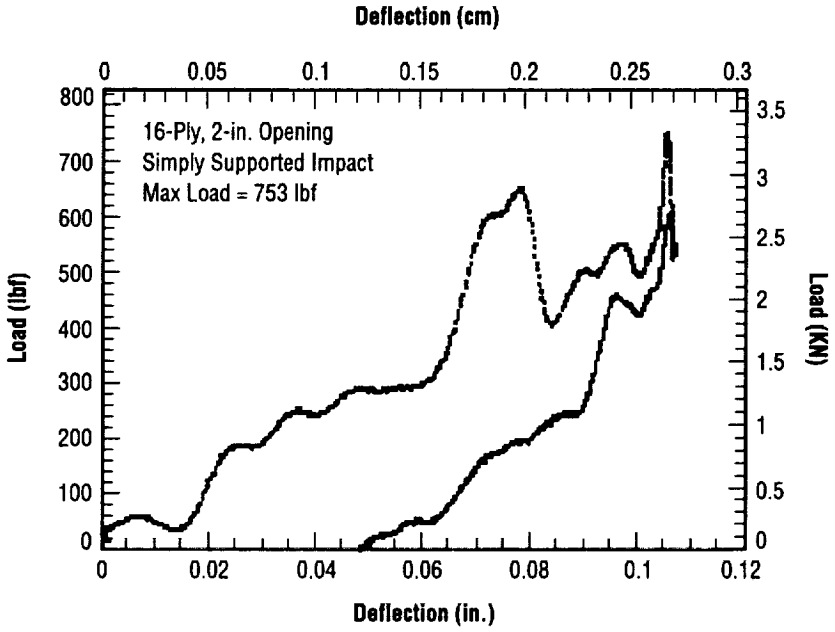

Figure 51. Load versus deflection specimen 727–22s.

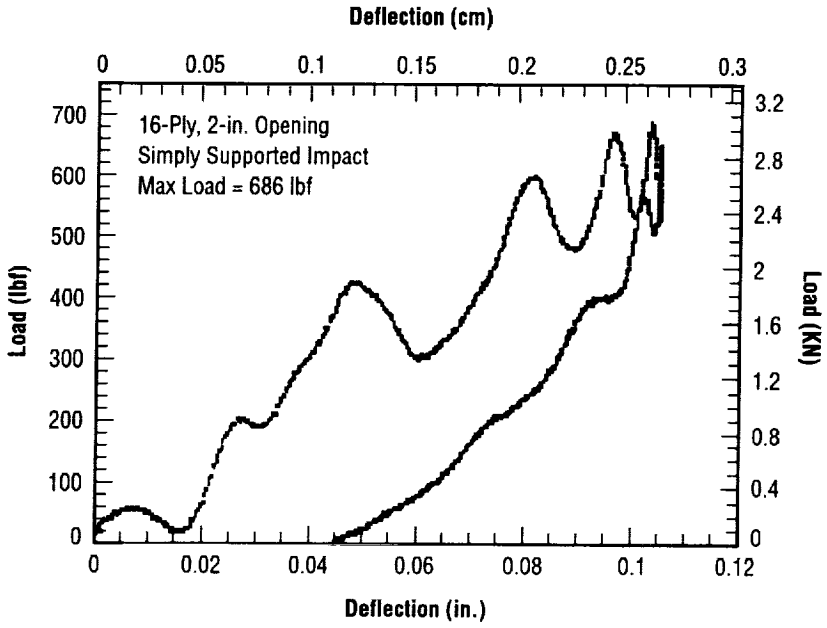

Figure 52. Load versus deflection specimen 728–01s.

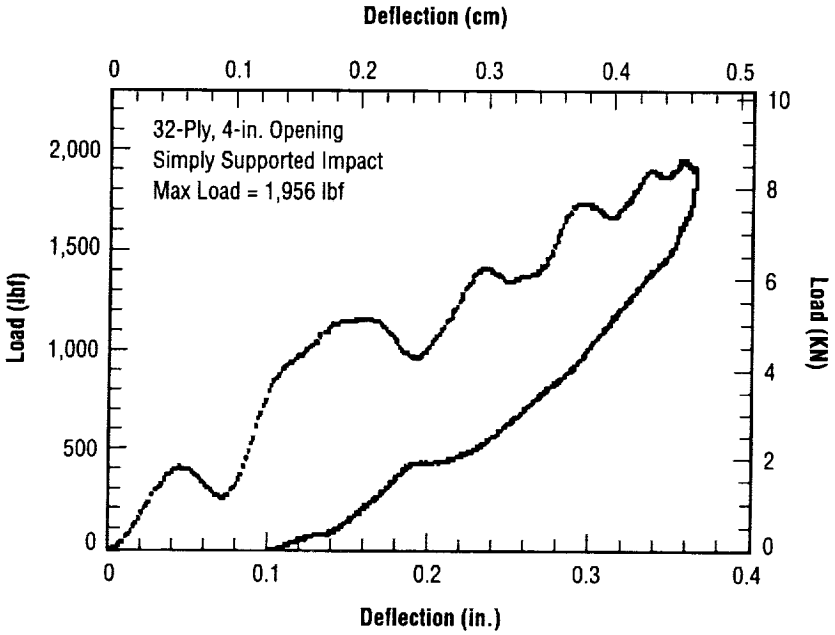

Figure 53. Load versus deflection specimen 727–16s.

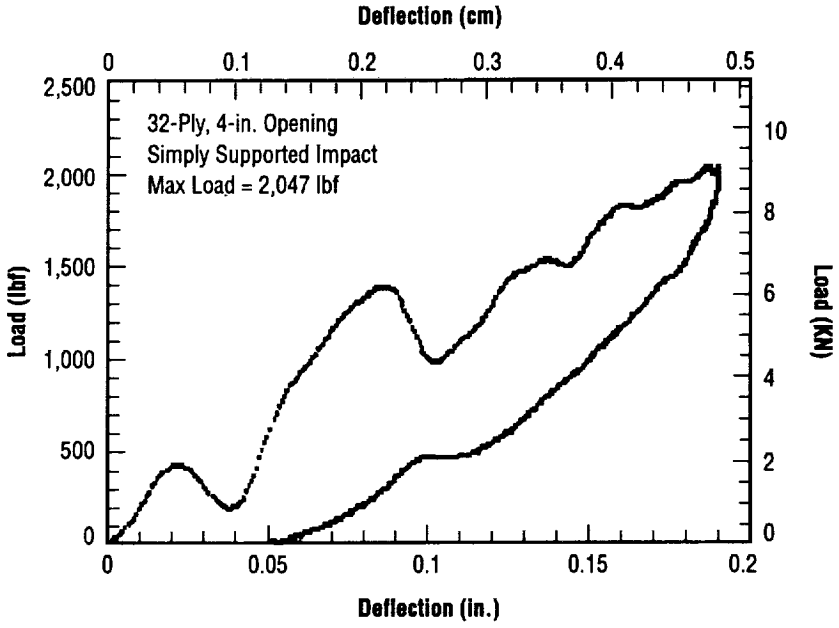

Figure 54. Load versus deflection specimen 727–17s.

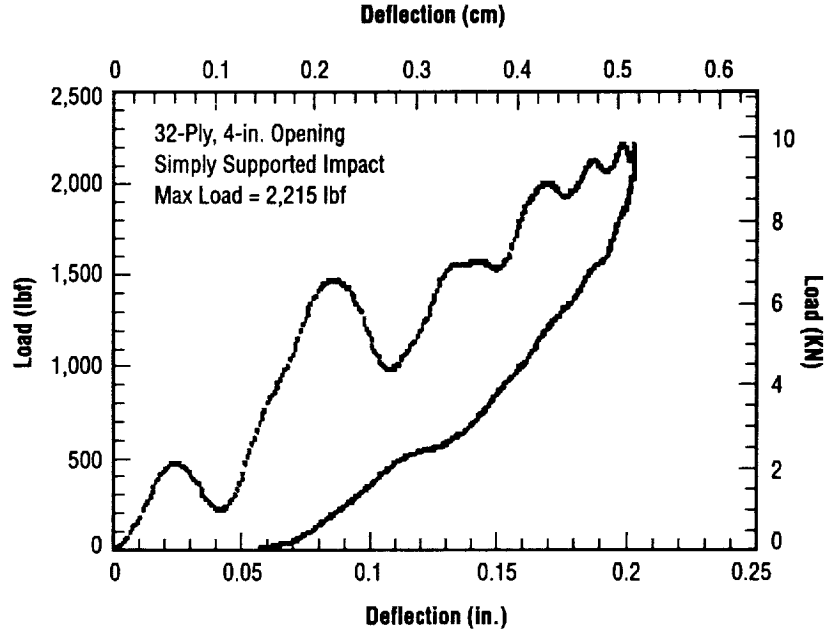

Figure 55. Load versus deflection specimen 727–18s.

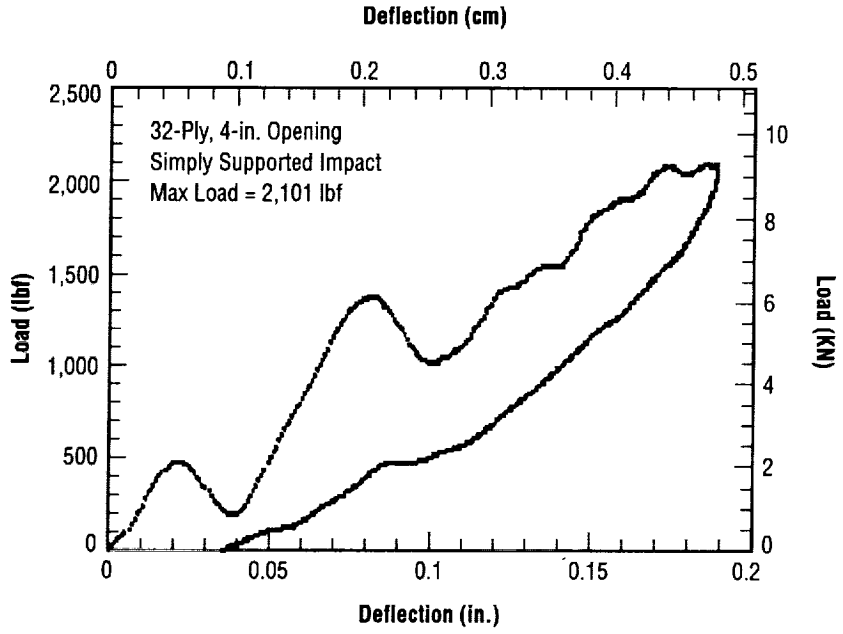

Figure 56. Load versus deflection specimen 727–19s.

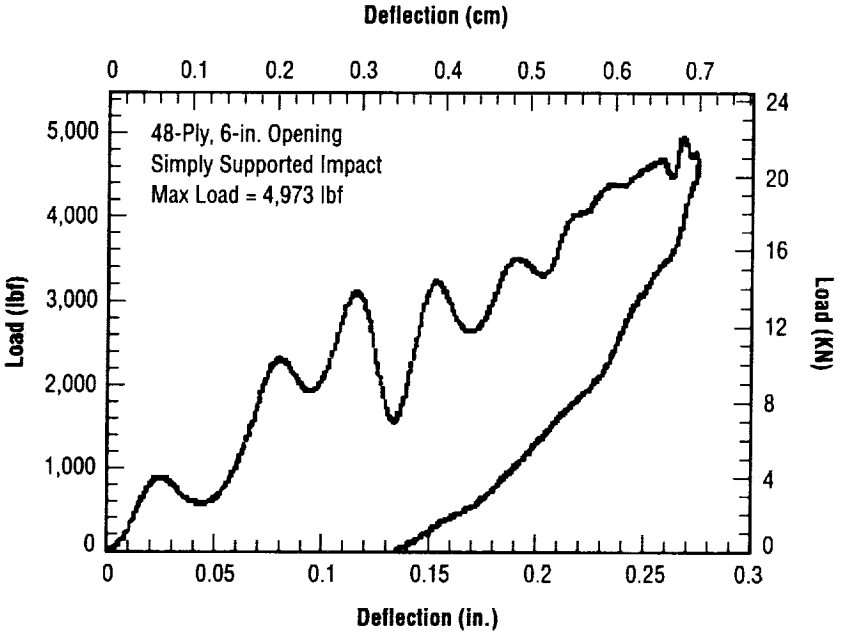

Figure 57. Load versus deflection specimen 727–02s.

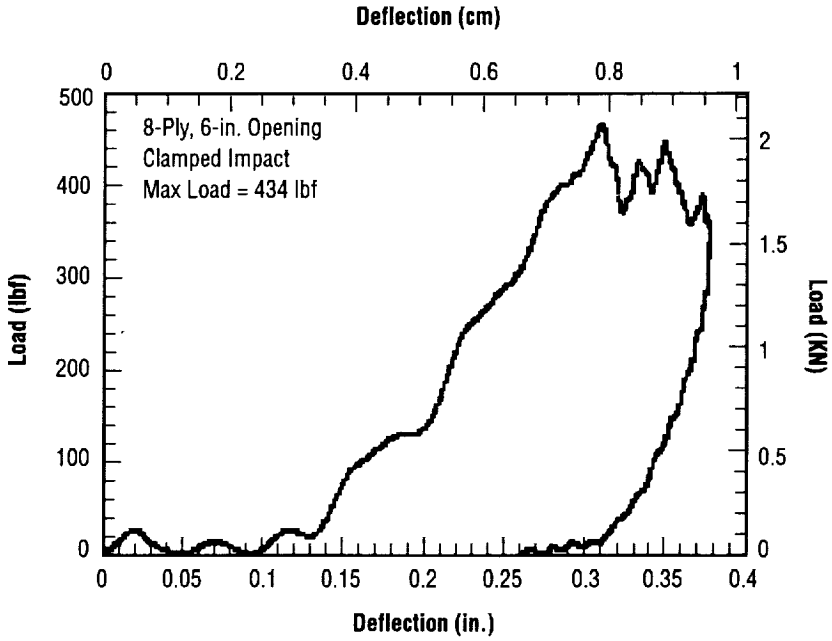

Figure 58. Load versus deflection specimen 616–15f.

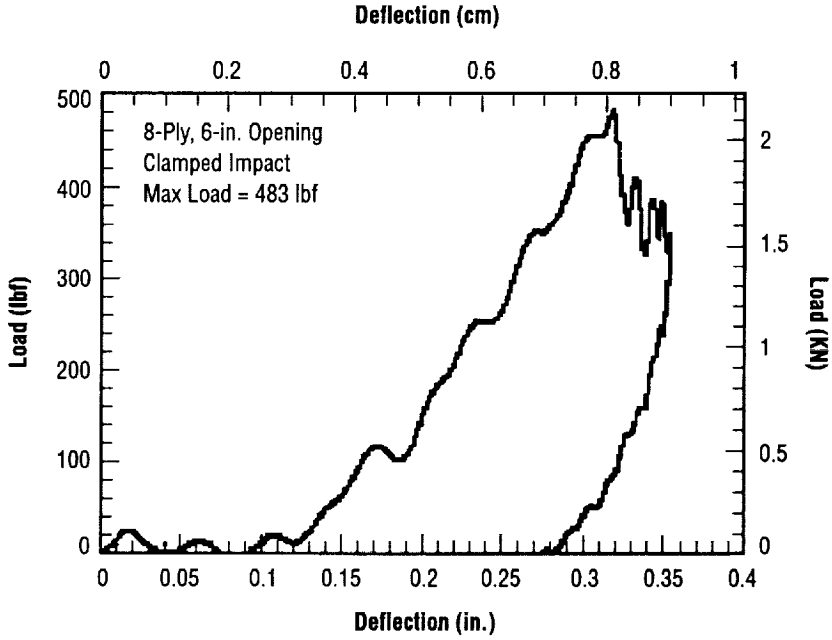

Figure 59. Load versus deflection specimen 616–16f.

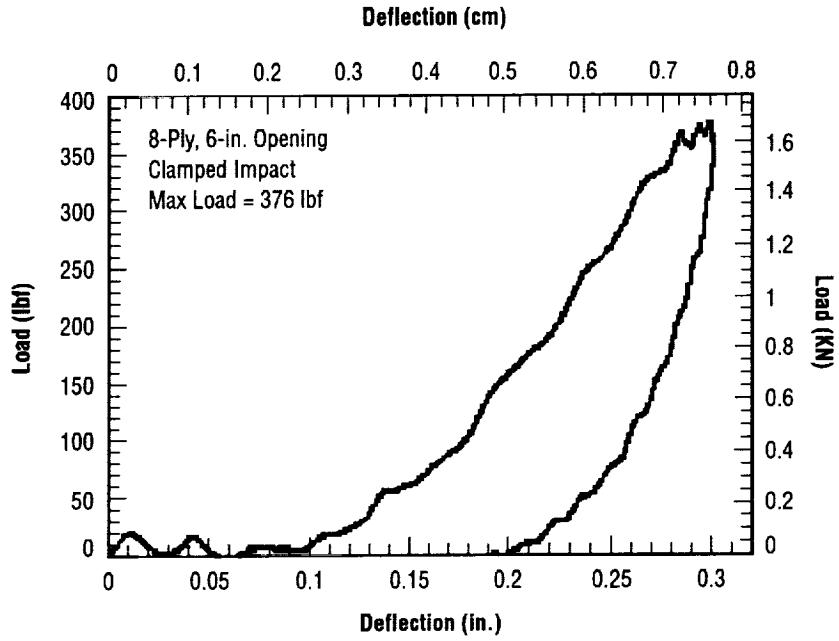

Figure 60. Load versus deflection specimen 616–17f.

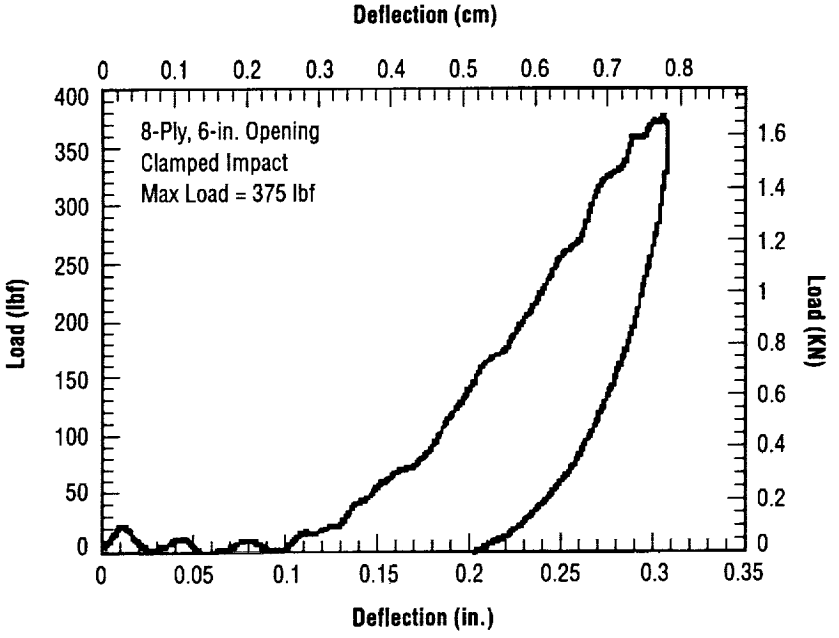

Figure 61. Load versus deflection specimen 616–18f.

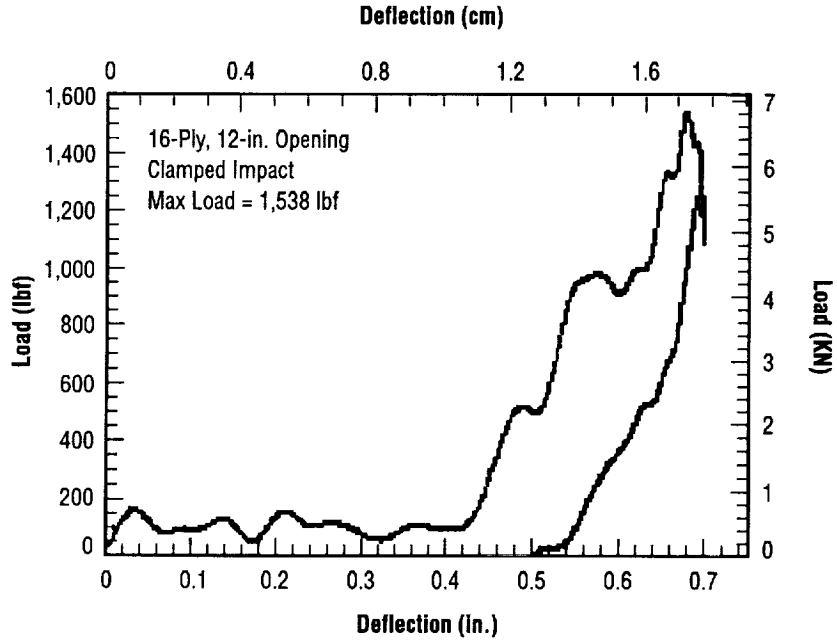

Figure 62. Load versus deflection specimen 616–01f.

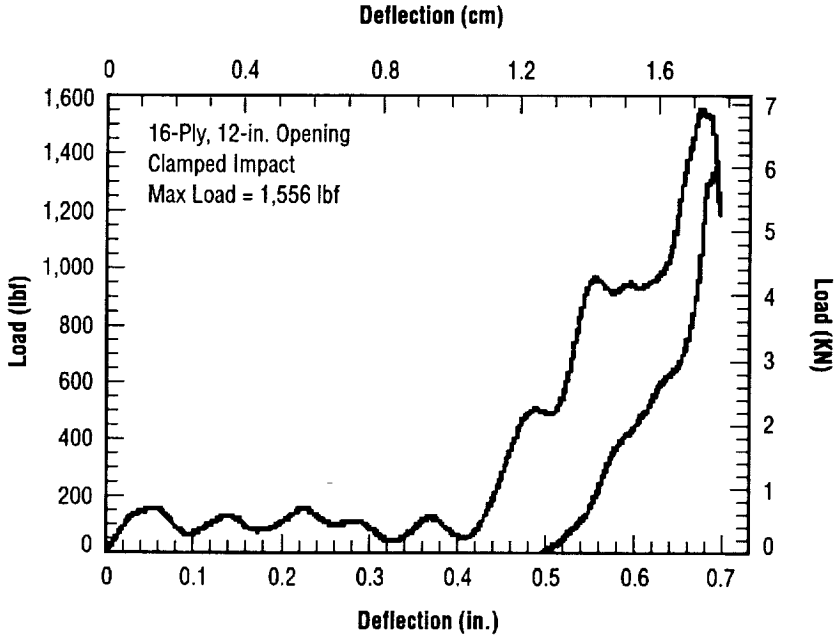

Figure 63. Load versus deflection specimen 616–02f.

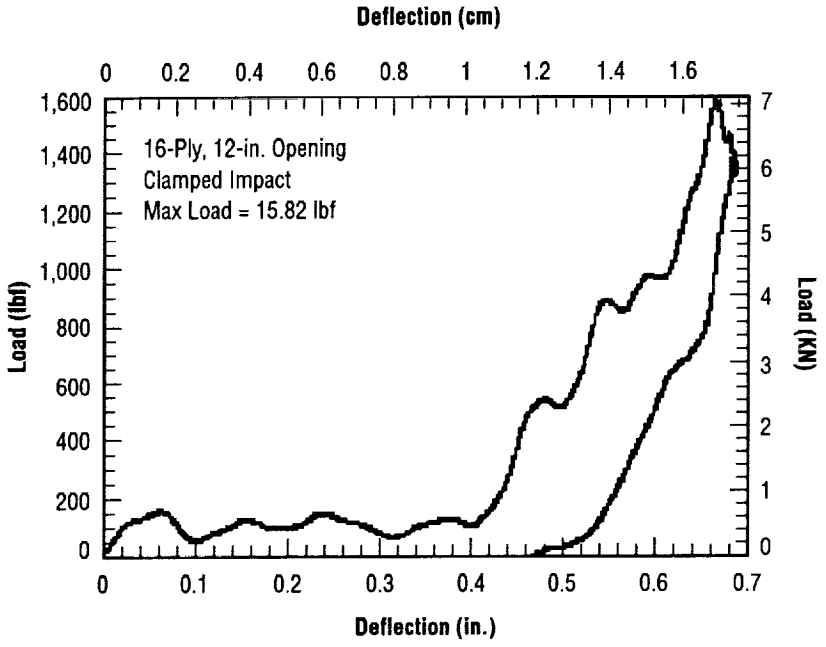

Figure 64. Load versus deflection specimen 616–03f.

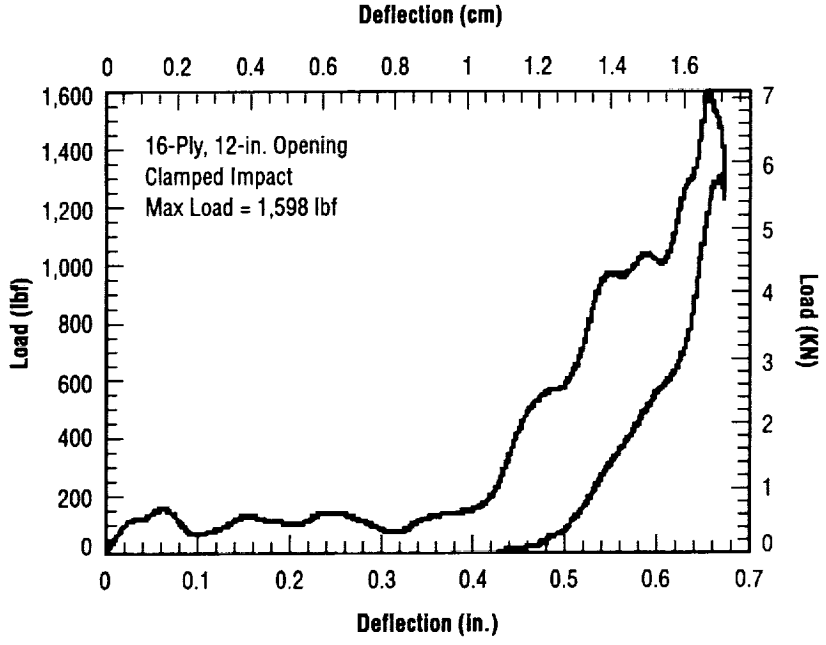

Figure 65. Load versus deflection specimen 616–04f.

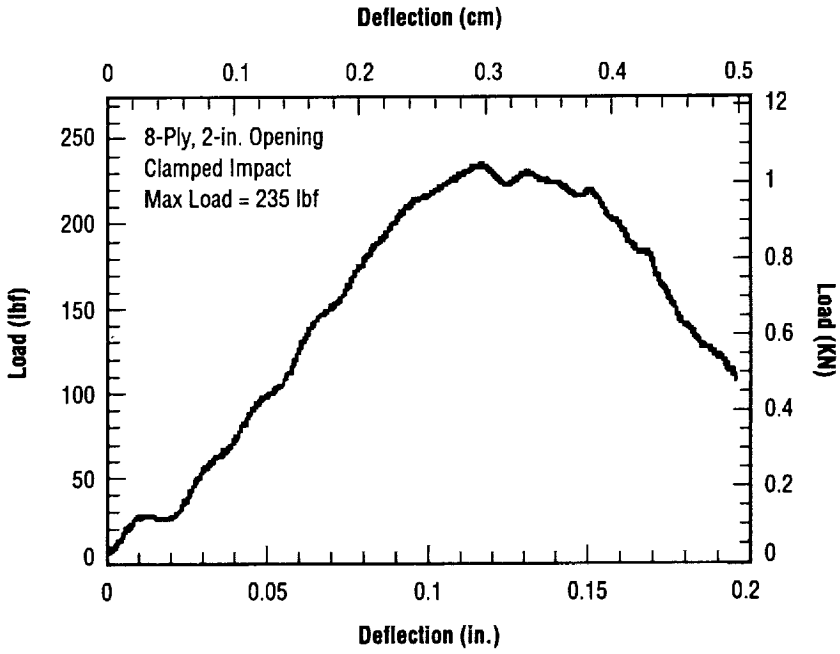

Figure 66. Load versus deflection specimen 616–37m.

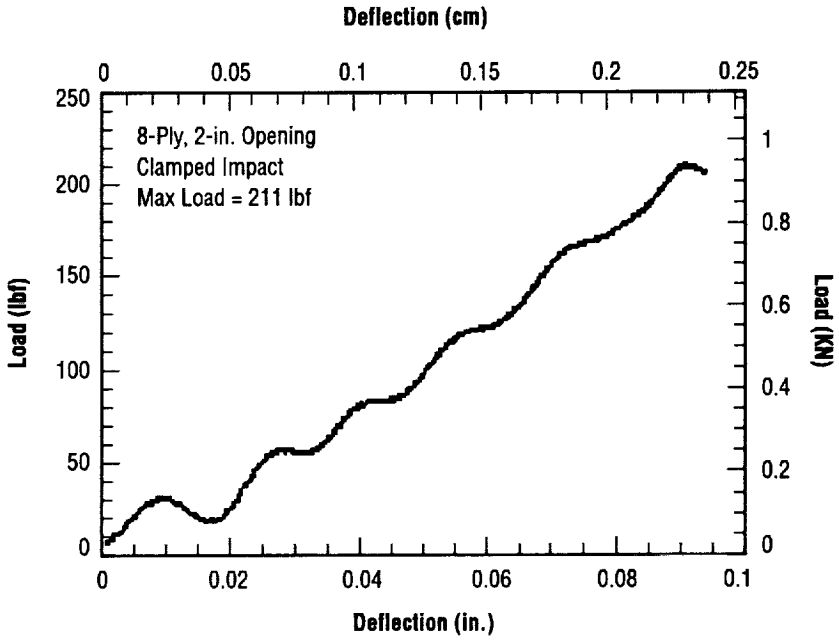

Figure 67. Load versus deflection specimen 616–38m.

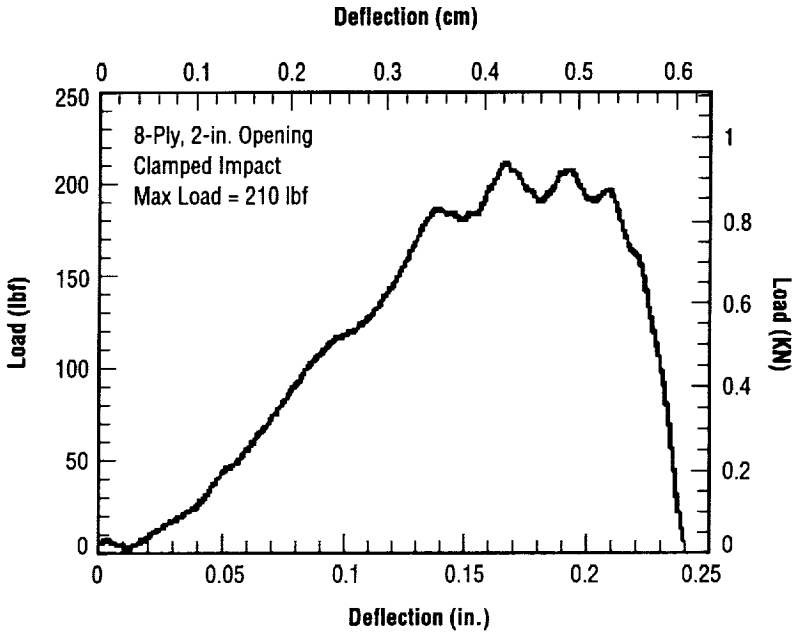

Figure 68. Load versus deflection specimen 728–09m.

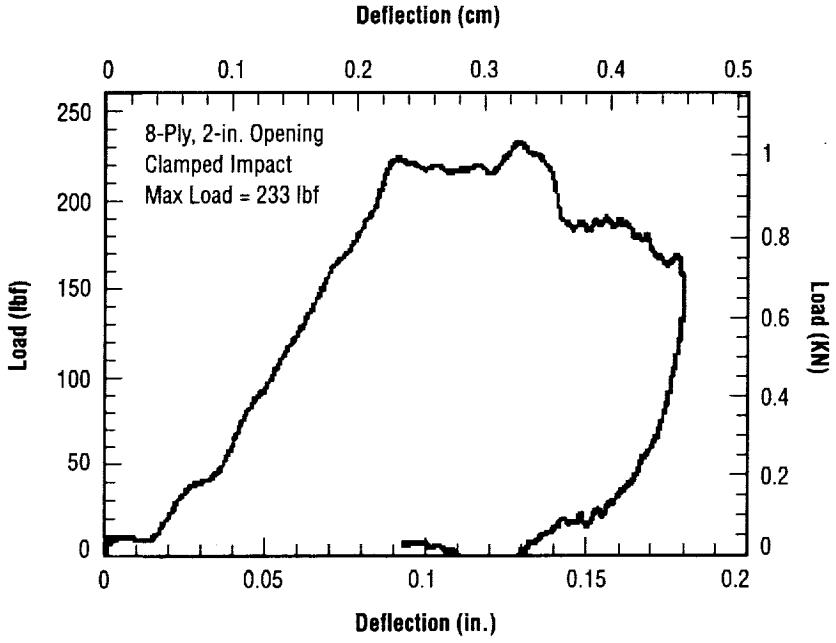

Figure 69. Load versus deflection specimen 728–11m.

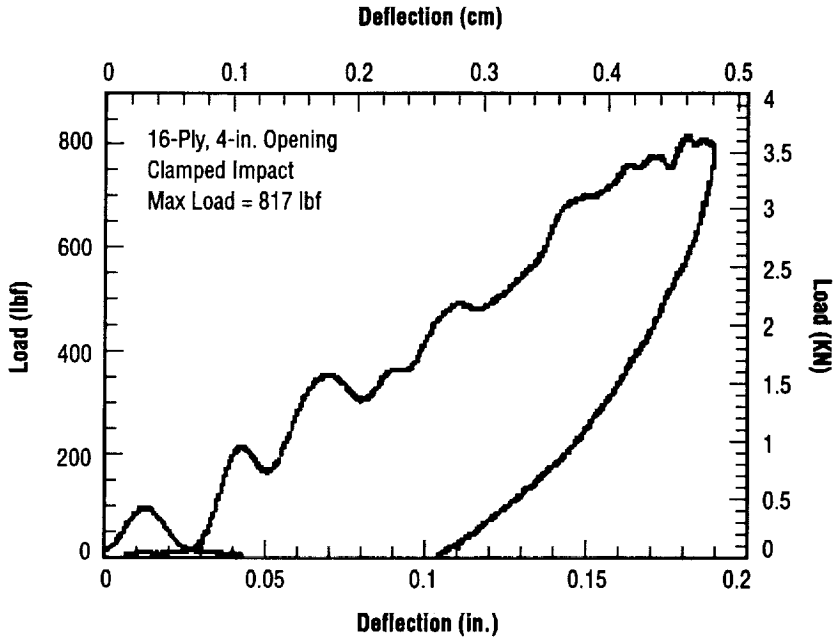

Figure 70. Load versus deflection specimen 616–25m.

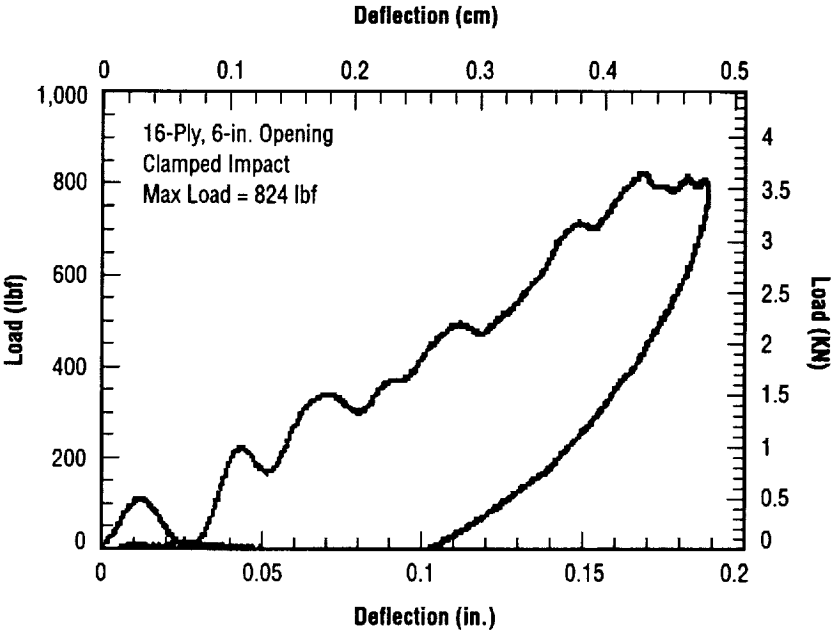

Figure 71. Load versus deflection specimen 616–26m.

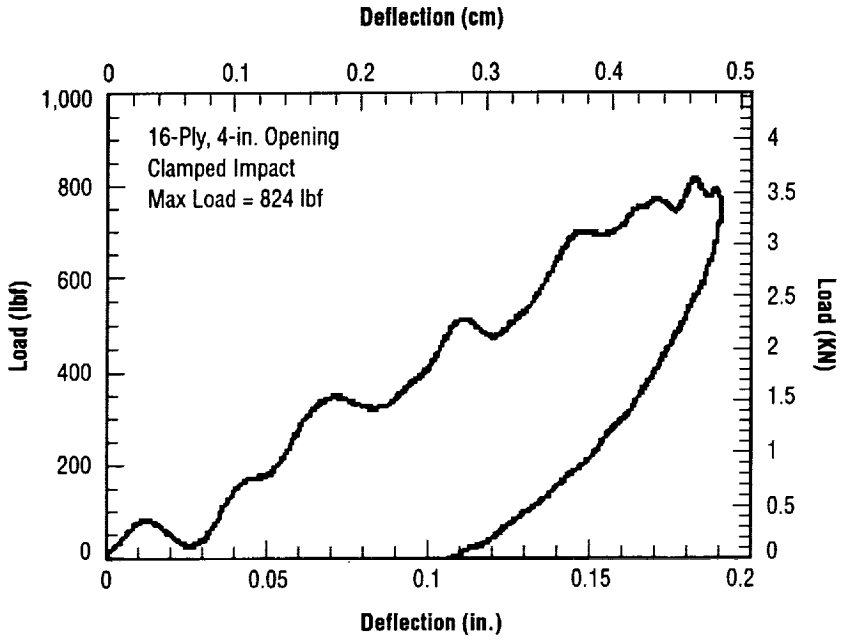

Figure 72. Load versus deflection specimen 616–27m.

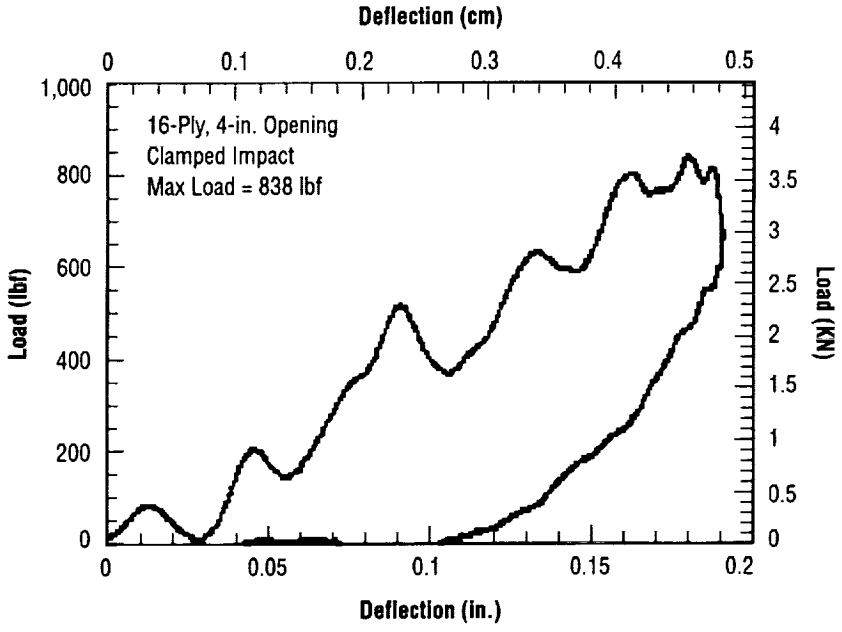

Figure 73. Load versus deflection specimen 616–28m.

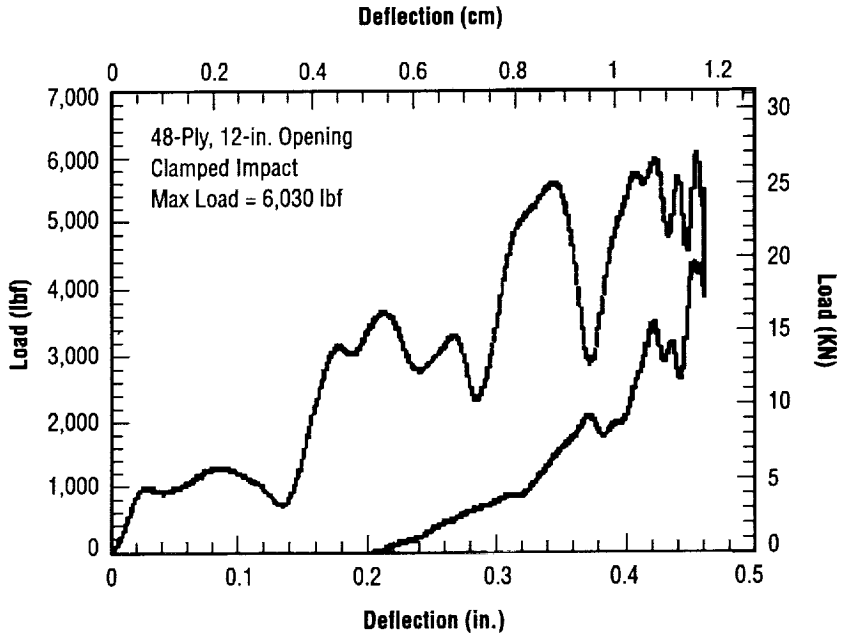

Figure 74. Load versus deflection specimen 61599–04m.

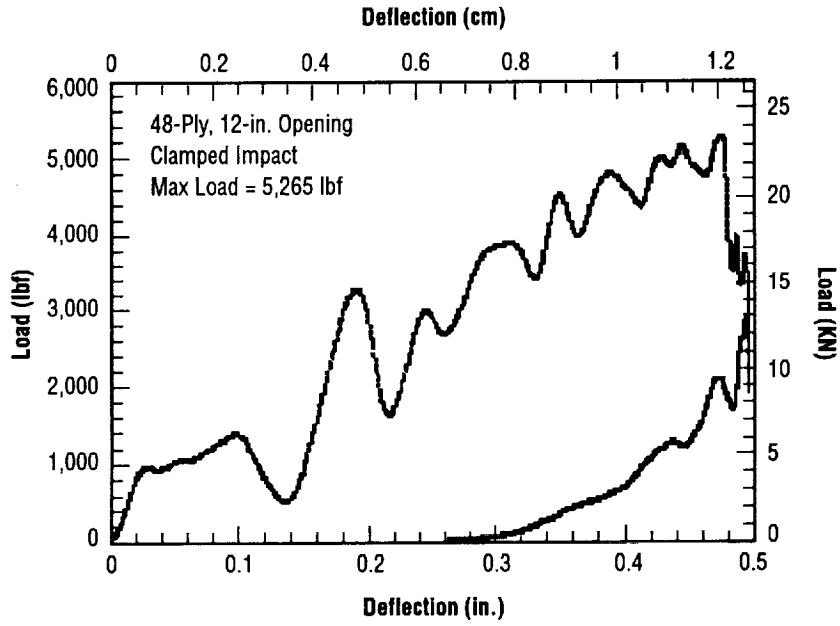

Figure 75. Load versus deflection specimen 61599–05m.

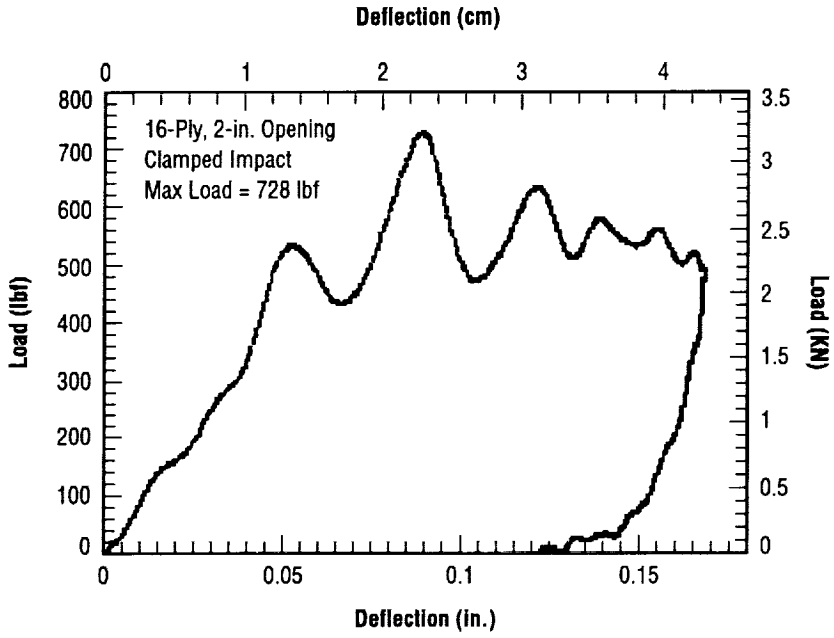

Figure 76. Load versus deflection specimen 616–29s.

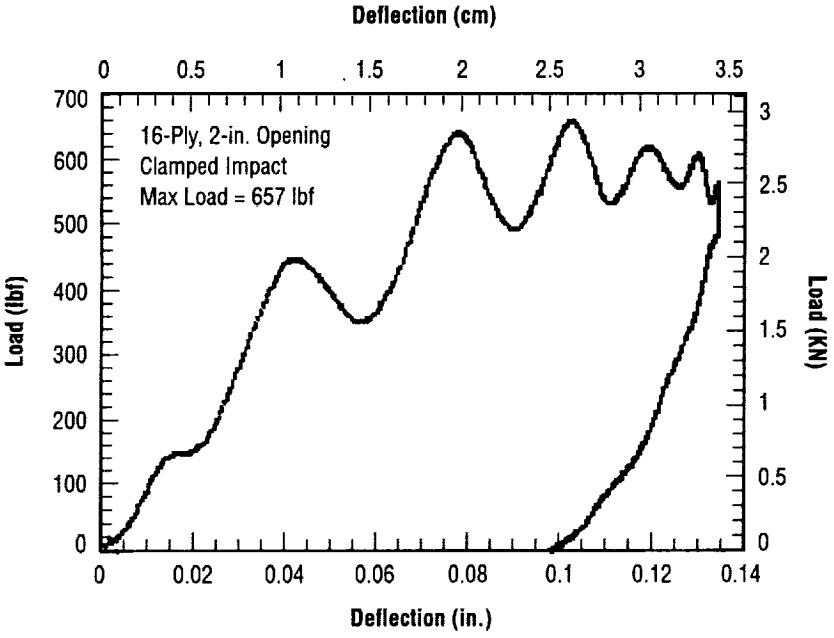

Figure 77. Load versus deflection specimen 616–30s.

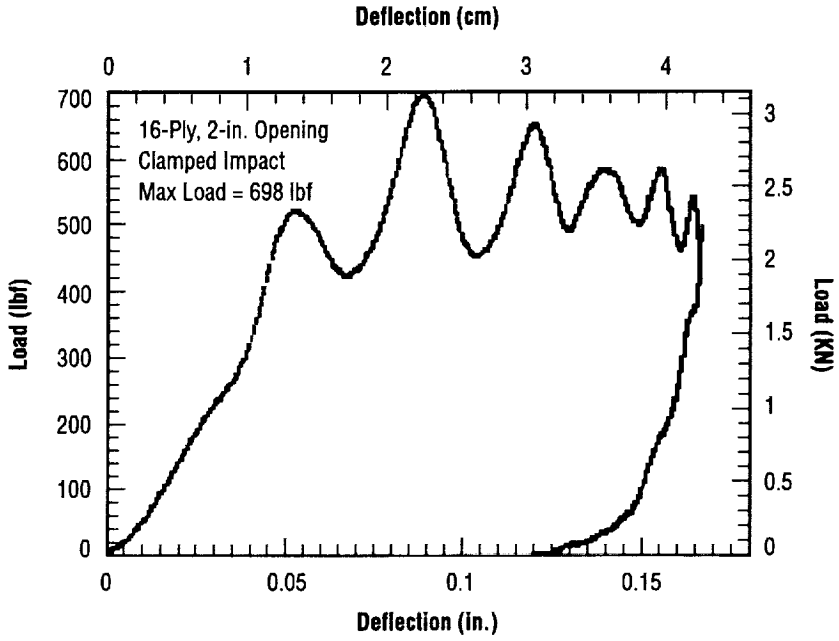

Figure 78. Load versus deflection specimen 616–31s.

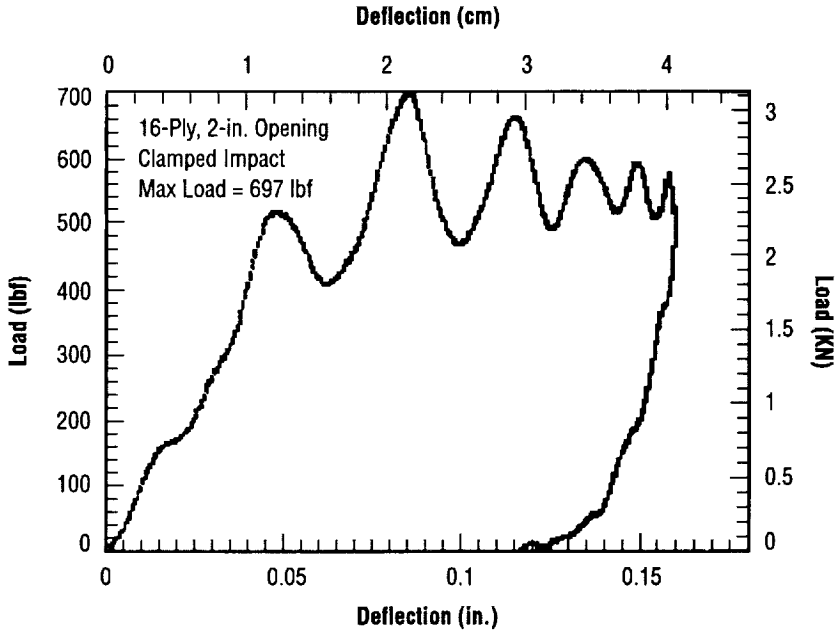

Figure 79. Load versus deflection specimen 616–32s.

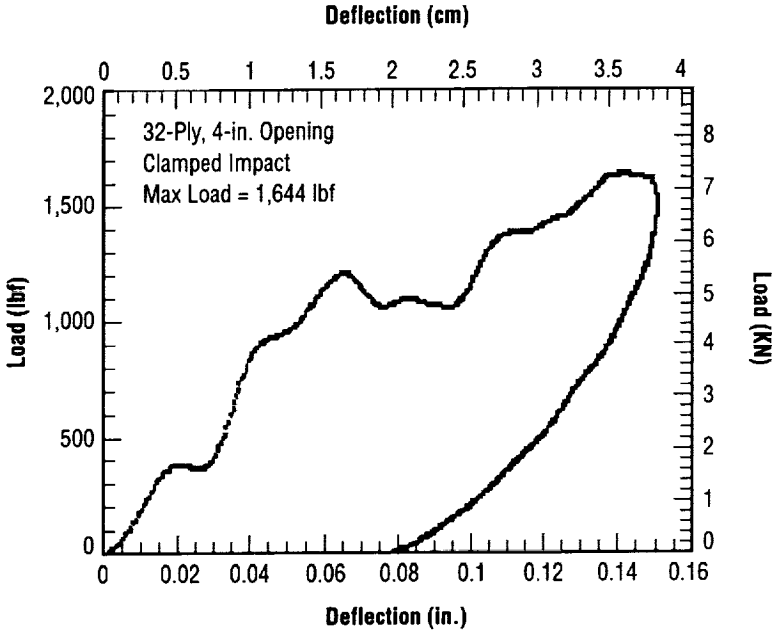

Figure 80. Load versus deflection specimen 616–20s.

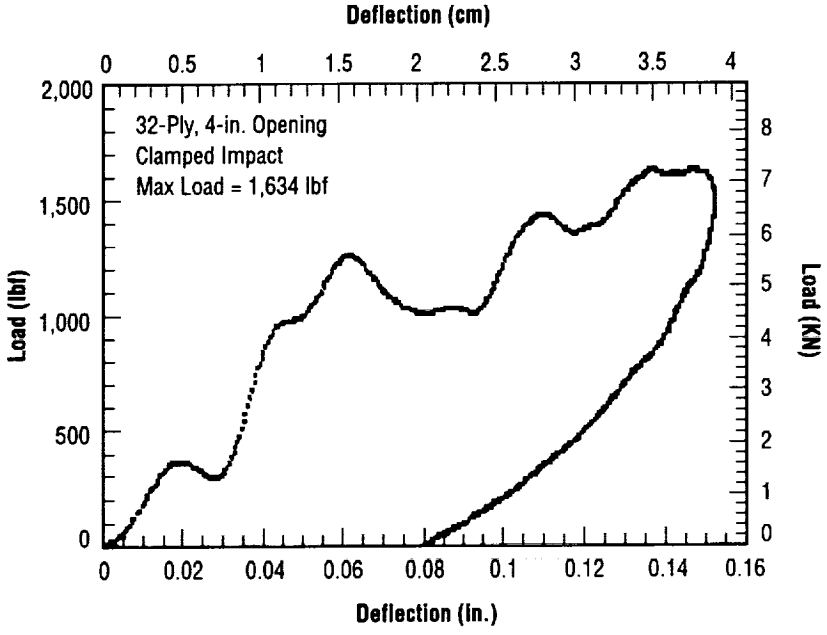

Figure 81. Load versus deflection specimen 616–21s.

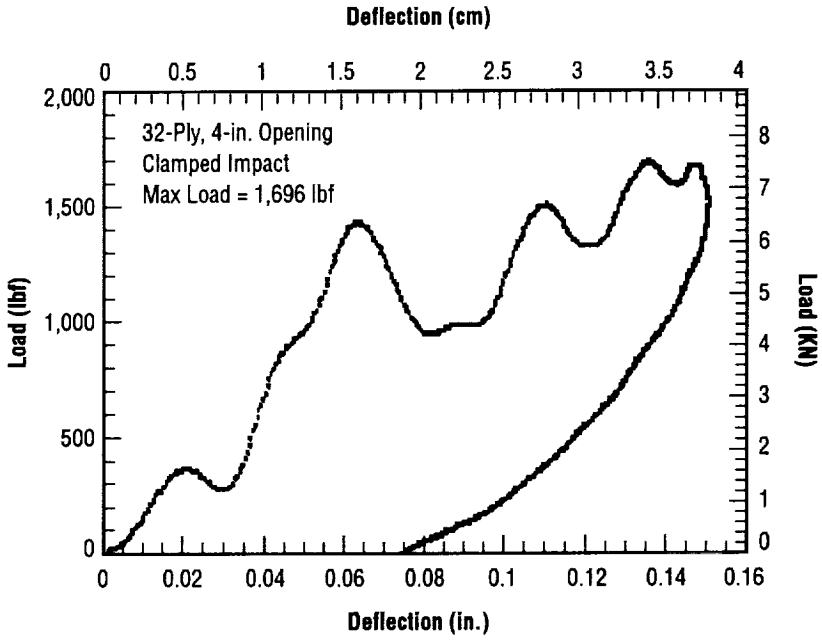

Figure 82. Load versus deflection specimen 616–22s.

APPENDIX C—LOAD VERSUS DEFLECTION PLOTS FOR QUASI-STATIC INDENTATION TESTS

Figures 83–97 show load versus deflection plots for quasi-static indentation tests.

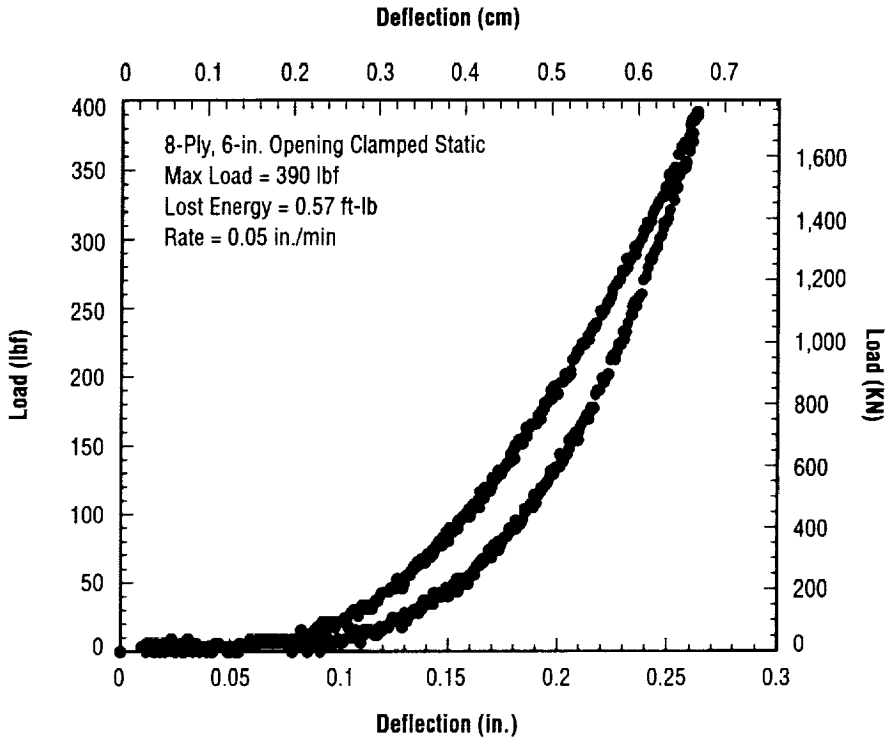

Figure 83. Load versus deflection specimen 708–10f.

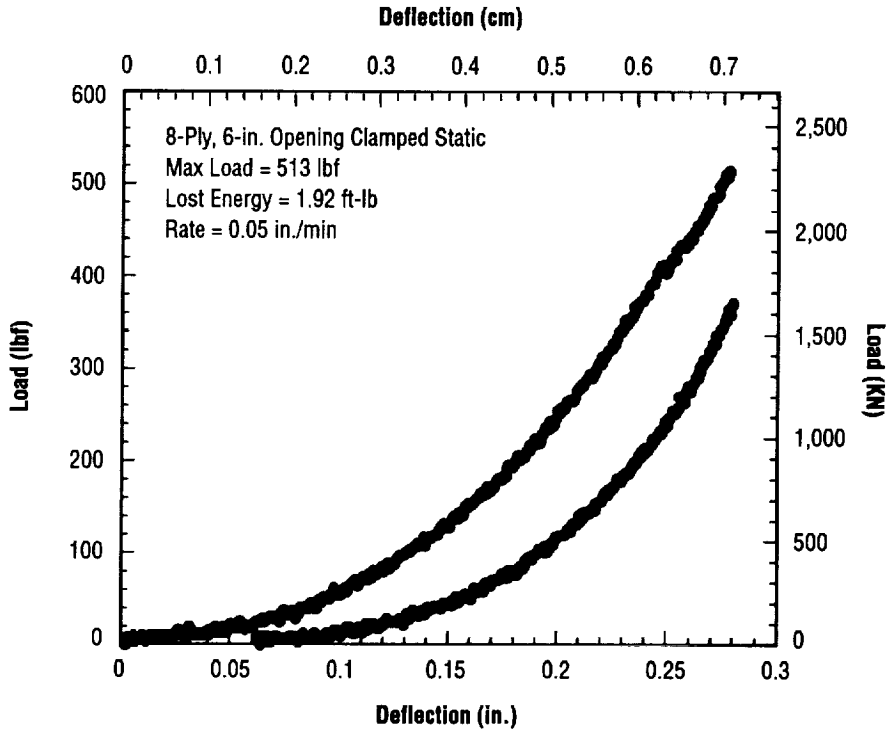

Figure 84. Load versus deflection specimen 708–11f.

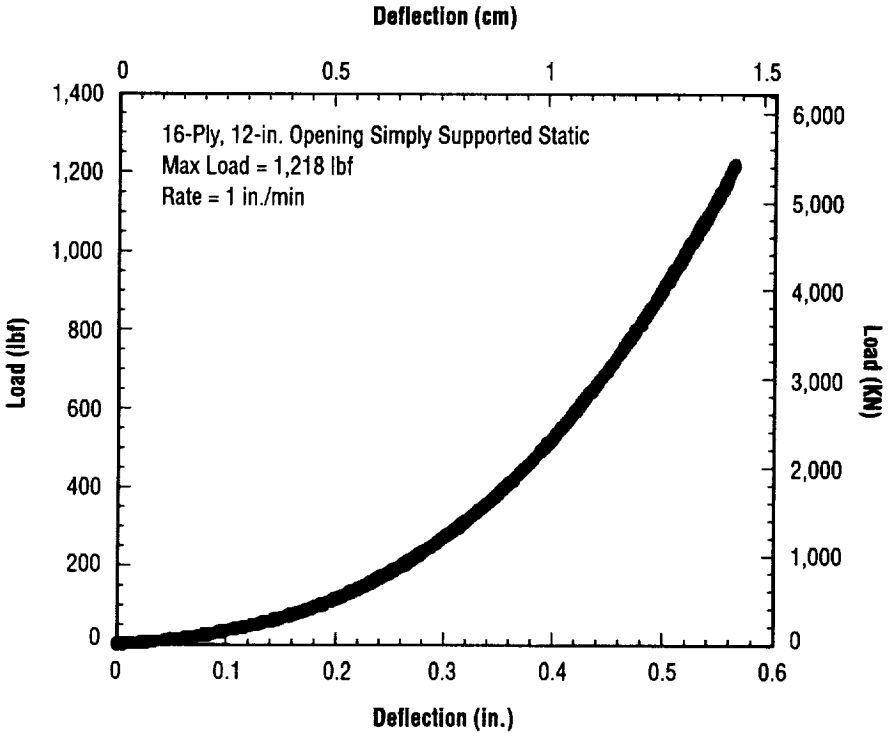

Figure 85. Load versus deflection specimen 1018–02f.

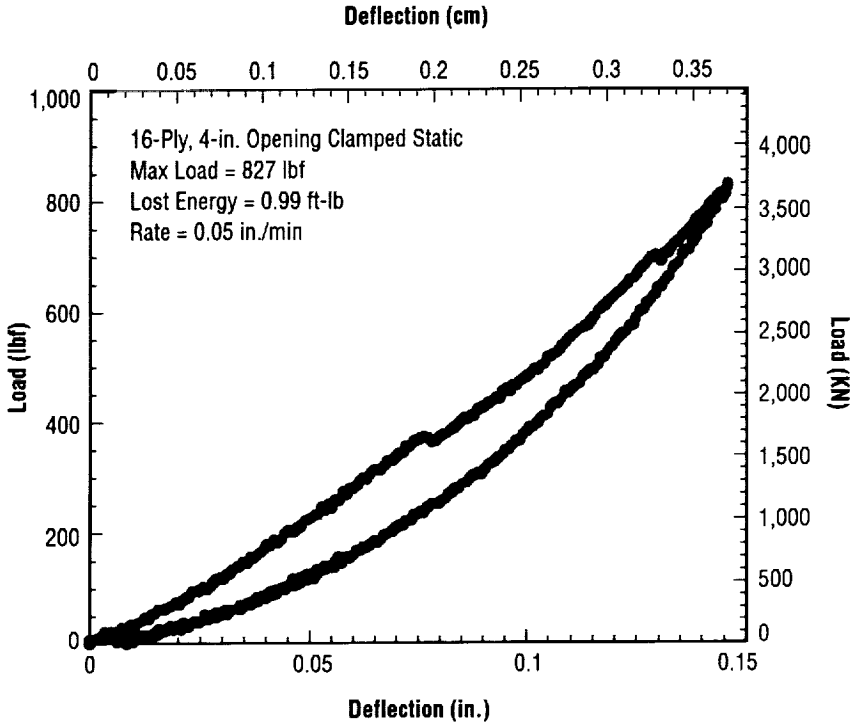

Figure 86. Load versus deflection specimen 708–03m.

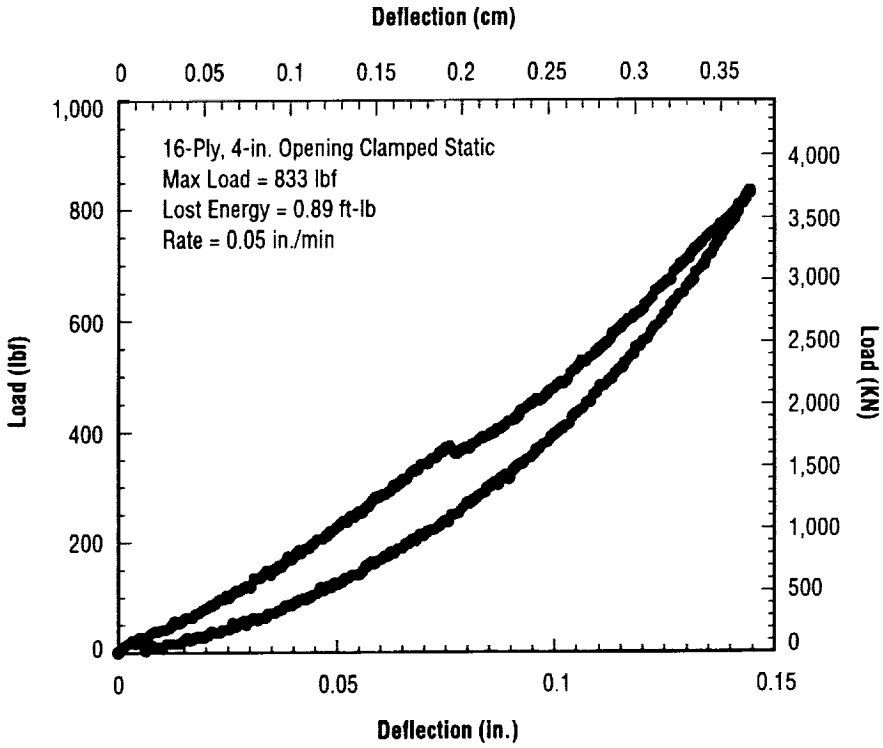

Figure 87. Load versus deflection specimen 708–02m.

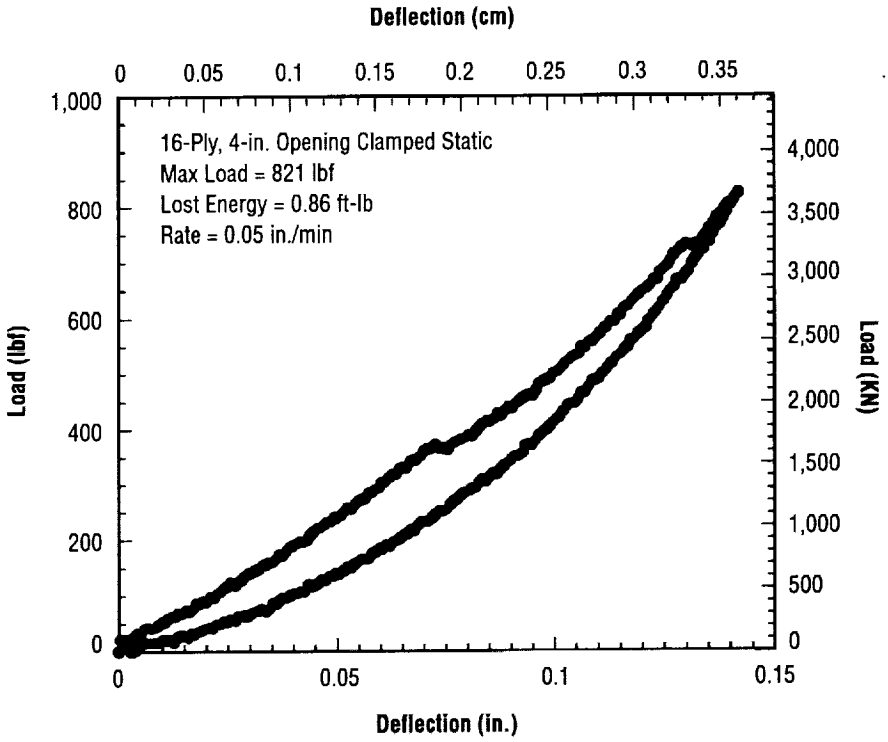

Figure 88. Load versus deflection specimen 708–04m.

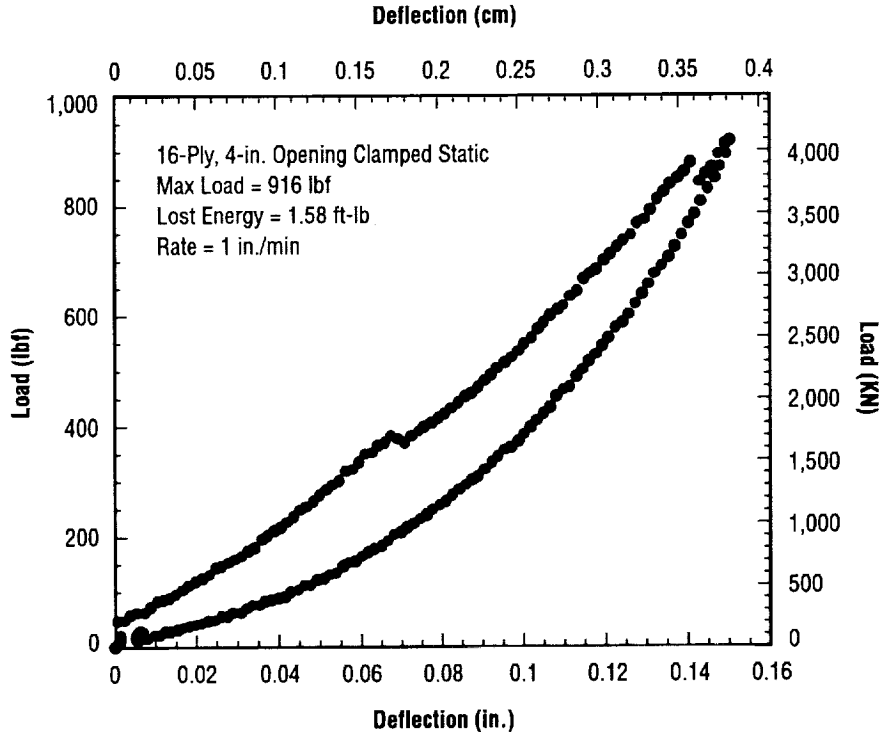

Figure 89. Load versus deflection specimen 708–05m.

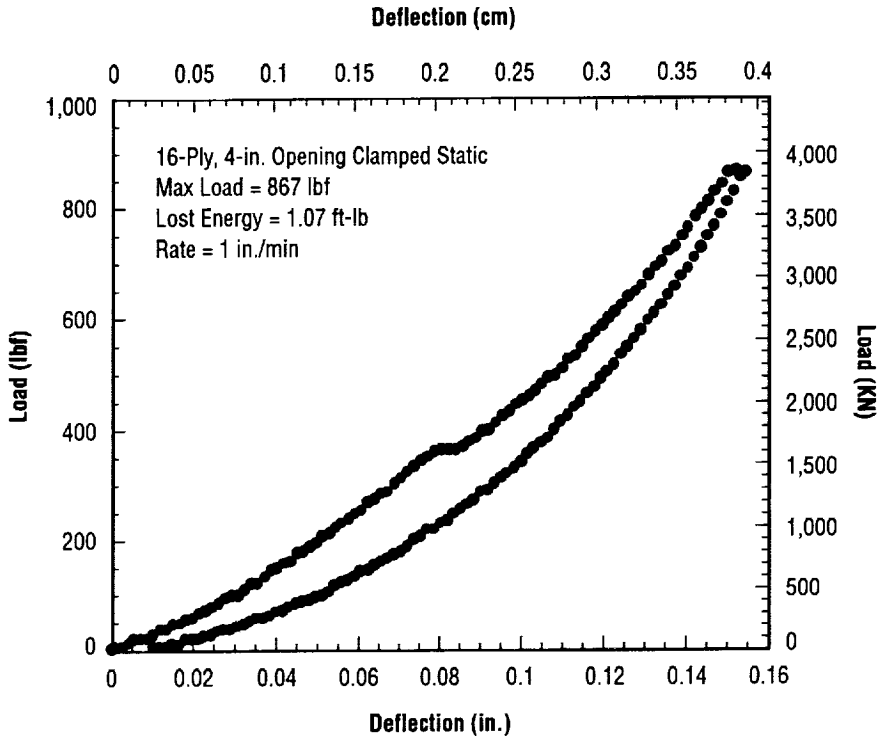

Figure 90. Load versus deflection specimen 708–06m.

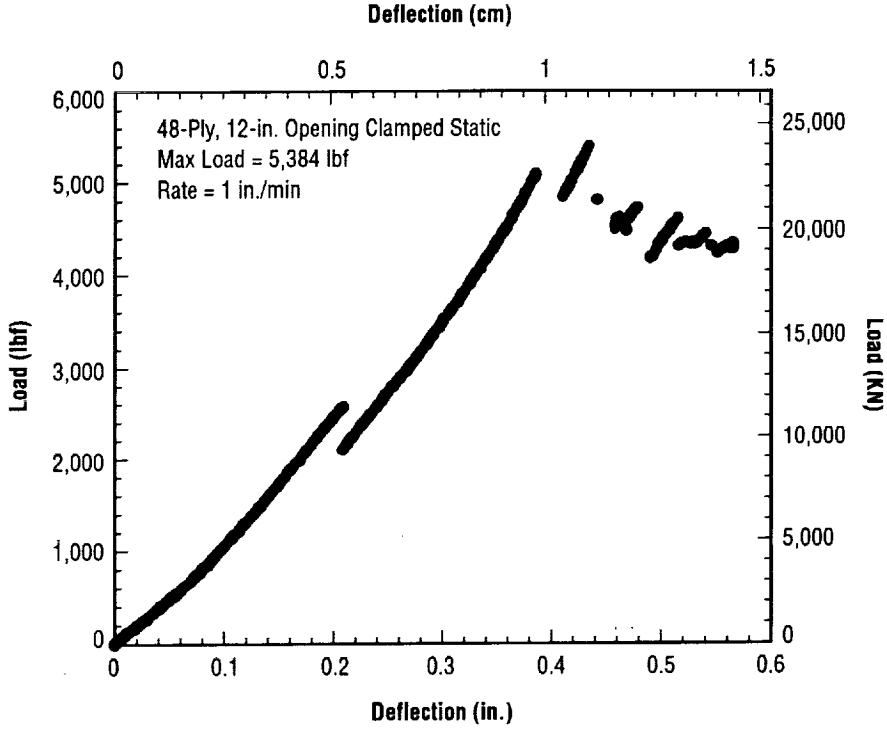

Figure 91. Load versus deflection specimen 1015–01m.

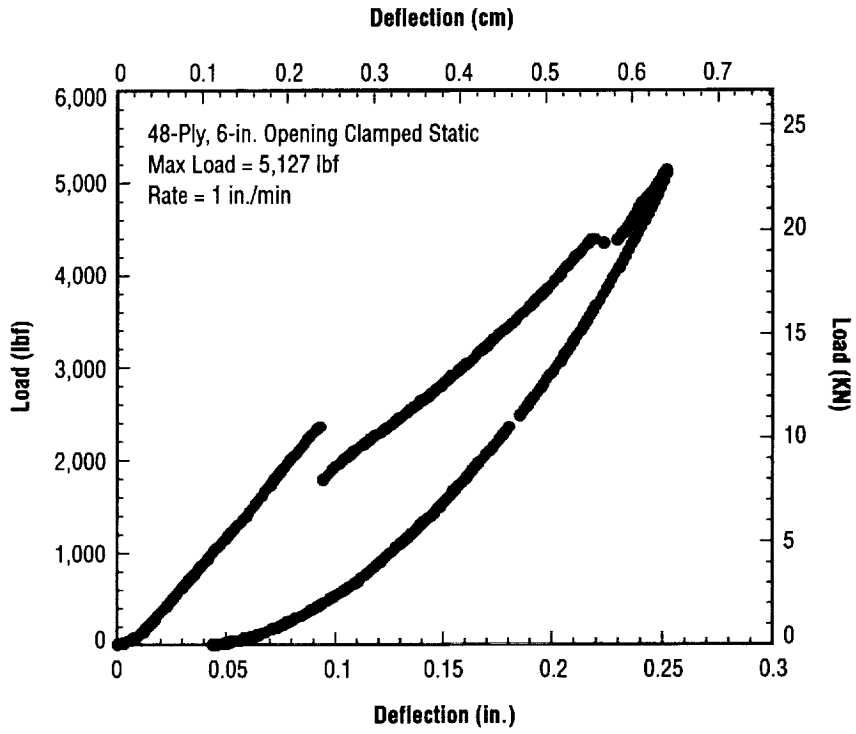

Figure 92. Load versus deflection specimen 1015–02s.

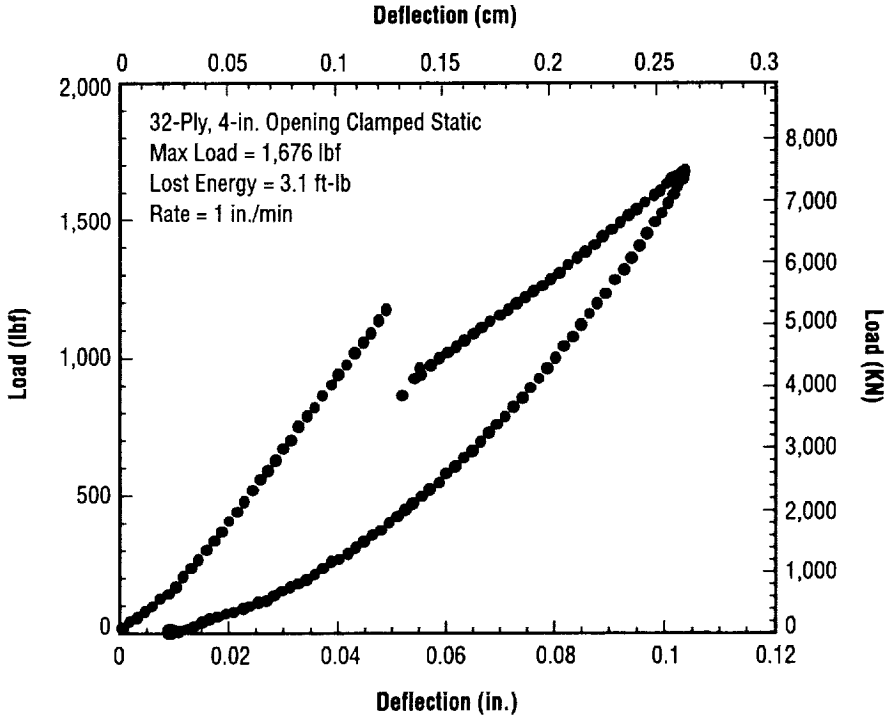

Figure 93. Load versus deflection specimen 708–07s.

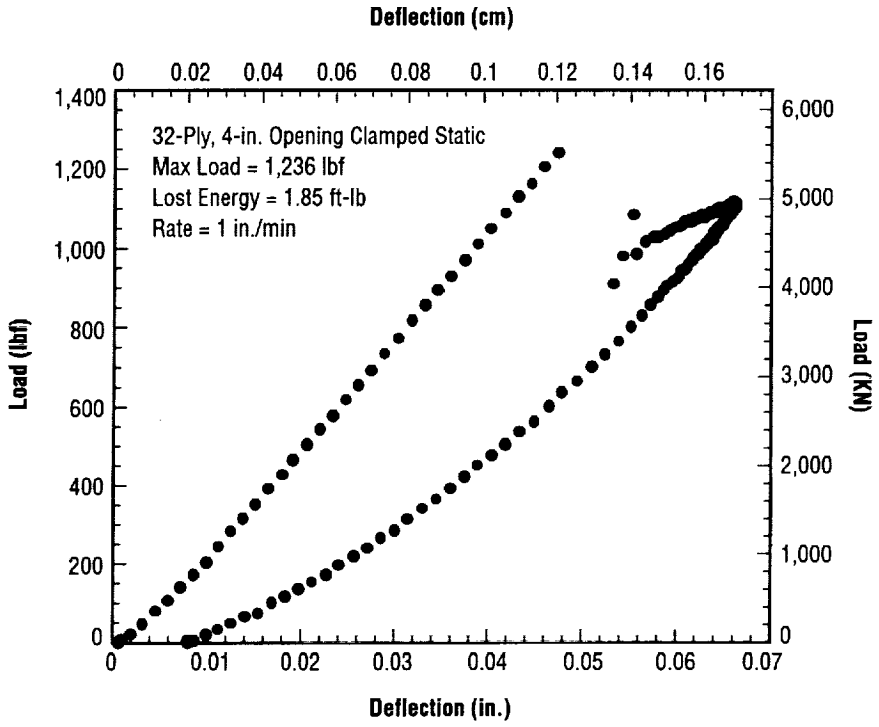

Figure 94. Load versus deflection specimen 708–08s.

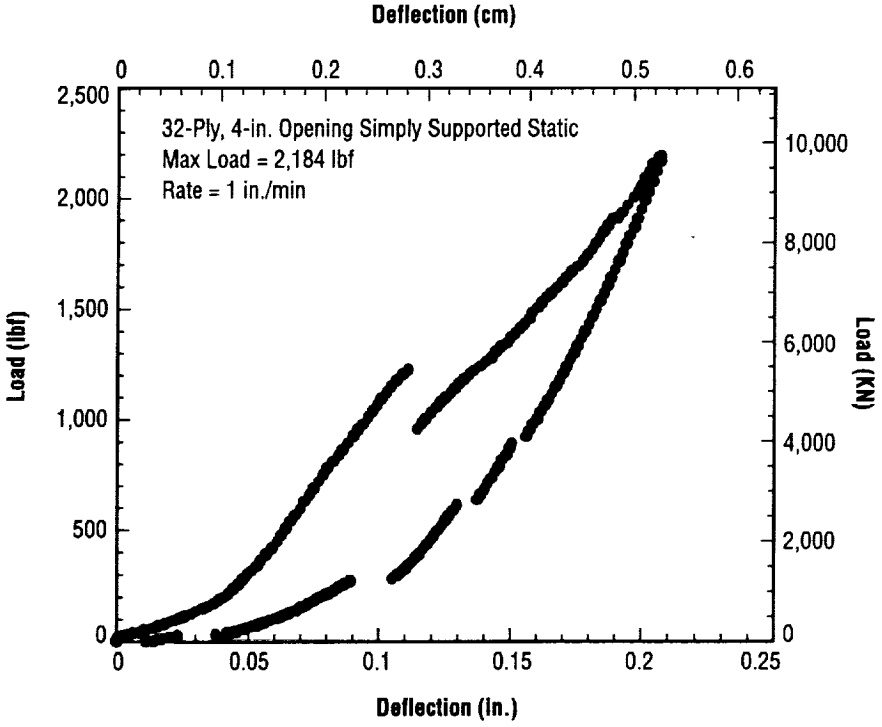

Figure 95. Load versus deflection specimen 1015–03s.

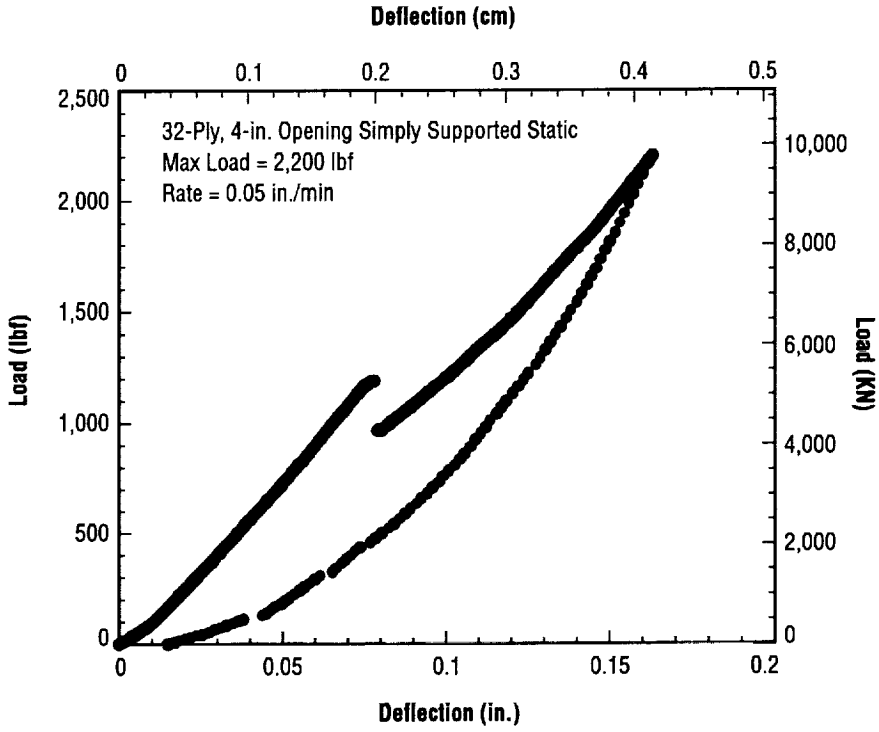

Figure 96. Load versus deflection specimen 1018–03s.

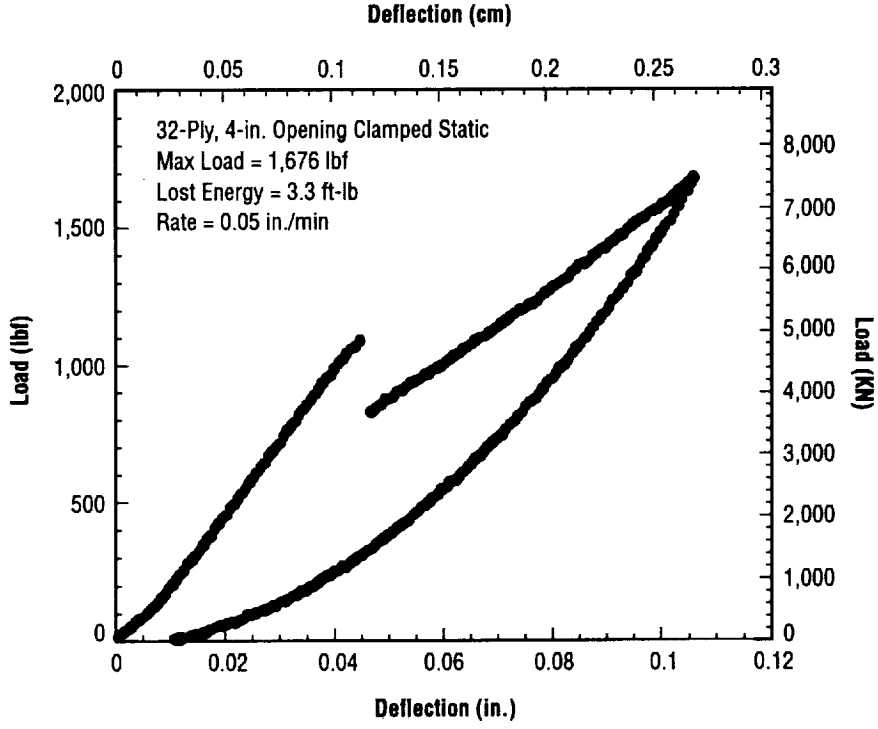

Figure 97. Load versus deflection specimen 706–01s.

APPENDIX D—NONDESTRUCTIVE EVALUATION ANALYSIS DATA

Tables 15–20 display simply supported and clamped flex data for nondestructive evaluation analysis.

Table 15. Simply supported flex.

8 Ply on 6-in. Platen				
Impact				
Specimen ID No.	**Max Load N (lbf)**	**Dent Depth mm (in.)**	**Crack Length mm (in.)**	**Delamination Area mm^2 ($in.^2$)**
727–06F	1,850 (416)	0.102 (0.004)	16.00 (0.63)	170 (0.28)
727–07F	1,766 (397)	0.075 (0.003)	47.75 (1.88)	216 (0.33)
727–08F	1,850 (416)	0.075 (0.003)	22.35 (0.88)	157 (0.24)
727–09F	1,873 (421)	0.075 (0.003)	25.4 (1.00)	223 (0.34)
727–10F	1,873 (421)	Not measurable	31.75 (1.25)	190 (0.29)
Quasi-Static				
817–10F	1,819 (409)	0.102 (0.004)	0.075 (0.003)	177 (0.27)
817–11F	1,859 (418)	0.102 (0.004)	Not measurable	111 (0.17)
817–04F	1,859 (418)	0.075 (0.003)	19.05 (0.75)	190 (0.29)
817–05F	1,850 (416)	0.075 (0.003)	22.35 (0.88)	190 (0.29)

16 Ply on 12-in. Platen				
Impact				
Specimen ID No.	**Max Load N (lbf)**	**Dent Depth mm (in.)**	**Crack Length mm (in.)**	**Delamination Area mm^2 ($in.^2$)**
728–05F	4,862 (1,093)	0.102 (0.004)	Not measurable	426 (0.65)
728–06F	5,400 (1,214)	0.102 (0.004)	31.75 (1.25)	499 (0.76)
728–07F	5,373 (1,208)	0.051 (0.002)	35.05 (1.38)	590 (0.90)
Quasi-Static				
818–05F	5,360 (1,205)	0.152 (0.006)	6.35 (0.25)	505 (0.77)
818–06F	5,458 (1,227)	0.127 (0.005)	6.35 (0.25)	538 (0.82)
818–03F	5,809 (1,306)	0.127 (0.005)	4.83 (0.19)	433 (0.66)
818–04F	5,667 (1,270)	0.127 (0.005)	9.65 (0.38)	472 (0.72)
1018–02F	5,420 (1,218)	No data	No data	416 (0.64)

Table 16. Simply supported medium.

8 Ply on 6-in. Platen				
Impact				
Specimen ID No.	**Max Load N (lbf)**	**Dent Depth mm (in.)**	**Crack Length mm (in.)**	**Delamination Area mm^2 ($in.^2$)**
728–02M	1,023 (230)	0.076 (0.003)	16.00 (0.63)	85 (0.13)
728–03M	974 (219)	0.076 (0.003)	16.00 (0.63)	79 (0.12)
728–04M	907 (204)	0.051 (0.002)	9.65 (0.38)	52 (0.08)
Quasi-Static				
819–01M	734 (165)	0.025 (0.001)	6.35 (0.25)	39 (0.06)
819–02M	907 (204)	0.076 (0.003)	4.83 (0.19)	46 (0.07)
819–07M	1,059 (238)	0.152 (0.006)	16.00 (0.63)	79 (0.12)
819–08M	1,059 (238)	0.127 (0.005)	19.05 (0.75)	105 (0.16)

16 Ply on 4-in. Platen				
Impact				
Specimen ID No.	**Max Load N (lbf)**	**Dent Depth mm (in.)**	**Crack Length mm (in.)**	**Delamination Area mm^2 ($in.^2$)**
727–11M	3,723 (837)	Penetrated	No data	No data
727–12M	3,701 (832)	0.279 (0.011)	28.70 (1.13)	492 (0.75)
727–13M	3,670 (825)	0.102 (0.004)	25.40 (1.00)	321 (0.49)
727–14M	2,998 (674)	0.051 (0.002)	6.35 (0.25)	171 (0.26)
727–15M	2,963 (666)	0.076 (0.003)	19.05 (0.75)	262 (0.40)
Quasi-Static				
819–16M	3,677 (827)	No data	No data	400 (0.61)
819–17M	3,670 (825)	0.102 (0.004)	9.65 (0.38)	308 (0.47)
819–09M	4,003 (900)	0.152 (0.006)	31.75 (1.25)	315 (0.48)
819–10M	3,777 (849)	0.203 (0.008)	31.75 (1.25)	328 (0.50)

48 Ply on 12-in. Platen				
Impact				
Specimen ID No.	**Max Load N (lbf)**	**Dent Depth mm (in.)**	**Crack Length mm (in.)**	**Delamination Area mm^2 ($in.^2$)**
61599–02M	23,557 (5,296)	0.614 (0.024)	112.13 (4.38)	3,214 (4.90)
61599–03M	29,496 (6,631)	0.205 (0.008)	118.53 (4.63)	3,011 (4.59)
Quasi-Static				
818–07M	23,878 (5,368)	0.635 (0.25)	Numerous cracks	25.80 (4.00)
818–01M	28,304 (6,363)	No data	No data	26.38 (4.09)

Table 17. Simply supported stiff.

16 Ply on 2-in. Platen				
Impact				
Specimen ID No.	**Max Load N (lbf)**	**Dent Depth mm (in.)**	**Crack Length mm (in.)**	**Delamination Area mm^2 ($in.^2$)**
727–20S	2,922 (657)	0.127 (0.005)	31.75 (1.25)	288 (0.44)
727–21S	2,771 (623)	0.178 (0.007)	35.05 (1.38)	334 (0.51)
727–22S	3,350 (753)	0.102 (0.004)	16.00 (0.63)	269 (0.41)
728–01S	3,051 (686)	0.152 (0.006)	26.92 (1.06)	295 (0.45)
Quasi-Static				
819–03S	2,904 (653)	Not measurable	1.27 (0.50)	269 (0.41)
819–04S	2,918 (656)	0.178 (0.007)	16.00 (0.63)	328 (0.50)
819–05S	2,758 (620)	0.356 (0.014)	38.10 (1.50)	348 (0.53)
819–06S	2,931 (659)	0.279 (0.011)	30.22 (1.19)	308 (0.47)

32 Ply on 4-in. Platen				
Impact				
Specimen ID No.	**Max Load N (lbf)**	**Dent Depth mm (in.)**	**Crack Length mm (in.)**	**Delamination Area mm^2 ($in.^2$)**
727–16S	8,696 (1,955)	0.152 (0.006)	38.10 (1.50)	984 (1.53)
727–17S	9,106 (2,047)	0.152 (0.006)	Not measurable	1,154 (1.76)
727–18S	9,853 (2,215)	0.178 (0.007)	Not measurable	1,141 (1.74)
727–19S	9,346 (2,101)	0.152 (0.006)	47.75 (1.88)	1,207 (1.84)
Quasi-Static				
819–14S	9,866 (2,218)	0.330 (0.013)	47.75 (1.88)	1,220 (1.86)
819–15S	9,844 (2,213)	0.330 (0.013)	47.75 (1.88)	1,233 (1.88)
819–12S	10,898 (2,450)	0.254 (0.010)	41.40 (1.63)	1,586 (2.42)
819–13S	10,925 (2,456)	0.279 (0.011)	28.70 (1.13)	1,614 (2.46)
1015–03S	9,718 (2,184)	No data	No data	1,232 (1.91)
1018–03	9,790 (2,200)	No data	No data	1,297 (2.01)

48 Ply on 6-in. Platen				
Impact				
Specimen ID No.	**Max Load N (lbf)**	**Dent Depth mm (in.)**	**Crack Length mm (in.)**	**Delamination Area mm^2 ($in.^2$)**
727–02S	22,121 (4,973)	0.279 (0.011)	1.27 (0.50)	3,339 (5.09)
727–03S	22,810 (5,128)	0.686 (0.027)	63.50 (2.50)	4,284 (6.53)
Quasi-Static				
817–08S	22,726 (5,109)	0.457 (0.018)	Numerous cracks	4,146 (6.32)
817–09S	22,383 (5,032)	1.067 (0.042)	55.63 (2.19)	4,146 (6.32)
817–06S	21,476 (4,828)	1.497 (0.059)	Numerous cracks	4,211 (6.42)
817–07S	20,987 (4,718)	1.016 (0.040)	31.75 (1.25)	3,765 (5.74)

Table 18. Clamped flex.

8 Ply on 6-in. Platen				
Impact				
Specimen ID No.	**Max Load N (lbf)**	**Dent Depth mm (in.)**	**Crack Length mm (in.)**	**Delamination Area mm^2 ($in.^2$)**
616–15F	1,930 (434)	0.203 (0.008)	85.85 (3.38)	676 (1.03)
616–16F	2,148 (483)	0.381 (0.015)	74.68 (2.94)	479 (0.73)
616–17F	1,673 (376)	0.051 (0.002)	19.05 (0.75)	112 (0.17)
616–18F	1,668 (375)	0.076 (0.003)	22.35 (0.88)	112 (0.17)
Quasi-Static				
708–10F	1,735 (390)	No data	No data	No data
708–11F	2,277 (512)	0.635 (0.025)	44.45 (1.75)	348 (0.53)
720–07F	1,415 (318)	0.152 (0.006)	12.70 (0.50)	92 (0.14)
720–08F	1,899 (427)	0.127 (0.005)	9.53 (0.38)	85 (0.13)

16 Ply on 12-in. Platen				
Impact				
Specimen ID No.	**Max Load N (lbf)**	**Dent Depth mm (in.)**	**Crack Length mm (in.)**	**Delamination Area mm^2 ($in.^2$)**
616–01F	6,841 (1,538)	0.152 (0.006)	41.28 (1.63)	774 (1.18)
616–02F	6,921 (1,556)	0.127 (0.005)	57.15 (2.25)	741 (1.13)
616–03F	7,037 (1,582)	0.127 (0.005)	38.10 (1.50)	833 (1.27)
616–04F	7,108 (1,598)	0.127 (0.005)	42.07 (1.66)	781 (1.19)
Quasi-Static				
720–03F	6,935 (1,559)	0.178 (0.007)	44.45 (1.75)	643 (0.98)
720–04F	6,993 (1,572)	0.203 (0.008)	44.45 (1.75)	708 (1.08)
720–05F	7,357 (1,654)	0.152 (0.006)	25.4 (1.00)	715 (1.09)
720–06F	7,517 (1,690)	0.178 (0.007)	35.05 (1.38)	840 (1.28)

Table 19. Clamped medium.

8 Ply on 2-in. Platen				
Impact				
Specimen ID No.	**Max Load N (lbf)**	**Dent Depth mm (in.)**	**Crack Length mm (in.)**	**Delamination Area mm^2 ($in.^2$)**
616–37M	1,045 (235)	Extensive damage		No data
616–38M	939 (211)	0.229 (0.009)	Numerous cracks	190 (0.29)
728–09M	936 (210)	0.102 (0.004)	22.35 (0.88)	92 (0.14)
728–11M	1,036 (233)	Extensive damage		131 (0.20)
Quasi-Static				
722–03M	1,183 (266)	0.076 (0.003)	16.00 (0.63)	66 (0.10)
722–04M	1,045 (235)	0.102 (0.004)	9.65 (0.38)	59 (0.09)
722–05M	939 (211)	0.127 (0.005)	6.35 (0.25)	52 (0.08)
722–06M	894 (201)	Not measurable	Not visible	46 (0.07)

16 Ply on 4-in. Platen				
Impact				
Specimen ID No.	**Max Load N (lbf)**	**Dent Depth mm (in.)**	**Crack Length mm (in.)**	**Delamination Area mm^2 ($in.^2$)**
616–25M	3,634 (817)	0.076 (0.003)	22.23 (0.88)	276 (0.42)
616–26M	3,629 (816)	0.076 (0.003)	34.93 (1.38)	348 (0.53)
616–27M	3,665 (824)	0.076 (0.003)	38.10 (1.50)	230 (0.35)
616–28M	3,728 (838)	0.127 (0.005)	44.45 (1.75)	335 (0.51)
Quasi-Static				
708–02M	3,705 (833)	0.152 (0.006)	Not measurable	348 (0.53)
708–03M	3,679 (827)	0.152 (0.006)	25.4 (1.00)	374 (0.57)
708–04M	3,652 (821)	0.152 (0.006)	22.35 (0.88)	308 (0.47)
708–05M	4,075 (916)	0.152 (0.006)	16.00 (0.63)	420 (0.64)
708–06M	3,857 (867)	0.127 (0.005)	Not measurable	420 (0.64)

48 Ply on 12-in. Platen				
Impact				
Specimen ID No.	**Max Load N (lbf)**	**Dent Depth mm (in.)**	**Crack Length mm (in.)**	**Delamination Area mm^2 ($in.^2$)**
61599–04M	26,823 (6,030)	0.794 (0.031)	80.00 (3.16)	3,640 (5.55)
61599–05M	23,420 (5,265)	1.434 (0.059)	70.40 (2.75)	3,378 (5.15)
Quasi-Static				
817–01M	26,293 (5,911)	0.333 (0.013)	99.20 (3.88)	4,159 (6.34)
817–02M	28,290 (6,360)	0.435 (0.017)	107.20 (4.19)	3,241 (4.94)

Table 20. Clamped stiff.

16 Ply on 2-in. Platen				
Impact				
Specimen ID No.	**Max Load N (lbf)**	**Dent Depth mm (in.)**	**Crack Length mm (in.)**	**Delamination Area mm^2 ($in.^2$)**
616–29S	3,239 (728)	0.457 (0.018)	50.80 (2.00)	382 (0.592)
616–30S	2,922 (657)	0.203 (0.008)	55.56 (2.19)	512 (0.794)
616–31S	3,105 (698)		66.68 (2.63)	624 (0.967)
616–32S	3,100 (697)	0.356 (0.014)	68.26 (2.69)	676 (1.048)
Quasi-Static				
722–01S	3,272 (736)	0.203 (0.008)	9.65 (0.38)	432 (0.670)
722–02S	3,109 (699)	0.178 (0.007)	19.05 (0.75)	560 (0.868)
722–07S	2,989 (672)	0.178 (0.007)	9.65 (0.38)	528 (0.818)
722–08S	3,003 (675)	0.305 (0.012)	22.35 (0.88)	536 (0.831)

32 Ply on 4-in. Platen				
Impact				
Specimen ID No.	**Max Load N (lbf)**	**Dent Depth mm (in.)**	**Crack Length mm (in.)**	**Delamination Area mm^2 ($in.^2$)**
616–20S	7,313 (1,644)	0.127 (0.005)	22.53 (0.88)	1,006 (1.56)
616–21S	7,268 (1,634)	0.152 (0.006)	19.20 (0.75)	1,012 (1.57)
616–22S	7,544 (1,696)	0.178 (0.007)	19.20 (0.75)	1,012 (1.57)
616–24S	7,322 (1,646)	0.152 (0.006)	28.93 (1.14)	987 (1.53)
Quasi-Static				
706–01S	7,455 (1,676)	0.203 (0.008)	Not measurable	1,256 (1.947)
708–07S	7,455 (1,676)	0.203 (0.008)	19.05 (0.75)	904 (1.401)
708–08S	5,498 (1,236)	0.203 (0.008)	Not measurable	

48 Ply on 6-in. Platen				
Impact				
Specimen ID No.	**Max Load N (lbf)**	**Dent Depth mm (in.)**	**Crack Length mm (in.)**	**Delamination Area mm^2 ($in.^2$)**
727–04S	22,788 (5,123)	0.381 (0.015)	73.03 (2.88)	5,412 (8.39)
727–05S	23,100 (5,193)	0.483 (0.019)	77.78 (3.06)	4,128 (6.40)
Quasi-Static				
720–01S	23,429 (5,267)	1.321 (0.052)	28.70 (1.18)	5,648 (8.754)
720–02S	22,196 (4,990)	1.19 (0.047)	22.35 (0.88)	5,244 (8.128)
817–02S	23,389 (5,258)	0.838 (0.033)	16.00 (0.63)	3,186 (4.94)
817–03S	23,389 (5,258)	1.19 (0.047)	31.75 (1.25)	4,880 (7.564)

REFERENCES

1. ASTM Standard D6264–8, *1999 ASTM Book of Standards*, Vol. 15.03.

2. Cantwell, W.J.; and Morton, J.: "Comparison of the Low- and High-Velocity Impact Response of CFRP," *Composites*, Vol. 20, No. 6, pp. 545–551, November 1989.

3. Wu, E.; and Chang, L.: "Loading Rate Effect on Woven Glass Laminated Plates by Penetration Force," *Journal of Composite Materials*, Vol. 32, No. 8, pp. 702–721, 1998.

4. Jackson, W.C.; and Poe, C.C.: "The Use of Impact Force as a Scale Parameter for the Impact Response of Composite Laminates," *NASA Technical Memorandum 104189*, January 1992.

5. Bucinell, R.B.; Nuismer, R.J.; and Koury, J.L.: "Response of Composite Plates to Quasi-Static Impact Events," Composite Materials: Fatigue and Fracture (Third Volume), ASTM STP 1110, pp. 528–549, 1998.

6. Swanson, S.R.: "Limits of Quasi-Static Solutions in Impact of Composite Structures," *Composites Engineering*, Vol. 2, No. 4, pp. 261–267, 1992.

7. Kwon, Y.S.; and Sankar, B.V.: "Indentation-Flexure and Low-Velocity Impact Damage in Graphite Epoxy Laminates," *Journal of Composites Technology and Research*, Vol. 15, No. 2, pp. 101–111, Summer 1993.

8. Lagace, P.A.; Williamson, J.E.; Wilson Tsang, P.H.; Wolf, E.; and Thomas, S.: "A Preliminary Proposition for a Test Method to Measure (Impact) Damage Resistance," *Journal of Reinforced Plastics and Composites*, Vol. 12, pp. 584–601, May 1993.

9. Kaczmarek, H.; and Maison, S.: "Comparative Ultrasonic Analysis of Damage in CFRP Under Static Indentation and Low-Velocity Impact," *Composites Science and Technology*, Vol. 51, pp. 11–26, 1994.

10. Wardle, B.L.; and Lagace, P.A.: "On the Use of Dent Depth as an Impact Damage Metric for Thin Composite Structures," *Journal of Reinforced Plastics and Composites*, Vol. 16, No. 12, pp. 1093–1110, 1997.

11. Nettles, A.T.; Douglas, M.J.; and Estes, E.E.: "Scaling Effects in Carbon/Epoxy Laminates Under Transverse Quasi-Static Loading," *NASA Technical Memorandum 209103*, March 1999.

12. Cheresh, M.C.; and McMichael, S.: "Instrumented Impact Test Data Interpretation," Instrumented Impact Testing of Plastics and Composite Materials, *ASTM STP 936*, pp. 9–23, 1987.

13. Found, M.S.; Howard, I.C.; and Paran, A.P.: "Interpretation of Signals from Drop-Weight Impact Tests," *Composite Structures*, Vol. 42, pp. 353–363, 1998.

14. Lee, S.M.; and Zahuta, P.: "Instrumented Impact and Static Indentation of Composites," *Journal of Composite Materials*, Vol. 25, pp. 204–222, February 1991.

15. Sjoblom, P.O.; Hartness, T.J.; and Cordell, T.M.: "On Low-Velocity Impact Testing of Composite Materials," *Journal of Composite Materials*, Vol. 22, pp. 30–52, January 1988.

16. Iber, W.: "Failure Mechanics in Low-Velocity Impacts on Thin Composite Plates," *NASA Technical Paper 2152*, 1983.

17. Highsmith, A.L.: "A Study of the Use of Contact Loading to Simulate Low-Velocity Impact," *NASA Contractor Report 97–206121*, January 1997.

REPORT DOCUMENTATION PAGE

Form Approved
OMB No. 0704-0188

1. AGENCY USE ONLY *(Leave Blank)*	2. REPORT DATE	3. REPORT TYPE AND DATES COVERED
	August 2000	Technical Publication

4. TITLE AND SUBTITLE

A Comparison of Quasi-Static Indentation to Low-Velocity Impact

5. FUNDING NUMBERS

6. AUTHORS

A.T. Nettles and M.J. Douglas*

7. PERFORMING ORGANIZATION NAMES(S) AND ADDRESS(ES)

George C. Marshall Space Flight Center
Marshall Space Flight Center, AL 35812

8. PERFORMING ORGANIZATION REPORT NUMBER

M–991

9. SPONSORING/MONITORING AGENCY NAME(S) AND ADDRESS(ES)

National Aeronautics and Space Administration
Washington, DC 20546–0001

10. SPONSORING/MONITORING AGENCY REPORT NUMBER

NASA/TP—2000–210481

11. SUPPLEMENTARY NOTES

Prepared by the Materials, Manufacturing, and Processes Department, Engineering Directorate
*Old Dominion University, Norfolk, VA

12a. DISTRIBUTION/AVAILABILITY STATEMENT

Unclassified-Unlimited
Subject Category 24
Standard Distribution

12b. DISTRIBUTION CODE

13. ABSTRACT *(Maximum 200 words)*

A static test method for modeling low-velocity foreign object impact events to composites would prove to be very beneficial to researchers since much more data can be obtained from a static test than from an impact test. In order to examine if this is feasible, a series of static indentation and low-velocity impact tests were carried out and compared. Square specimens of many sizes and thicknesses were utilized to cover the array of types of low-velocity impact events. Laminates with a $\pi/4$ stacking sequence were employed since this is by far the most common type of engineering laminate. Three distinct flexural rigidities under two different boundary conditions were tested in order to obtain damage ranging from that due to large deflection to contact stresses and levels in-between to examine if the static indentation-impact comparisons are valid under the spectrum of damage modes that can be experienced. Comparisons between static indentation and low-velocity impact tests were based on the maximum applied transverse load. The dependent parameters examined included dent depth, back surface crack length, delamination area, and to a limited extent, load-deflection behavior. Results showed that no distinct differences could be seen between the static indentation tests and the low-velocity impact tests, indicating that static indentation can be used to represent a low-velocity impact event.

14. SUBJECT TERMS

composite materials, impact, static indentation

15. NUMBER OF PAGES

94

16. PRICE CODE

A05

17. SECURITY CLASSIFICATION OF REPORT	18. SECURITY CLASSIFICATION OF THIS PAGE	19. SECURITY CLASSIFICATION OF ABSTRACT	20. LIMITATION OF ABSTRACT
Unclassified	Unclassified	Unclassified	Unlimited